2017

Theoretical And Phenomenological Viability Of Scalar Field Theories

Benjamin Elder
University of Pennsylvania, benelder@sas.upenn.edu

Theoretical And Phenomenological Viability Of Scalar Field Theories

Abstract

The objective of this Thesis is to explore several related questions with regards to criteria for viability in scalar field theories. Roughly the first half is devoted to theoretical criteria, while the second half focuses on phenomenological ones. We begin with an overview of theories that violate the null energy condition, highlighting the pathologies that inevitably appear. We then present a theory that violates the null energy condition while remaining free of the problems that plagued previous attempts. Next we explore a global condition for classical stability in scalar field theories, namely, the requirement that the total energy of the space-time be positive. This property is guaranteed if the theory admits a positive energy theorem. After reviewing existing proofs of positive energy for canonical scalar fields, we then extend those proofs to theories with derivative interactions, proving a positive energy theorem for a wide class of P(X) theories. The second half of this Thesis considers experimental constraints on scalar field theories. We focus on what may be learned from atom interferometry experiments, which have been a powerful probe of fundamental physics for over two decades but only recently gained the ability to constrain screened scalar field theories. We present a general analytic and numerical framework for precise predictions of scalar field theories in atom interferometry experiments, and use those techniques to derive new limits on chameleon and symmetron field theories.

Degree Type

Dissertation

Degree Name

Doctor of Philosophy (PhD)

Graduate Group

Physics & Astronomy

First Advisor

Justin Khoury

Subject Categories

Other Physics

THEORETICAL AND PHENOMENOLOGICAL VIABILITY OF SCALAR FIELD THEORIES

Benjamin Elder

A DISSERTATION

in

Physics and Astronomy

Presented to the Faculties of the University of Pennsylvania

in

Partial Fulfillment of the Requirements for the

Degree of Doctor of Philosophy

2017

Supervisor of Dissertation

Justin Khoury, Professor of Physics and Astronomy

Graduate Group Chairperson

Joshua Klein, Professor of Physics and Astronomy

Dissertation Committee:

Mark Trodden, Fay R. and Eugene L. Langberg Professor of Physics and Astronomy

Joshua Klein, Professor of Physics and Astronomy

Adam Lidz, Associate Professor of Physics and Astronomy

Tom Lubensky, Christopher H. Browne Distinguished Professor of Physics and Astronomy

THEORETICAL AND PHENOMENOLOGICAL VIABILITY OF SCALAR FIELD THEORIES

Acknowledgements

Nobody writes a thesis alone, and I am no exception. I am infinitely grateful to my advisor, Justin Khoury, for all of his generous support, encouragement, and knowledge over the past four years. Working with him has been truly inspiring. I admit that there were many times I wished I could stay a graduate student for a decade just so I could stay and keep working on projects with him.

I would also like to thank Mark Trodden, who has patiently explained many ideas and concepts to me. There were numerous occasions where I chanced upon him while lost in thought, and he was always happy to hear what I was thinking about and to help un-muddle my thoughts. Thanks are also due to Josh Klein for always having exciting new ideas to discuss, as well as for serving on my thesis committee. On that note, I'd also like to thank Adam Lidz, Tom Lubensky, and Mark Trodden (again) for being on my committee. Warm thanks are also due to all of my collaborators, without whom I would not have been able to do the work presented in this Thesis.

I'm also extremely grateful to Austin Joyce for all of his long and elucidating discussions, as well as his encouragement. Arriving at Penn to work on ideas I didn't understand was a daunting prospect and Austin patiently explained a great many things to me, especially in those first few months. I'm similarly grateful to Lasha Berezhiani, Yi-Zen Chu, Garrett Goon, Adam Solomon, Mariana Carrillo Gonzalez, and Rehan Deen. Special thanks are due to Jeremy Sakstein for saving my life by introducing me to BibTeX. I've also been very glad to share an office with Ashley, Mariana, and Yuedong.

I'd be remiss not to mention all the care and support I've gotten from my parents, who have always encouraged me to pursue my ambitions, and from Charlotte, who has

been a steady companion throughout this journey. Bonus points are also due to her for bringing along Nubi and Tink, who quickly became my favorite furry co-authors.

ABSTRACT

THEORETICAL AND PHENOMENOLOGICAL VIABILITY OF SCALAR FIELD THEORIES

Benjamin Elder

Justin Khoury

The objective of this Thesis is to explore several related questions with regards to criteria for viability in scalar field theories. Roughly the first half is devoted to theoretical criteria, while the second half focuses on phenomenological ones. We begin with an overview of theories that violate the null energy condition, highlighting the pathologies that inevitably appear. We then present a theory that violates the null energy condition while remaining free of the problems that plagued previous attempts. Next we explore a global condition for classical stability in scalar field theories, namely, the requirement that the total energy of the space-time be positive. This property is guaranteed if the theory admits a positive energy theorem. After reviewing existing proofs of positive energy for canonical scalar fields, we then extend those proofs to theories with derivative interactions, proving a positive energy theorem for a wide class of $P(X)$ theories. The second half of this Thesis considers experimental constraints on scalar field theories. We focus on what may be learned from atom interferometry experiments, which have been a powerful probe of fundamental physics for over two decades but only recently gained the ability to constrain screened scalar field theories. We present a general analytic and numerical framework for precise predictions of scalar field theories in atom interferometry experiments, and use those techniques to derive new limits on chameleon and symmetron field theories.

Contents

1 Introduction **1**

1.1 Scalar fields: kinetic classification 8

1.2 Effective field theory pathologies 17

1.3 Atom Interferometry 21

2 Violating the Null Energy Condition **26**

2.1 Attempts to violate the NEC 33

2.2 A no-go argument for interpolating solutions 43

2.3 Construction of the theory 45

2.4 Radiative stability 51

2.5 NEC violation and neglecting gravity 52

2.6 Cosmological Evolution 56

2.7 Stability of perturbations 57

2.8 Conclusions 61

3 A Positive Energy Theorem for $P(X)$ Theories **64**

3.1 Two-Field Description 69

3.2 Direct derivation 72

3.3 Special Cases 75

3.4 Conclusions 78

4 Constraints on Chameleon Field Theories **81**

4.1 Chameleons: A Brief Review 87

4.2 Existing Constraints and Motivations for this Work 93

4.3 Numerical Method 97

4.4 Successive Steps Towards Realistic Set-Up 100
4.5 Simulation of the Experiment 106
4.6 Forecasts for ongoing and upcoming experiments 108
4.7 Conclusions 112

5 Constraints on Symmetron Field Theories **113**
5.1 Symmetrons: A Brief Review 115
5.2 Numerical analysis 118
5.3 Conclusion 121

6 Conclusions **123**

A Screening Factors **125**
A.1 The field from a single object 125
A.2 Motion of an extended object 128

References **131**

List of Tables

2.1 Checklist of properties of various theories which possess null energy condition-violating solutions. See Section 1.2 for a discussion of the pathologies in this Table. 42

4.1 Densities of the materials in the experiment. 97

List of Figures

1.1 Schematic of the effective potential felt by a chameleon field (solid line), given by the sum of the bare potential of runaway form, $V(\phi)$ (dashed line), and a density-dependent piece, from coupling to matter (dotted line). As the density ρ increases, so does the effective mass of the chameleon $m_\phi^2 = V_{\rm eff},_{\phi\phi}$, which depends on the second derivative of the effective potential about the minimum. 12

1.2 Schematic of the effective potential felt by a symmetron field. At low densities, the quadratic term in the effective potential is negative and the field rolls to a local minimum at a nonzero value of ϕ (green line). At high densities the sign of the quadratic term flips and the minimum of the effective potential is at $\phi = 0$. 13

1.3 Acceleration of an unscreened test particle towards a massive body in $P(X)$ and Galileon theories, divided by the Newtonian gravitational force. We have arbitrarily chosen $\Lambda = M_{\rm Pl}$, and both forces have been normalized such that $F_\phi/F_{\rm N} \to 1$ at large radii. For $P(X)$, this corresponds to $M = \sqrt{2}M_{\rm Pl}$, while for the cubic galileon the choice is $M = M_{\rm Pl}/\sqrt{3}$. In both cases the scalar force is strongly suppressed relative to gravity for $r < r_*$, and $P(X)$ screening is actually *more* efficient due to the greater degree of non-linearity in its equation of motion. Note also that the expression for r_* is slightly different in the two theories. 15

1.4 Left: Experimental setup. The acceleration $a_{\rm cyl}$ of cesium atoms towards a source mass suspended in ultra-high vacuum is measured. Making a differential measurement isolates the effect of any interactions due to the source mass. Note that the source mass is depicted here as a cylinder, while an earlier version of the experiment used a spherical source mass. This is why much of the analysis in this Section is for a spherical source mass. Right: Mach-Zehnder interferometer based on Raman transitions in an optical cavity. Three laser pulses manipulate the cesium atoms during free-fall. The pulses 1) split the atomic wave packet along two different trajectories, 2) reflect the two trajectories near their apex, and 3) recombine and interfere the matter waves to measure the phase difference accumulated between the two paths during the interferometer time of 2T = 110 ms. 24

2.1 In a dilation invariant theory, we must have $Z = 0$ at both $e^{-2\pi}\dot{\pi}^2 = 0$ and $e^{-2\pi}\dot{\pi}^2 = Y$, as well as $Z' > 0$ at both of these points. It is impossible to connect these two solutions without having a region where $Z' < 0$, as is clear from the plot. 44

2.2 NEC-satisfying and NEC-violating regions in the (ϕ, ϕ') phase space, for the parameter values $\frac{f_\infty}{f_0} = 10$ and $\mathcal{J}_0 = 0.75$. The solution of interest, $\phi = 1 + t/t_*$, corresponding to $\phi' = 1$, is plotted as a black dashed line. It first obeys the NEC for a period of time, and then crosses into the NEC-violating regime. 53
2.3 Timeline for the evolution. Our approximation of neglecting gravity is valid for the range $t_{\rm beg} \leq t \leq t_{\rm end}$. For $t < t_{\rm beg}$, the universe asymptotes to a big bang singularity (since the NEC is satisfied in this regime). At approximately t_*, the universe transitions from a NEC-satisfying phase to a NEC-violating one. For $t > t_{\rm end}$, cosmological expansion is important, and the universe must transition from the NEC-violating phase to a standard, radiation-dominated phase. 55
2.4 The Hubble parameter is plotted for two values of H_i with the fiducial parameters $\mathcal{J}_0 = 0.75$, $f_\infty/f_0 = 10$, $\Lambda = 0.1$, $t_* = -1$, and $C = -6.3 \times 10^{-4} M_{\rm Pl}$. The vertical dashed line marks the boundary between the NEC-satisfying and NEC-violating phases. As we would expect, $\dot{H} < 0$ when the NEC holds, and $\dot{H} > 0$ when it is violated. The dashed solution (corresponding to $H_i = 0.001 M_{\rm Pl}$) always has $H > 0$. It represents an initially expanding universe with decelerating expansion, and could match onto a big-bang type solution for $t < t_{\rm beg}$. The solid line (with $H_i = -0.001 M_{\rm Pl}$) represents an initially contracting universe ($H < 0$) which enters the phase of NEC-violation and undergoes a cosmological bounce to an accelerating phase ($H > 0$), all within the regime of validity of our effective theory. . . 57
2.5 The shaded regions represent parts of the (ϕ, ϕ') phase space where perturbations (a) suffer from gradient instabilities; (b) propagate superluminally; (c) are strongly coupled. The parameter values are $\frac{f_\infty}{f_0} = 10$ and $\mathcal{J}_0 = 0.75$. The solution of interest, $\phi = 1 + t/t_*$, corresponding to $\phi' = 1$, is plotted as a black dashed line. It avoids all pathological regions. 59
2.6 Phase portrait with all constraints overlaid, again for the fiducial choice of parameters $\frac{f_\infty}{f_0} = 10$ and $\mathcal{J}_0 = 0.75$. The shaded region represents the union of all pathological regions shown in Fig. 2.5. The green long-dashed line separates the NEC-satisfying and NEC-violating regions. The black short-dashed line corresponds to the background solution of interest, given by (2.51). The solid lines represent other background solutions (with different initial conditions). 62

4.1 Schematic of the effective potential felt by a chameleon field (solid line), given by the sum of the bare potential of runaway form, $V(\phi)$ (dashed line), and a density-dependent piece, from coupling to matter (dotted line). . . . 87
4.2 Effective potential for low ambient matter density (Left) and high ambient density (Right). As the density increases, the minimum of the effective potential, $\phi_{\rm min}$, shifts to smaller values, while the mass of small fluctuations, m_ϕ, increases. 90

4.3 Current constraints due to atom interferometry and torsion pendulum experiments. We are mainly concerned with $\Lambda = \Lambda_0$, indicated by the black line on the first plot, so that the chameleon field can drive the observed accelerated expansion of the universe. The narrow light blue stripes on the left panel show the influence of varying the fudge parameter over $0.55 \leq \xi \leq 0.68$. The second plot shows $M_{\rm Pl}/M$ *vs.* n, and also assumes $\Lambda = \Lambda_0$. The "torsion pendulum" region shown in green has been corrected from [96] to accurately reflect the constraints imposed by that experiment, following [225]. 94

4.4 The chameleon field as a function of distance along the center of the spherical vacuum chamber. The black horizontal line marks the central value of ϕ predicted inside an empty chamber using (4.18). The red vertical line denotes the location of the interferometer. We find essentially no difference between letting ϕ minimize its potential in atmosphere *vs* in steel at the walls. 101

4.5 **Diagram and dimensions of experimental setup.** The cross marks the center of the vacuum chamber. The vacuum chamber walls are ~ 2 cm thick, which is much greater than the Compton wavelength of the chameleon inside steel in all cases examined. 102

4.6 **Spherical *vs* cylindrical vacuum chamber.** Chameleon profile and acceleration as a function of distance from the center of the spherical source mass, for a spherical (blue curve) and cylindrical (green curve) vacuum chamber. The dimensions of the cylindrical vacuum chamber are chosen to match that of the experiment in [96] and are shown in Fig. 4.5. The radius of the sphere is chosen to match the inner radius of the cylinder. At the location of the interferometer (red vertical line), the acceleration in the spherical case is 18% larger than in the cylindrical chamber. 103

4.7 **Source mass centered *vs* offset.** Same plot as the previous figure, now comparing a source mass at the center (blue curve) and offset by 2.55 cm from the center (green curve), as in the actual experiment. As in the previous figure, the dimensions of the cylindrical chamber match those of the experiment. Although the field profile is altered by the offset, the acceleration at the interferometer (red vertical line) changes by less than 1%. . . . 104

4.8 **Source mass with *vs* without bore.** Same as the previous two figures, but now comparing a solid source mass (blue curve) against one with a 3 mm diameter circular bore through the center (green curve), as in the experiment. All other dimensions are chosen to match those of the experiment. The only significant difference is inside the sphere, as the green line passes through the center of the bore, so it is still in vacuum. The acceleration at the interferometer (red vertical line) again changes by less than 1%. 105

4.9 Simulation of the experimental configuration, for values of M ranging from $10^{-5}M_{\rm Pl}$ to $M_{\rm Pl}$. We find that the profiles in vacuum are nearly identical, differing only in the walls. The field values inside the metal of the source mass also scale with M, but we are showing a path that passes through the center of the bore in the source mass. The bore acts as a miniature vacuum chamber, so instead the chameleon field goes to an M-independent value such that the Compton wavelength is of order the radius of the bore. . . . 107

4.10 **Spherical source mass** *vs* **cylindrical source.** Comparison between two experimental setups: that of [96] (blue line) and of an improved version of the experiment that is currently underway (green line). The main difference is that the latter employs a tungsten cylinder as the source mass, while the former used an aluminum sphere. The cylinder has a wedge cut out of it, allowing for vastly improved control over systematics. These show that the cutout comes at no cost to the chameleon signal, in fact, the cylinder confers a 5% stronger chameleon force over the previous setup. 109

4.11 Same plot as Fig. 4.9, but for the empty rectangular vacuum chamber of the CAL experiment. The field profiles are taken along the long axis of the vacuum chamber. Again, we find that the profiles in vacuum are nearly identical. 110

5.1 Symmetron field profiles for $M = 10^3$ GeV, $\lambda = 10^{-5}$, and $\mu = 10^{-1}, 10^{-1.5}$ meV, plotted along the vertical axis of the vacuum chamber. The atoms follow a vertical path that takes them near the source mass; the interferometry measurement occurs in the red region near the apex of their trajectory. The combination $\lambda\phi\vec{\nabla}\phi$ is displayed because it is independent of M and λ and is easily relatable to the scalar acceleration Eq. (5.11). (Note that this is the λ that appears in the Lagrangian, not the thin-shell factor $\lambda_{\rm atom}$.) The two curves illustrate the window of measurable μ nicely: for larger μ, the overall force is stronger, yet shorter-ranged, and much larger μ would result in a force that cannot reach to the interferometer. For smaller μ, the force is weaker yet longer-ranged, suppressed because the vacuum chamber is not large enough for the field to reach its VEV. 120

5.2 Shaded areas are excluded regions of parameter space. The areas in blue are constrained by the latest atom interferometry data [4]. For comparison we have included older atom interferometry [96], as well as data from torsion balance experiments [225]. 122

Preface

This thesis is based on work I have done at Penn over the past four years with Prof. Justin Khoury at Penn. I owe him, as well as my collaborators, a huge debt of gratitude, without whom this work certainly would not have been possible.

Chapter 1 contains introductory background material and lays the groundwork for the rest of the theory. Many of the topics which are common across multiple Chapters are introduced here.

In Chapter 2 I consider the problem of violating the Null Energy Condition (NEC) with a healthy scalar field theory. All previous examples of NEC violation have come with some sort of pathological instability in the theory, leading some to wonder if healthy NEC violation is possible. In this Chapter I provide a counterexample by constructing a theory which, for the first time, can smoothly interpolate between a Poincarè invariant vacuum and a NEC violating solution while remaining stable throughout. The work in this Chapter first appeared in [1].

Chapter 3 presents a positive energy theorem for derivatively-coupled $P(X)$ theories. Positive energy is a necessary requirement for the vacuum of a theory to be classically stable. This proof builds on earlier proofs for canonical field theories, extending them to $P(X)$ theories. At the end I briefly consider the extension to galileons, and describe the obstruction one faces in proving a positive energy theorem for them. This chapter is based on work that appeared in [2].

Chapters 4 and 5 are concerned with constraints on chameleon and symmetron theories from atom interferometry (AI) tests. Recent AI experiments have recently become enormously more sensitive to scalar forces by miniaturizing the interferometer and including a small metal object inside the vacuum chamber a few millimeters away.

Their precise measurements of the interaction between the atoms and the metal object necessitates detailed predictions of scalar forces in such environments. These Chapters present the theoretical groundwork for such predictions and develop a numerical scheme that accurately accounts for the highly irregular geometry of the experimental setup. This work was published in [3, 4].

Chapter 1

Introduction

The past two decades have seen a great deal of activity on theories that modify Einstein's General Relativity. There are many reasons to modify our theory of gravity: to model the effects of cosmic acceleration, dark matter, or the early universe, or perhaps the modification is merely a side effect of some other theory. Massive gravity, string theory, and higher dimensional constructions of gravity are all examples of theories that modify general relativity (GR).

Whatever the motivation may be, it is important to take care: GR is an incredibly precise and well-developed theory, and even the slightest modification may have far-reaching and unintended consequences. It is therefore crucial to have a solid understanding of baseline viability in the theory — is the theory stable? Does it have the desired phenomenology? Does it conflict with existing tests of gravity?

This thesis will explore each of these questions in turn. Since Einstein gravity is the unique interacting massless spin-2 theory [5], modifications generically introduce new degrees of freedom. We therefore focus on scalar-tensor theories, in which there is a new degree of freedom in the form of a scalar field. Furthermore, we adopt the viewpoint of effective field theory (EFT), where we focus on the low-energy dynamics only. Beyond a certain energy scale (the *cutoff*), the theory is no longer predictive and a more complete theory (termed the *UV completion*) is needed.

There exists a dizzying number of theories which modify GR [6, 7]. We will be

as general as possible, making sweeping statements about broad classes of theories whenever we can. There are three main classes of theories to consider, distinguished by the form of their kinetic term.

The first, known as *canonical* field theories, have a kinetic form of the typical form $X = -\frac{1}{2}(\partial\phi)^2$, where ϕ is the scalar field and Lorentz contraction is implied. Such theories have a long history — even the Klein-Gordon field is canonical. One of the most historically significant theories of modified gravity, Brans-Dicke theory [8], also takes this form.

The second class, termed $P(X)$ theories, involves higher powers of X in the Lagrangian. Without a potential the field is invariant under a shift symmetry $\phi \to \phi + a$. The first example of a $P(X)$ theory was a version of electrodynamics due to Born and Infeld [9]. The Dirac-Born-Infeld (DBI) action for the fluctuations of a brane in string theory also belongs to this class [10, 11]. Another significant theory in this class is the Ghost Condensate, which has been used to violate the null energy condition [12]. Models have also been introduced that can drive cosmic acceleration [13, 14], and exhibit that screening [15, 16]. One of the primary motivations for studying $P(X)$ theories is that they describe the low energy dynamics of a superfluid [17], a fact that has been utilized recently to describe superfluid dark matter [18–21].

The third and final class, called *galileons*, involves terms in the Lagrangian with more than one derivative per field. Galileons first attracted interest via their appearance in the decoupling limit of DGP gravity [22], where our universe is embedded as a 3-brane in a 5-dimensional space-time. It was noted that the action was invariant under a *Galilean transformation*,

$$\phi \to \phi + a + b_\mu x^\mu \ , \tag{1.1}$$

for constants a, b_μ, which is inherited from higher-dimensional Poincaré symmetry [23]. The most general possible scalar field invariant under Eq. (1.1) while retaining second order equations of motion was constructed in [24]. Any theory that has this property is known as a galileon.

The requirement that the equations of motion be second order is a non-trivial one. Many of the terms that are invariant under Eq. (1.1) involve two derivatives per field, which generally leads to third derivatives in the equation of motion. This presents a challenge, since equations of motion with higher than second order derivatives are unstable [25]. Galileons avoid this issue by carefully balancing the coefficients of terms so that the terms with higher-order derivatives cancel each other out.

There exists a finite number of terms that simultaneously exhibit the galilean symmetry and retain second order equations of motion. To be exact, in n dimensions there are $n+1$ unique galileon terms. Each successive term is just $(\partial\phi)^2$ times the equation of motion of the previous term's equation of motion [26], a structure known as an Euler hierarchy [27–30]. The galileon terms may also be understood as Wess-Zumino terms for spontaneously broken space-time symmetries [31].

Galileons have been used as a model for inflation [32–44] and its alternatives [45–54], as well as late time acceleration of the universe [55–71]. They are also notable for their appearance in the decoupling limit of massive gravity [72], and have been generalized to other theories such as supersymmetry and supergravity [73–77]. One important generalization is Horndeski theory, which constructs galileons in arbitrarily curved space-times [78, 79].

Extra care must be taken with higher derivative theories (*i.e.* $P(X)$ and galileons), as they are susceptible to various instabilities and other similar problems. The ques-

tion of pathologies is a powerful one, as we may immediately deem a pathologically unstable theory to be unpredictive. Section 1.2 details a number of criteria, which we summarize here.

Instabilities manifest in some (or all) of the Fourier modes growing without bound. Furthermore, demanding that the UV completion be a local quantum field theory allows us to rule out theories with superluminal propagation or a non-analytic S-matrix. Finally, there may be barriers preventing access to certain solutions — if it is impossible for the field to evolve from a vacuum state to a given solution without becoming strong coupled, then such solutions should be regarded as inaccessible.

Pathologies often go hand in hand with *energy conditions*, which are covariant statements about the energy content of the theory. They are demands that the stress-energy tensor be sufficiently positive for all observers, or that energy not flow faster than the speed of light. The four most common energy conditions (weak, strong, dominant, and null) are detailed in the introduction to Chapter 2.

Since the stress-energy tensor dictates the curvature of space-time, energy conditions are often assumed or required when constructing particular solutions to the Einstein Field Equations. For example, a universe going from a contracting phase ($\dot{a} < 0$) to an expanding one ($\dot{a} > 0$) requires violating the null energy condition which, incidentally, is the *only* energy condition that can not be violated with a canonical scalar field without encountering an instability. In Chapter 2 we review previous attempts to violate the null energy condition, and show that all have encountered some kind of pathology. We go on to give an example of a galileon field theory which can do so while avoiding all of the above issues.

Another concern is that the vacuum of the theory should be stable in the presence

of gravity. This is equivalent to asking whether the theory admits a positive energy theorem, which states that the total energy of the space-time should be positive, and should be zero only for Minkowski space-time. The quantity of interest here is the Arnowitt, Deser, and Misner (ADM) mass [80], which combines the energy contributions from the space-time and the energy sources in it. It is well defined for asymptotically flat space-times, and is computed by the deviation of the metric tensor from flatness at spatial infinity in a manner similar to Gauss' Law in Newtonian gravity.

If the ADM mass is positive, then the space-time is guaranteed to have positive energy. This theorem was originally proven provided that the energy content of the space-time obeys the Dominant Energy Condition (DEC) [81–83]. The requirement that the fields satisfy the DEC was later relaxed; it was shown that canonical scalars with a certain type of potential would have positive energy [84–86]. Until recently it was unknown whether a similar proof held for derivatively coupled scalar fields. A proof of the positive energy theorem for $P(X)$ theories, which originally appeared in [2], is detailed in Chapter 3.

Finally, it is important to note that if scalar fields are currently present in the universe, then their effects should be consistent with existing tests of gravity. The main motivation for introducing scalar fields comes from the empirical discovery of late-time cosmic acceleration (dark energy). If dark energy is shown to be varying in time, then by Lorentz invariance it can also vary in space, and is therefore a scalar field. This general idea for minimally-coupled scalars goes under the the name *quintessence* [87, 88].

A more theoretical motivation for introducing scalar fields in the late universe is the problem of the cosmological constant (CC). There is strong evidence that the universe

is undergoing a period of accelerated expansion, and that expansion is consistent with a cosmological constant of size $\Lambda \sim \text{meV}^4 \sim 10^{-120} M_{\text{Pl}}^4$. This is far smaller than the value we might have guessed, since $M_{\text{Pl}} \sim 10^{30}$ meV is the typical scale for gravitational phenomena [89]. A related problem is that the ground state energy of standard model matter fields should also contribute a cosmological constant of at least $\Lambda_{\text{SM}} \sim 10^{-60} M_{\text{Pl}}^4$. A full solution of the cosmological constant problem would explain why the CC is so small when measured in Planck units, and would also explain how the large contribution from standard model fields gets neutralized to a scale of order $\sim \text{meV}^4$ without fine-tuning.

Scalar fields provide one possible avenue to solving the CC problem. For example, a uniformly varying scalar field $\phi = \phi(t)$ is a perfect fluid with an equation of state $P = w_\phi \rho$, where

$$w_\phi = \frac{\frac{1}{2}\dot{\phi}^2 - V(\phi)}{\frac{1}{2}\dot{\phi}^2 + V(\phi)} \ . \tag{1.2}$$

If the scalar field is slowly rolling $\dot{\phi}^2 \ll V(\phi)$, then $w \approx -1$ and the fluid behaves like a cosmological constant. The idea is that perhaps the scalar field can dynamically relax to the present day's value of the CC. Unfortunately, this particular approach is a dead end — Weinberg's no-go theorem shows that scalar fields under certain assumptions (namely, a finite number of scalar fields with constant solutions) cannot accomplish this without fine-tuning the potential to the same degree as an ordinary CC [89].

We will not directly address the CC problem here, but instead study the general effect of introducing a scalar field in the present universe. If that field is coupled to matter, it implies a "fifth force."[1] The staggering experimental success of Einstein's general relativity up to solar system scales [90] would seem to rule out any such force, or at

[1]Since the charges of any two objects have the same sign, this force is always attractive.

least require fine tuning such that the coupling is extremely weak.

However, there is a second possibility, where the modification to gravity is $O(1)$ typically, but dynamically weakens in or near massive bodies and dense environments. Such forces would go undetected in conventional tests of gravity, while still having significant long-range effects in the Universe. Theories that have this property are said to contain a *screening mechanism*.

Screening mechanisms fall into two types. The first type, called *potential screening*, involves theories that develop non-linear equations of motion based on the local value of the scalar field ϕ. This phenomenon is due to the particular form of the scalar field's self-interaction potential $V(\phi)$, hence their name. Theories exhibiting potential screening couple not to the entire mass of an object but to just a thin shell of matter near the surface. Large, dense objects like planets or stars have such thin shells that the scalar force is negligible compared to ordinary gravity.

The second type, called *derivative screening*, involves screening due to derivative couplings in the Lagrangian. Derivative screening is exhibited in some $P(X)$ theories and in galileons. In this case, the scalar force is comparable to gravity at large distances, but as one gets closer there is a point (the *Vainshtein radius*) at which non-linear terms in the field's equation of motion begin to dominate, suppressing the scalar force. In this scenario, we do not experience the scalar force from an object like the Sun because we are well inside its Vainshtein radius.

Active searches are ongoing to detect the effects of screened scalar field theories. Historically, the strongest constraints have come from solar system tests of gravity and torsion balance experiments. Recently, two promising new techniques have entered the mix. Gravity Resonance Spectroscopy [91–93] measures the quantum states of

cold neutrons in Earth's gravitational potential, determining Earth's acceleration from the energy levels of the eigenstates. Atom Interferometry [3, 4, 94–96] splits a wavepacket of cold atoms into two parts, with one part on a trajectory to pass near a dense sphere, while the other remains distant. The groups are then recombined, and the degree of interference in the final packet is proportional to the force felt by the atoms near the sphere.

These new techniques are ideal for measuring theories with potential screening — since neutrons and atoms are so small, they are much more likely to be unscreened, making them far more sensitive probes of gravity. Chapters 4 and 5 are devoted to translating the results of atom interferometry, which is described in Section 1.3, into constraints on chameleon and symmetron theories, two examples of screened canonical field theories. They are based on work that appeared in [3, 4] .

1.1 Scalar fields: kinetic classification

In this Section we introduce the mathematical formalism underlying all three classes of field theories, and provide a few examples of specific theories in each classes.

Canonical scalar fields can be written in the general form

$$S = \int d^4x\sqrt{-g}\left(\frac{M_{\rm Pl}^2}{2}R - \frac{1}{2}(\partial\phi)^2 - V(\phi)\right) + S_{\rm m}[A^2(\phi)g_{\mu\nu};\psi] \ , \qquad (1.3)$$

where R is the Ricci scalar in the Einstein frame, ϕ is a scalar field, and $S_{\rm m}$ is the action for the matter fields, generically denoted by ψ.[2]

[2]Throughout this Thesis we adopt a mostly-plus metric signature, the reduced Planck mass is defined as $M_{\rm Pl} = (8\pi G)^{-1/2}$, and the Ricci scalar is a contraction of the Ricci tensor $R = R^{\mu}{}_{\mu}$, which is a contraction of the Riemann tensor $R_{\mu\nu} = R^{\alpha}{}_{\mu\alpha\nu}$. Dots refer to time derivatives $\dot{\phi} = \partial_t\phi$, primes refer to radial derivatives $\phi' = \partial_r\phi$, and commas indicate derivatives with respect to the field following the comma $A_{,\phi} = \partial_\phi A$. Furthermore, indices will be suppressed where there structure may be inferred, as in the above action where $(\partial\phi)^2 = \partial_\mu\phi\partial^\mu\phi$.

Brans-Dicke theory [8] is perhaps the most historically significant modification to gravity, originally arising from the idea that Newton's constant $G_{\rm N}$ might vary from one point to the next. It corresponds to choosing $V(\phi) = 0$ and $A^2(\phi) = \exp[-\phi/(M_{\rm Pl}\sqrt{\omega + 3/2})]$, where ω is the Brans-Dicke parameter. In the limit $\omega \to \infty$ the field decouples from matter ($A(\phi) \to 1$) and GR is recovered.

$f(R)$ gravity [97, 98] is a theory which can be written without a scalar field but instead includes higher powers of the Ricci scalar. This theory, with $f(R) = R + R^2$ was the first model of inflation [99] as well as cosmic acceleration in the late universe [100–102] Under a conformal rescaling it may be rewritten as the ordinary Einstein-Hilbert action plus a canonical scalar [103, 104], in fact, the theory is exactly that of Brans and Dicke with $\omega = 0$ and a potential $V(\phi)$ that depends on the form of $f(R)$.

The matter fields are coupled to the Jordan frame metric $\tilde{g}_{\mu\nu} = A^2(\phi) g_{\mu\nu}$. Point particles still follow geodesics, but with respect to the Jordan frame:

$$S = \int \sqrt{-A^2(\phi) g_{\mu\nu} dx^\mu dx^\nu} \ . \tag{1.4}$$

In the non-relativistic limit with static matter fields, the above action tells us that test particles accelerate as

$$\vec{a} = -\vec{\nabla}\Phi - \frac{\mathrm{d} \ln A(\phi)}{\mathrm{d}\phi} \vec{\nabla}\phi \ . \tag{1.5}$$

The first term is the standard acceleration due to the Newtonian potential Φ (computed in the Einstein frame), while the second term represents an anomalous "fifth force" due to the scalar field ϕ.

Note that if $A(\phi) = 1$ (*i.e.* minimal coupling), the fifth force vanishes. In this

scenario matter fields are only able to interact with the scalar field through the metric. However, it is certainly worthwhile to study the rich phenomenology possible when $A(\phi) \neq 1$.

Extensive tests of gravity, in a wide range of scenarios, are consistent with the scalar field acceleration being zero, *i.e.* standard GR. Unscreened theories like that of Brans and Dicke are therefore strongly constrained by existing measurements. For example, the Brans-Dicke parameter is constrained by the Cassini spacecraft to be $\omega \gtrsim 10^4$ [90].

However, screened theories evade these constraints because the local environment where the tests are performed is very dense, causing the scalar force to weaken. Potential screening may be accomplished by suitably choosing $V(\phi)$ and $A(\phi)$. The scalar field's equation of motion responds not just to its own potential, but is also influenced by the matter fields. The scalar field sees an effective potential which dynamically varies with the local environmental density:

$$\begin{aligned} \Box\phi &= V_{\text{eff},\phi}\left(\phi\right) \ , \\ V_{\text{eff}}(\phi) &= V(\phi) + A(\phi)\rho \ , \end{aligned} \tag{1.6}$$

where we have assumed that the matter is non-relativistic ($\tilde{T} = -\tilde{\rho}$) and have expressed the density in a form which is conserved in the Einstein frame ($\rho = A^{-1}\tilde{\rho}$) .

One particular example of potential screening is the *chameleon mechanism*, which relies on a scalar particle mass that increases with the matter density of the local environment. A prototypical potential and coupling function that accomplishes this is :

$$V(\phi) = \Lambda^4\left(1 + \frac{\Lambda}{\phi}\right) \ , \qquad A(\phi) = 1 + \frac{\phi}{M} \ . \tag{1.7}$$

These choices yield an effective potential

$$V_{\rm eff}(\phi) = \Lambda^4 \left(1 + \frac{\Lambda}{\phi}\right) + \frac{\rho}{M}\phi \ , \tag{1.8}$$

resulting in a variable scalar particle mass $m_\phi^2 = V_{{\rm eff},\phi\phi}$ which increases with ρ. Inside a dense extended object like a star or planet, the effective mass is large and the force is short-ranged. Only within a thin shell of matter near the surface of the object is the field sufficiently long-ranged to be able to reach the surface; it is this matter only (and not the entire mass) that contributes to the scalar force. Effectively the "scalar charge" carried by an object is not αm, the mass and coupling strength of the object (as it is for GR) but instead is $\lambda_m \alpha m$, where λ_m is a *screening factor* between 0 and 1. For chameleons this is given by the size and density of the object and the ambient field value, $\lambda_m = M\phi_{\rm bg}/(\rho_{\rm obj} R^2)$. For a very small or light object, the thin shell may be comparable to the size of the object and the entire mass is able to contribute to the external field and the object is unscreened. If $M \sim M_{\rm Pl}$, the force on unscreened objects is comparable to gravity.

Another scenario is the *symmetron mechanism*, which relies on a coupling to matter that becomes small in regions of large environmental matter density. A simple potential and coupling that achieve this are

$$V(\phi) = -\frac{1}{2}\mu^2\phi^2 + \frac{\lambda}{4}\phi^4 \ , \qquad A^2(\phi) = 1 + \frac{\phi^2}{2M^2} \ , \tag{1.9}$$

resulting in an effective potential

$$V_{\rm eff}(\phi) = \frac{1}{2}\left(\frac{\rho}{M^2} - \mu^2\right)\phi^2 + \frac{\lambda}{4}\phi^4 \ . \tag{1.10}$$

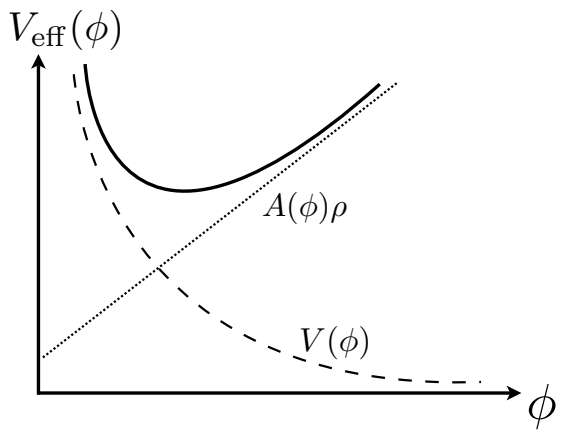

Figure 1.1: Schematic of the effective potential felt by a chameleon field (solid line), given by the sum of the bare potential of runaway form, $V(\phi)$ (dashed line), and a density-dependent piece, from coupling to matter (dotted line). As the density ρ increases, so does the effective mass of the chameleon $m_\phi^2 = V_{\rm eff},_{\phi\phi}$, which depends on the second derivative of the effective potential about the minimum.

In regions of low density, the effective potential has a non-zero minimum at $\phi_0 \equiv \mu/\sqrt{\lambda}$, and the scalar mediates an $O(1)$ modification to general relativity. However, in dense regions, the sign of the quadratic term flips and the minimum of the potential becomes 0. In this limit the coupling term in Eq. (1.5), $\frac{{\rm d}\ln A(\phi)}{{\rm d}\phi} = \frac{\phi}{M^2}$, switches off. The symmetron effectively decouples from matter deep inside dense environments such as planets and stars, making the symmetron force between such objects very weak. Once again, the scalar charge is some fraction of the mass $\lambda_m m$, for $\lambda_m = M^2/(6M_{\rm Pl}^2\Phi)$, where Φ is the surface Newtonian potential of the object.

$P(X)$ theories are a generalization of Eq. (1.3) that add to or replace the ordinary kinetic term $X = -\frac{1}{2}(\partial\phi)^2$ with a function of X, often denoted $P(X)$ (hence their name). A simple example of a $P(X)$ theory is

$$\mathcal{L}_\phi = X + \frac{\alpha}{\Lambda^4}X^2 \,, \qquad A(\phi) = 1 + \frac{\phi}{M} \,, \tag{1.11}$$

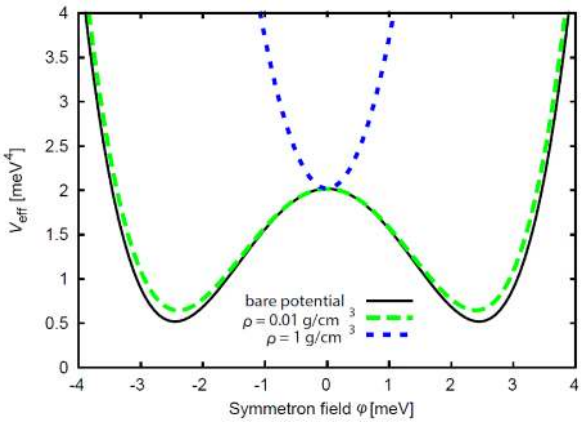

Figure 1.2: Schematic of the effective potential felt by a symmetron field. At low densities, the quadratic term in the effective potential is negative and the field rolls to a local minimum at a nonzero value of ϕ (green line). At high densities the sign of the quadratic term flips and the minimum of the effective potential is at $\phi = 0$.

where $\Lambda \ll M_{\rm Pl}$ is the strong-coupling scale of the theory and $\alpha = \pm 1$. This theory has been used to violate the Null Energy Condition [12], and the $\alpha = -1$ case is interesting in that it admits a positive energy theorem *despite* having superluminal perturbations and violating the standard S-matrix analyticity properties (a fact that will be shown in Chapter 3). It also provides a simple example of derivative screening, which we illustrate here [7, 105].

We will solve for the static, spherically symmetric solutions $\phi = \phi(r)$ around some stationary point mass, so that $T = -m\delta^{(3)}(\vec{x})$. The static equation of motion following from Eq. (1.11) is

$$\vec{\nabla} \cdot \left(\vec{\nabla}\phi - \frac{\alpha}{\Lambda^4} (\vec{\nabla}\phi)^2 \vec{\nabla}\phi \right) = \frac{1}{M} m\delta^{(3)}(\vec{x}) \ . \tag{1.12}$$

This equation is readily integrated once, yielding

$$\phi' - \frac{\alpha}{\Lambda^4} \phi'^3 = \frac{1}{4\pi r^2} \frac{m}{M} \ . \tag{1.13}$$

Note that the above equation only has real solutions for ϕ' if $\alpha = -1$, so we are restricted to this choice. (Although we will not show this here, this choice of α implies that perturbations around a spherically-symmetric and static background propagate superluminally along radial directions. Furthermore, this choice violates the standard S-matrix analyticity criteria, suggesting that the UV completion of the theory is non-standard [7].)

This equation, being cubic in ϕ', may be solved algebraically. It is instructive to consider two limits depending on the size of ϕ'. When ϕ' is small the linear term dominates, and when ϕ' is large the non-linear term dominates. Their corresponding solutions are

$$\phi'(r) \sim \begin{cases} \frac{\Lambda^2}{(4\pi)^{1/3}}\left(\frac{r_*}{r}\right)^{2/3} & r \ll r_* \ , \\ \frac{\Lambda^2}{4\pi}\left(\frac{r_*}{r}\right)^2 & r \gg r_* \ . \end{cases} \tag{1.14}$$

We have introduced a crossover scale $r_* = \frac{1}{\Lambda}\left(\frac{m}{M}\right)^{1/2}$, which represents the closest point at which non-linearities begin to dominate. This is the *Vainshtein radius*, although the term is sometimes reserved for galileon theories despite the mechanism being the same.

Note that the acceleration on a test particle from the Newtonian gravitational force is

$$a_{\rm N} = \frac{Gm}{r^2} = \frac{m}{8\pi M_{\rm Pl}^2 r^2} \ . \tag{1.15}$$

At distances $r > r_*$, the scalar field's force law is similar:

$$a_\phi = \frac{m}{4\pi M^2 r^2} \ , \tag{1.16}$$

where we have used Eq. (1.5) and $A_{,\phi} \approx \frac{1}{M}$ for $\phi \ll M$. If $M \approx M_{\rm Pl}$, the scalar force

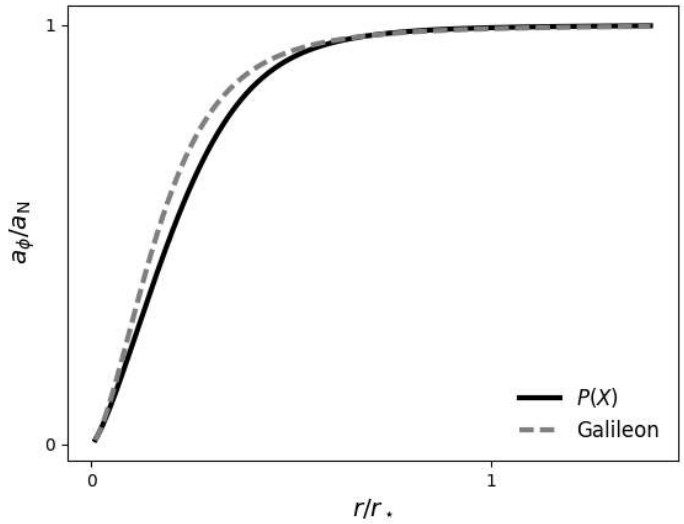

Figure 1.3: Acceleration of an unscreened test particle towards a massive body in $P(X)$ and Galileon theories, divided by the Newtonian gravitational force. We have arbitrarily chosen $\Lambda = M_{\rm Pl}$, and both forces have been normalized such that $F_\phi/F_{\rm N} \to 1$ at large radii. For $P(X)$, this corresponds to $M = \sqrt{2}M_{\rm Pl}$, while for the cubic galileon the choice is $M = M_{\rm Pl}/\sqrt{3}$. In both cases the scalar force is strongly suppressed relative to gravity for $r < r_*$, and $P(X)$ screening is actually *more* efficient due to the greater degree of non-linearity in its equation of motion. Note also that the expression for r_* is slightly different in the two theories.

is approximately gravitational strength at large distances.

At small distances $r \ll r_*$, the non-linear term dominates and the force grows only as $r^{-2/3}$, so the force grows much more slowly than a standard $1/r^2$ force. This behavior is typical of derivative screening, and is illustrated in Fig. 1.3.

Galileons are a further generalization of Eq. (1.3) to terms that involve more than one derivative per field in the Lagrangian. The simplest example is the cubic galileon, which has a Lagrangian

$$\mathcal{L}_\phi = -\frac{1}{2}c_2(\partial\phi)^2 - \frac{c_3}{\Lambda^3}\frac{1}{2}(\partial\phi)^2\Box\phi \ , \qquad A^2(\phi) = 1 + \frac{\phi}{M} \ , \tag{1.17}$$

where the c_i and g are dimensionless parameters. DGP gravity [22] corresponds to choosing $c_2 = 6, c_3 = 2$, and $M = M_{\rm Pl}$. Adopting those c_i, the static and spherically symmetric equation of motion following from Eq. (1.17) is

$$\vec{\nabla} \cdot \left(6\vec{\nabla}\phi + \hat{r}\frac{4}{\Lambda^3}\frac{(\vec{\nabla}\phi)^2}{r} \right) = \frac{m}{M}\delta^{(3)}(\vec{x}) \ . \tag{1.18}$$

Note that this equation is second order, despite the $\Box\phi$ appearing in Eq. (1.17)! Integrating the equation of motion once gives an algebraic equation for ϕ':

$$6\phi' + \frac{4}{\Lambda^3}\frac{\phi'^2}{r} = \frac{m}{4\pi r^2 M} \ . \tag{1.19}$$

This time the Vainshtein radius appears as $r_* = \frac{1}{\Lambda}\left(\frac{m}{M}\right)^{1/3}$. As in the $P(X)$ example, we find the solution to this equation in two limits [7, 23]

$$\phi' \sim \begin{cases} \frac{\Lambda^2}{4\sqrt{\pi}}\left(\frac{m}{M}\right)^{1/3}\left(\frac{r_*}{r}\right)^{1/2} & r \ll r_* \ , \\ \frac{\Lambda^2}{24\pi}\left(\frac{m}{M}\right)^{1/3}\left(\frac{r_*}{r}\right)^{2} & r \gg r_* \ , \end{cases} \tag{1.20}$$

Again we see the Vainshtein mechanism at work: near the source, the non-linear terms dominate the equation of motion leading to a scalar force that grows much more slowly than $1/r^2$. This behavior is also demonstrated in Fig. 1.3. We find that the force law for $P(X)$ falls off faster for $r < r_*$, this is because Eq. (1.13) is cubic in ϕ' while Eq. (1.19) is only quadratic. Note also that for a given massive object, the Vainshtein radius for the $P(X)$ theory is larger than for the cubic galileon, again due to the increased non-linearity.

1.2 Effective field theory pathologies

Derivatively coupled field theories have generated a great deal of interest in recent years, in part because their kinetic structure affords them a much greater degree of flexibility in their phenomenology. However, along with this flexibility comes a danger: instabilities can more easily appear in the theory, and care must be taken to ensure that a particular solution is stable. A good first step[3] is to look at the quadratic Lagrangian for fluctuations about some background solution: $\phi \to \bar{\phi} + \varphi$. The general form of the quadratic action for φ is

$$\mathcal{L}_\phi = \frac{1}{2} f_0(\bar{\phi}, \partial\bar{\phi})\dot{\varphi}^2 - \frac{1}{2} f_{ij}(\bar{\phi}, \partial\bar{\phi})\partial_i\varphi\partial_j\varphi - \frac{1}{2} f_m(\bar{\phi}, \partial\bar{\phi})m_\varphi^2\varphi^2 \ , \tag{1.21}$$

where the partial derivatives within the f_J (for $J = 0 - 3, m$) collectively denote space and time derivatives and there is an implied sum over $i = 1, 2, 3$. The functions f_J can be arbitrary functions of the background solution, except that they must be positive for the theory to be stable.

If $f_0(\bar{\phi}) < 0$, the mode is a *ghost*, signifying that the field carries negative energy. If the scalar is coupled to ordinary matter fields, the decay rate for the vacuum to produce two ϕ particles and two healthy particles is infinite [106, 107]. The vacuum therefore immediately decays into an infinite number of ghostly and healthy particles, making the theory lose all predictive power. A ghostly mode is only acceptable if its mass lies above the cutoff of the EFT, signifying that the field is non-dynamical at the energy scales of interest.

If $f_i(\bar{\phi}) < 0$, the theory contains a *gradient instability*. This is a disaster for the theory, since all Fourier modes allowed in the EFT grow like $\phi_k \sim e^{kt}$. The fastest-

[3]See Appendix D of [7] for a more detailed discussion these pathologies and their resolutions.

growing mode is the largest value of k allowed within the EFT, $k \sim \Lambda$, so the EFT is unstable on timescales $\tau \sim \Lambda^{-1}$. But any dynamics on timescales faster than this would involve $k > \Lambda$, and therefore lie outside the regime of validity of the EFT. Theories with gradient instabilities are non-predictive at all scales [7].

If $f_3(\bar{\phi}) < 0$, the field is *tachyonic*, indicating that the mass is negative. This is a much milder form of instability, as a tachyon's instability only manifests on timescales longer than m_φ^{-1}. As long as this is longer than the timescales of interest, the theory will be stable for all practical purposes. Physically, a tachyonic instability indicates that the solution being perturbed around is unstable and will evolve to a different (hopefully stable) state. This behavior is exhibited in the symmetron model Eq. (1.9): if the quadratic term in the effective potential is negative and we try to expand around $\phi = 0$, the perturbations appear tachyonic. But if we perturb around the true vacuum $\phi_0 = \mu/\sqrt{\lambda}$, the instability disappears.

We must also be careful that the propagation speed of the perturbations is *subluminal*. This requirement expresses a prejudice that the EFT has a Lorentz invariant UV completion. A Lorentz invariant theory has operators that commute outside the light cone [7, 108]:

$$[O_1(x), O_2(y)] = 0 \qquad \text{if } (x-y)^2 > 0 \ . \tag{1.22}$$

A superluminally propagating signal, even within a low energy limit (such as the EFT), violates this criterion.

The speed of perturbations along the ith direction is $c_i^2 = f_{ii}/f_0$, so we must have $f_{ii}/f_1 < 0$. Although this is a simple check on the theory, superluminal propagation does not necessarily break causaulity. The quantity c_s is the *phase* velocity, which can be superluminal without breaking causality as long as the *front* velocity is less

than or equal to the speed of light [109]. Nonetheless, in the present work we will be conservative and demand $c_s \leq 1$. Canonical scalars always exhibit subluminal perturbations, while $P(X)$ and galileon theories can have superluminal perturbations around certain backgrounds. We have already encountered this behavior: recall that perturbations in the $P(X)$ theory Eq. (1.11) are superluminal if $\alpha = -1$.

A related concern is that an EFT that appears to be locally Lorentz-invariant secretly exhibits macroscopic non-locality. This situation may be avoided if the S-matrix for perturbations satisfies standard analyticity requirements. This is essentially a requirement that is inherited from the demand that the EFT descends from a Lorentz invariant UV completion. In many theories this amounts to requiring that the overall signs of certain higher dimensional operators are positive [7, 110].

Something else to watch out for is that quantum corrections can introduce new operators in the effective field theory. Such terms could easily ruin the screening mechanism, so we must be sure that quantum corrections are under control, that is, that the EFT is technically natural.

For instance, the one-loop correction to a canonical scalar field goes as $\Delta V \sim m_{\text{eff}}^4 \ln(m_{\text{eff}}^2/\mu^2)$ for some mass scale μ [111]. Screening mechanisms in canonical scalar field theories generally rely on m_{eff} becoming large, but this is precisely the limit in which the effective field theory breaks down. As shown in [112], the one-loop correction is sub-leading so long as $m_{\text{eff}} \lesssim (\alpha\rho)^{1/3}$, where α is the strength of the matter coupling and ρ is the density of the surrounding matter. For gravitational-strength couplings and laboratory densities, this is roughly $\sim$meV. This is safely above the present experimental bounds on m_{eff} [113], so there is still enough room for these theories to screen and remain predictive.

Derivatively coupled field theories have a similar issue [23, 114, 115] — quantum corrections introduce new operators which would, at first glance, seem to get large whenever screening occurs. In $P(X)$ theories, there are two types of terms to worry about: higher powers of X, and operators involving derivatives of X. Since screening occurs when X becomes large, one would expect that in this limit all higher powers of X would become large as well, signaling a breakdown of the theory.

The resolution relies on the fact that that $P(X)$ theories have *two* important scales [114]. The first is the strong coupling scale Λ, which is when loop effects become important and tree-level unitarity breaks down. In this regime, unitarity can be restored by re-summing loop effects, so the theory is still predictive. The second scale is the cutoff $\Lambda_{\rm c} \geq \Lambda$, where unitarity completely breaks down and new high energy physics must be accounted for. Since there can be a hierarchy between Λ and Λ_c, there is a window in which it is possible for the field to acquire classical non-linearities (which can screen macroscopic objects) while still remaining safely below the cutoff of the theory.

The story for galileons is very similar, although galileons fare much better than $P(X)$ theories when it comes to quantum corrections. Surprisingly, the tree level galileon terms do not receive any quantum corrections at all. Only terms with at least two derivatives per field are generated by quantum corrections [7, 23], so the galileon coefficients remain unchanged to all loop orders. This is because the galileon terms are only invariant under galilean transformations up to a total derivative, so the transformations are a symmetry of the action but not of the Lagrangian. The quantum terms do not share that luxury, and must be strictly invariant under galilean transformations [23, 26, 115, 116].

The higher order terms are still a concern, though, because we wish for them to

remain small compared to tree level terms. It would seem that once again we are doomed: screening occurs when, say, the $(\partial\phi)^2\Box\phi$ term becomes large compared to the ordinary $(\partial\phi)^2$ term, but this is exactly the limit in which one might expect all the higher order terms become important as well. It turns out that this is not the case, as there are in fact two expansion parameters at work. The first is a classical expansion parameter, $\alpha_{\rm cl} = \partial^2\phi/\Lambda^3$, which quantifies the strength of non-linearities, and a quantum expansion parameter, $\alpha_{\rm q} = \partial^2/\Lambda^2$, which measures the strength of the higher-order quantum mechanically generated terms. Galileon screening relies on $\alpha_{\rm cl}$ becoming large, to enable screening, while $\alpha_{\rm q}$ is still small, so that higher order terms are sub-leading and the classical EFT can be trusted [7, 23].

1.3 Atom Interferometry

So far we have been mainly concerned with the theoretical properties of scalar field theories. We now turn to their experimental predictions. For theories with potential screening in particular, atom interferometry has emerged as a powerful experimental probe. The experiment used for the constraints computed in Sections 4 and 5 is the result of an effort by Prof. Holger Müller's group at UC Berkeley [3, 4, 96] as a follow-up to a proposal to use atom interferometry to measure the scalar-mediated force, introduced by the theory papers of Burrage *et al* [94, 95].

Interferometry is a standard technique used in many areas of physics, and gravitation is no exception. Indeed, the celebrated Michelson-Morley interferometer measured the relative speed of light in directions parallel and orthogonal to the motion of the Earth, dispelling the aether myth and paving the way towards relativity. More recently, interferometers have been used to detect gravitational waves by detecting the expansion and contraction of the two arms of the interferometer [117].

The first interferometers were based on light: an incoming light wave would be split into two parts with a half-silvered mirror, and each part is sent on a separate path. The paths are then recombined and the amplitude of the output wave is measured. If the two paths are identical then the output amplitude of the wave is unchanged. However, if the paths are different then a phase difference is accumulated between the two paths and the two waves will interfere destructively at the output. For instance, one path being slightly longer, or passing through a material with a different index of refraction, generally results in a phase difference between the two waves. This fact may be exploited to make extremely precise measurements of, for instance, the relative difference in path lengths, as a difference of order the wavelength of light will result in measurable interference pattern.

As is well known, interference is not a phenomenon restricted to classical waves like light. As was conclusively demonstrated by the famous two-slit experiment, matter particles may interfere as well due to quantum-mechanical effects under the right circumstances.

Atom interferometry [118] exploits the quantum-mechanical wave nature of atoms for a similar purpose. A cloud of atoms may be manipulated via laser pulses to split their matter-wave packets to travel along two different paths. The partial matter-wave packets may then be recombined, and any relative phase between the two paths results in destructive interference at the time of measurement. Atom interferometry has developed into a powerful tool for testing fundamental physics, and provides competitive measurements of G_{N} and the fine-structure constant, as well as tests of the equivalence principle [119]. Atom interferometry is also well equipped to deliver measurements on quantities crucial for an accurate determination of the anomalous magnetic moment of the muon [120].

Atom interferometry has been used to look for anomalous gravitational interactions before [121], however, such experiments were unable to directly constrain screened scalar fields. In the case of potential screening, this is because the atmosphere and vacuum chamber walls cause the scalar particle to become very massive. The scalar field quickly goes to a constant the value that minimizes its effective potential, effectively shielding the atoms from scalar forces sourced outside the vacuum chamber.

What sets the Berkeley experiment apart is the inclusion of a small, dense source mass *inside* the vacuum chamber in the immediate vicinity of the atoms. Inside the vacuum chamber the chameleon force is much longer-range, of order the size of the vacuum chamber. The scalar force between the source mass and the atoms is therefore much larger than in atmosphere, allowing one to place much stronger constraints on the theory.

The Berkeley experiment, illustrated in Fig. 1.4, consists of an atom interferometer inside a vacuum chamber. A fountain of cold ^{133}Cs atoms are launched vertically, passing near a small metal source mass at their apex. Two vertical counter-propagating laser beams are used to induce photon absorption and then stimulated emission in the opposite direction, resulting in a net change in the quantum state and momentum of $|a, p_0\rangle \rightarrow |b, p_0 + 2\hbar k\rangle$, where $k = k_1 + k_2$ is the sum of the individual lasers' wavenumbers.

The first laser pulse is tuned such that the atoms undergo the transition with 50% probability, so the wave function of each atom splits into two pieces, one along each path. A second pulse T seconds later is tuned for nearly 100% probability, so that the excited atoms drop back to the ground state and vice versa, so that the two paths begin to converge. Finally, a third pulse another T seconds later is timed for 50% probability, recombining the partial matter waves.

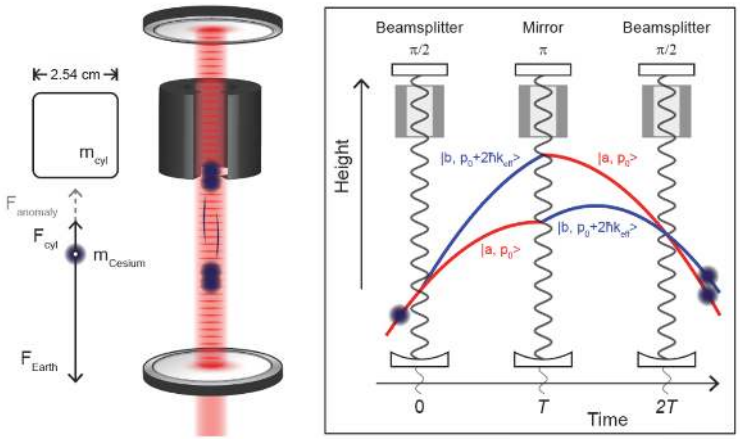

Figure 1.4: Left: Experimental setup. The acceleration a_{cyl} of cesium atoms towards a source mass suspended in ultra-high vacuum is measured. Making a differential measurement isolates the effect of any interactions due to the source mass. Note that the source mass is depicted here as a cylinder, while an earlier version of the experiment used a spherical source mass. This is why much of the analysis in this Section is for a spherical source mass. Right: Mach-Zehnder interferometer based on Raman transitions in an optical cavity. Three laser pulses manipulate the cesium atoms during free-fall. The pulses 1) split the atomic wave packet along two different trajectories, 2) reflect the two trajectories near their apex, and 3) recombine and interfere the matter waves to measure the phase difference accumulated between the two paths during the interferometer time of 2T = 110 ms.

The probability of observing any given atom at the output is [118]

$$P = \cos^2\left(\frac{\Delta\phi}{2}\right) \ , \tag{1.23}$$

where $\Delta\phi$ is the phase difference accumulated along the two different paths

$$\Delta\phi = kaT^2 \ . \tag{1.24}$$

The variable a represents the total acceleration experienced by the atoms during the measurement. The experiment is repeated with the source mass removed, so that any change in $\Delta\phi$ must be due to the force between the atoms and the source mass. After subtracting out the Newtonian gravitational forces from a, anything left over may be interpreted as an anomalous "fifth force."

The strongest bound at the time of writing of this Thesis was $a < 50$ nm/s^2 at the 95% confidence level, a number that was derived using the techniques developed in this Thesis [4]. This result is consistent with no scalar force at all. Placing the strongest possible constraints on chameleon field theories from this measurement requires accurately accounting for the experimental setup when computing the scalar field. The geometry of the experiment is described in Fig. 4.5, and the densities of the materials are in Table 4.1 . Chapters 4 and 5 detail a numerical method that allows us to include the exact setup in the calculation of the chameleon force, yielding the most precise prediction of the chameleon scalar force in atom interferometry to date.

Chapter 2

Violating the Null Energy Condition

In this Chapter we describe energy conditions in general relativity and their relationship with well-behaved quantum field theories. We show that violating the null energy condition, which is the most robust of the four standard energy conditions, generally comes hand-in-hand with pathologies in the field theory. We then construct a galileon field theory that violates the null energy condition while remaining well-behaved. This Chapter is based on work that originally appeared in [1].

The Einstein field equations relate the curvature of space-time (the Ricci tensor $R_{\mu\nu}$) to the energy content of gravitational sources (the energy-momentum tensor $T_{\mu\nu}$). The metric does not appear to discriminate between sources: for *any* given metric, one can use the field equations to calculate what $T_{\mu\nu}$ needs to be to give rise to that metric. However, this does not necessarily mean that $T_{\mu\nu}$ comes from a well-behaved source. For instance, the matter could be flowing faster than light, or the energy density could be negative for some observer on a timelike path. Such pathologies are avoided by imposing *energy conditions*, which place restrictions on $T_{\mu\nu}$.

Energy conditions are central to our understanding of the physics of matter in relativistic space-times yet, perplexingly, are not known to come directly from the axioms of general relativity. Rather than *deriving* these conditions, they are *imposed* directly on $T_{\mu\nu}$, based entirely on notions about what we deem to be physically reasonable

matter-energy sources. Since any new theory must contribute to $T_{\mu\nu}$, energy conditions have consequences for any physical theory which gravitates.

The most historically significant application of energy conditions is in the singularity theorems of Penrose, Hawking, Ellis, and others. Singularity theorems are are statements the inevitability of singularities appearing in a space-time under certain assumptions. For instance, the famous 1965 theorem of Penrose [122] shows that there are null geodesics inside a black hole that are *incomplete*, *i.e.* even null geodesics encounter a singularity, provided that the Ricci tensor satisfies the null convergence condition $R_{\mu\nu}n^\mu n^\nu \geq 0$ for null n^μ.

The null convergence condition, which constrains the geometry, may be interpreted via the Einstein field equations to be a requirement on the stress-energy tensor $T_{\mu\nu}$. In this context, it becomes the Null Energy Condition (NEC) $T_{\mu\nu}n^\mu n^\nu \geq 0$ for null n^μ. Interestingly, the proof of this singularity theorem (and many others) is independent of the field equations, only making statements about the geometry, such as the above null convergence condition. Einstein's equations are only invoked when interpreting the geometric requirements, which then take on the guise of an energy condition. This suggests that energy conditions are logically independent from Einstein's equation, and amount to "reasonable" statements about gravitational sources as well as space-time geometry [123].

There are a number of different energy conditions (see [123, 124] for reviews), but here we quickly mention the four most common ones. The *weak energy condition* requires that the energy density be non-negative for all observers on timelike geodesics. A timelike observer with 4-velocity v^μ therefore measures

$$T_{\mu\nu}v^\mu v^\nu \geq 0 \ . \tag{2.1}$$

The *dominant energy condition* states that, in addition to the weak energy condition being true, energy can never be seen flowing faster than light. An observer with timelike 4-velocity v^μ sees a 4-current of energy density $-T^\mu_\nu v^\nu$. The dominant energy condition requires this 4-current to be causal (timelike or null).

The *strong energy condition* requires that a timelike observer measure an energy density that is sufficiently larger than the trace of the stress tensor. It is equivalent to demanding

$$T_{\mu\nu}v^\mu v^\nu \geq -\frac{1}{2}T \ , \tag{2.2}$$

for a timelike 4-velocity v^μ.

The *null energy condition* states that an observer on a null path measures a positive energy density. It is similar to the weak energy condition, except with a null 4-velocity vector $n_\mu n^\mu = 0$:

$$T_{\mu\nu}n^\mu n^\nu \geq 0 \ . \tag{2.3}$$

For a more intuitive picture, the above formal statements may be translated into requirements on a perfect fluid, which has a rest-frame energy-momentum tensor $T_{\mu\nu} = \mathrm{diag}(\rho, P, P, P)$:

- Weak $\qquad \rho + P \geq 0$ and $\rho \geq 0$, ,
- Dominant $\qquad \rho \geq |P|$,
- Strong $\qquad \rho + P \geq 0$ and $\rho + 3P \geq 0$,
- Null $\qquad \rho + P \geq 0$.

A simple cosmological constant, which has an equation of state $P = -\rho$ and can also have $\rho < 0$, violates all of these conditions except the null energy condition. In the

same way, a healthy canonical scalar field with a suitable constant in its potential may violate all of these conditions except the NEC. In Section 2.1 we will see that a canonical scalar field that violates the NEC is necessarily ghostlike.

Violating the NEC with a healthy scalar field is the focus of this Chapter. The primary motivation is to better understand the relationship between the NEC and well-behaved relativistic quantum field theories. In [125] it was shown that any theory with at most one derivative per field that violates the NEC necessarily has an instability, such as a ghost, gradient instability, superluminality, absence of a Lorentz-invariant vacuum, *etc.*[4] These pathologies are described in Section 1.2. Progress has been made in avoiding some of these shortcomings [45, 51–53, 127, 128], as reviewed in Section 2.1 (see also Table 2.1 for a summary), though a fully satisfactory example remains elusive. It is important to push this program further, to sharpen the connection between the NEC and the standard assumptions of quantum field theory.

A secondary motivation is that the NEC precludes a non-singular cosmological bounce. Assuming spatial flatness, Einstein's equations imply that the Hubble parameter satisfies

$$M_{\rm Pl}^2 \dot{H} = -\frac{1}{2}(\rho + P) \ . \tag{2.4}$$

For a perfect fluid, the NEC implies $\rho + P \geq 0$, and thus $\dot{H} \leq 0$. Contraction ($H < 0$) cannot evolve to expansion ($H > 0$). Violating (2.3) is therefore central to any alternative to inflation relying on a contracting phase before the big bang [46, 50, 75, 129–175], or an expanding phase from an asymptotically static past [45, 47–49, 51–53, 127, 176–178].

The *DBI Genesis* scenario [52], based on the DBI conformal galileons [179], is the

[4]For example, the Hamiltonian of theories which violate the NEC was argued to be unbounded from below in [126].

closest any theory has come to achieving NEC violation while satisfying the standard properties of a local quantum field theory, and is reviewed in the following paragraphs and in Section 2.1. Specifically, as shown in [52], the coefficients of the five DBI galileon terms can be chosen such that:

1. The theory admits a stable, Poincaré-invariant vacuum. Further, the Lorentz-invariant S-matrix about this vacuum obeys the simplest dispersion relations for $2 \to 2$ scattering coming from analyticity constraints.

2. The theory admits a time-dependent, homogeneous and isotropic solution which violates the NEC in a stable manner. In fact, this NEC-violating background is an *exact* solution of the effective theory, including all possible higher-dimensional operators consistent with the assumed symmetries.

3. Perturbations around the NEC-violating background, and around small deformations thereof, propagate subluminally.

4. This solution is stable against radiative corrections and the effective theory for perturbations about this solution is well-defined.

This represents a significant improvement over ghost condensation [12] (which fails to satisfy 1) and the ordinary conformal galileons [45, 116] (which fail to satisfy 1 and 3), as will be reviewed in detail in Section 2.1.[5] Additionally, consistency with black hole thermodynamics is desirable [180]. This remains an open issue which deserves further study. It is worth pointing out that the non-minimal couplings to gravity inherent in the theory will modify the usual link between NEC violation and the black hole area law [181, 182].

[5]Note that the conformal galileon Lagrangian can be deformed in a straightforward way to remove superluminal propagation about the NEC-violating background [53].

Unfortunately, the DBI Genesis theory itself suffers from two drawbacks. Similar to the conformal galileons, one can find weak deformations of the Poincaré-invariant solution around which perturbations propagate superluminally. As pointed out recently [183, 184], however, galileon theories that admit superluminality can sometimes be mapped through field redefinitions to healthy galileon theories, indicating that the apparent superluminalty may be unphysical.[6] So in this sense superluminality may not offer a clear-cut criterion. But it would certainly be preferable to have an example where superluminality is manifestly absent.

A less ambiguous drawback was pointed out by Rubakov [128]: although the theory admits both Poincaré-invariant and NEC-violating solutions, any solution that attempts to interpolate between the two vacua inevitably hits a strong coupling point. In other words, the kinetic term of fluctuations around any interpolating solution goes to zero somewhere. In particular, it is impossible to create a NEC-violating region in the laboratory.[7] The argument, which we review in Sec. 2.2, is quite general — it only assumes that the theory describes a single field which is dilation-invariant, and that both Poincaré and NEC-violating solutions preserve this symmetry. Rubakov showed that the conclusions can be evaded by introducing additional scalar fields [128].

Since this work was written there have been further examples of well-behaved NEC violation. The approach described here was generalized to include quartic galileons [185] and a procedure for a graceful exit back to a NEC-satisfying phase [186]. Another approach, in which the galileon becomes a massless scalar field driving the expansion of the universe at later times is given in [187]. This problem has also been studied within the framework of the effective field theory of cosmological perturbations [188].

[6] We thank Claudia de Rham and Andrew Tolley for a discussion on this point.

[7] Although [128] focused on solutions which interpolate in a radial direction (a 'bubble' of NEC violation), the argument applies equally well to interpolation in the temporal direction.

In this Chapter, we stick to a single-field theory but relax the assumption of dilation invariance in order to construct a theory which admits a solution that obeys the null energy condition at early times but at late times crosses into a phase of NEC-violation. The theory of interest is a deformation of the Galilean Genesis Lagrangian,

$$\mathcal{L} = \mathcal{Z}(\pi)e^{2\pi}(\partial\pi)^2 + \frac{f_0^3}{\Lambda^3}(\partial\pi)^2\Box\pi + \frac{1}{\mathcal{J}(\pi)}\frac{f_0^3}{2\Lambda^3}(\partial\pi)^4 \ , \tag{2.5}$$

where the functions $\mathcal{Z}(\pi)$ and $\mathcal{J}(\pi)$ are constrained to allow a smooth interpolation between a NEC-satisfying phase at early times and a NEC-violating phase at late times. Specifically, at early times ($\pi \to \pi_\infty$) the cubic term is negligible, and the theory reduces to

$$\begin{aligned}\mathcal{L}_{\text{early}} &\simeq -\frac{f_\infty^2 e^{2\pi_\infty}}{\left(e^{\pi-\pi_\infty}-1\right)^4}(\partial\pi)^2 + \frac{1}{\mathcal{J}_0}\frac{f_0^3}{2\Lambda^3}\frac{(\partial\pi)^4}{\left(1-e^{-(\pi-\pi_\infty)}\right)^8} \\ &= -f_\infty^2 e^{2\pi_\infty}(\partial\phi)^2 + \frac{f_0^3}{8\mathcal{J}_0\Lambda^3}(\partial\phi)^4 \, ,\end{aligned} \tag{2.6}$$

where the second line follows after a field redefinition to the (almost) canonically-normalized variable ϕ. The quartic term has the correct sign demanded by locality [110], hence the S-matrix of this theory obeys the standard dispersion relations coming from analyticity.

At late times ($\pi \to \infty$), on the other hand, $\mathcal{Z}$ and $\mathcal{J}$ both tend to constants, $\mathcal{Z}(\pi) \to f_0^2 \gg \Lambda^2$, $\mathcal{J}(\pi) \to \mathcal{J}_0 \sim \mathcal{O}(1)$, such that (2.5) reduces to the Galilean Genesis action

$$\mathcal{L}_{\text{late}} \simeq f_0^2 e^{2\pi}(\partial\pi)^2 + \frac{f_0^3}{\Lambda^3}(\partial\pi)^2\Box\pi + \frac{1}{\mathcal{J}_0}\frac{f_0^3}{2\Lambda^3}(\partial\pi)^4 \ . \tag{2.7}$$

This gives rise to the usual, genesis NEC-violating solution. For suitable values of

$\mathcal{J}_0$, perturbations around this solution are comfortably subluminal, as in [53].[8] Note that $\mathcal{Z}(\pi)$ has the correct sign at early times, and the wrong (*i.e.*, ghost-like) sign at late times. Nevertheless, the kinetic term of fluctuations around the time-dependent interpolating solution is healthy during the entire evolution.

Of course, the presence of arbitrary functions in the Lagrangian makes it unlikely that the theory is radiatively stable. However, we will argue that quantum effects in the theory are under control both at early and late times. We imagine that, given this, the existence of a healthy interpolating solution is not extremely sensitive to quantum corrections, even though the functions $\mathcal{Z}$ and $\mathcal{J}$, and hence the explicit form of the solution itself, might be. In this sense, our explicit construction is designed to be a proof-of-principle.

2.1 Attempts to violate the NEC

We begin with a brief overview of the different theories that can violate the NEC, highlighting their successes and failures. For a more comprehensive review of the null energy condition and attempts to violate it, see [190]. In Table 2.1 we provide a scorecard for the different theories. A natural place to search for matter which can violate the NEC is in the context of scalar field theories, since scalars can develop nontrivial background profiles that preserve homogeneity and isotropy.

- **2-derivative theories:** Consider a non-linear sigma model with dynamical variables $\phi^I : \mathbb{R}^{3,1} \to \mathcal{M}$, where $\mathcal{M}$ is an arbitrary, N-dimensional real target space. At 2-derivative order, the action is given by

$$S = \int \mathrm{d}^4x \left(-\frac{1}{2} G_{IJ}(\phi) \partial_\mu \phi^I \partial^\mu \phi^J - V(\phi^I \phi_I) \right) , \tag{2.8}$$

[8] It was recently argued that including a matter component can reintroduce superluminality in some part of the cosmological phase space [189].

where G_{IJ} is the target-space metric. The stress-energy tensor for this field is readily computed, and the quantity relevant for the NEC is

$$T_{\mu\nu}n^\mu n^\nu = G_{IJ}(\phi)n^\mu n^\nu \partial_\mu \phi^I \partial_\nu \phi^J \,. \tag{2.9}$$

In the language of perfect fluids, focusing on time-dependent profiles, $\phi^I(t)$, this becomes

$$\rho + P = G_{IJ}(\phi)\dot{\phi}^I \dot{\phi}^J \,. \tag{2.10}$$

Now, the target-space metric G_{IJ} can be diagonalized, since it is symmetric and invertible. Therefore, in order to violate the NEC ($\rho + P \leq 0$), G_{IJ} must have at least one negative eigenvalue, that is, one of the ϕ^I's must be a ghost. At the 2-derivative level, violating the NEC comes hand in hand with ghosts.

- $P(X)$ **theories:** The obvious generalization is to consider higher-derivative theories. In order to avoid ghost instabilities, the equation of motion should remain 2^{nd}-order. A general class of such models is

$$S = M^4 \int \mathrm{d}^4 x P(X) \,, \tag{2.11}$$

where $X \equiv -\frac{1}{2M^4}(\partial\phi)^2$, and M is an arbitrary mass scale. The justification for considering theories of this type is effective field theory reasoning — we anticipate that at low enough energies, terms with more derivatives per field will be sub-leading. However, even in these theories, NEC violation generically introduces pathologies, albeit of a more subtle nature.

To see this, note that the combination $\rho + P$, assuming $\phi = \phi(t)$, is given by

$$\rho + P = 2XP_{,X} \ . \tag{2.12}$$

In order to violate the NEC, we therefore need $P_{,X} < 0$. Meanwhile, expanding (2.11) about the background $\phi = \bar{\phi}(t) + \varphi$, the action for quadratic fluctuations is [12]

$$S_\varphi = \frac{1}{2}\int \mathrm{d}^4x \left((P_{,X} + 2XP_{,XX}\,)\,\dot{\varphi}^2 - P_{,X}\,(\vec{\nabla}\varphi)^2 \right) \ . \tag{2.13}$$

A violation of the NEC ($P_{,X} < 0$) results in either gradient instabilities (wrong-sign spatial gradient term) or ghost instabilities (if we choose $P_{,X} + 2XP_{,XX} < 0$). More generally, it was shown in [125, 191] that violating the NEC in theories of the form $\mathcal{L}(\phi^I, \partial\phi^I)$ (*i.e.*, involving at most one derivative per field), implies either the presence of ghost or gradient instabilities *or* superluminal propagation.

- **Ghost condensation:** This general theorem about instabilities in such a wide class of theories would seem to preclude any sensible violations of the NEC. There is, however, a rather compelling loophole to the general logic. The theorem of [125] relies heavily on the standard organization of effective field theory, *i.e.*, the sub-dominance of terms of the form $\partial^2\phi$. There exist two well-studied situations where such terms can become important and, indeed, both lead to violations of the NEC free of the obvious pathologies.

  The first is *ghost condensation* [12]. This relies on an action of the $P(X)$ form (2.11), but chosen so that there exists a solution with $P_{,X} = 0$. Notice from (2.13) that this precisely corresponds to the vanishing of the spatial gra-

dient term in the quadratic Lagrangian about this background. This allows a higher-derivative term of the form $(\nabla^2\varphi)^2$ to become important in the quadratic Lagrangian *without* the effective field theory expansion breaking down. Since $\rho + P = 0$ on the background, this acts as a vacuum energy contribution. Deforming the background as $\phi = \bar{\phi}(t) + \pi(t)$, one finds

$$\rho + P \sim \dot{\pi}\,. \tag{2.14}$$

This is *linear* in π, and hence can have either sign. Violating the NEC once again will push the kinetic term of fluctuations slightly negative, but the dispersion relation is stabilized at high k by the $(\nabla^2\varphi)^2$ term [127]. The no-go theorem of [125] is thus evaded by relying on higher-derivative spatial gradient terms.

The main drawback of the ghost condensate is the absence of a Lorentz-invariant vacuum. Indeed, from (2.13) the absence of ghosts about the condensate $P_{,X} = 0$ solution requires $P_{,XX} > 0$, *i.e.*, the condensate is at a minimum of $P(X)$. As a result, the theory cannot be connected to a Lorentz-invariant vacuum ($P_{,X}|_{X=0} > 0$) without encountering pathologies in between. The theory is only well-defined in the neighborhood of the ghost condensate point.

A NEC-violating ghost condensate phase has been used in alternative cosmological models, including a universe starting from an asymptotically static past [127], the New Ekpyrotic Universe [150, 153], and the matter-bounce scenario [166].

- **Galileons:** A second class of theories which can violate the NEC without instabilities is given by the conformal *galileons* [24, 116].[9] These are conformally-

[9]For another construction which violates the NEC based on Kinetic Gravity Braiding [178], a cousin of the galileons, see [192].

invariant scalar field theories with derivative interactions. The simplest example is

$$\mathcal{L} = f^2 e^{2\pi}(\partial\pi)^2 + \frac{f^3}{\Lambda^3}\Box\pi(\partial\pi)^2 + \frac{f^3}{2\Lambda^3}(\partial\pi)^4 \ . \tag{2.15}$$

Each term is manifestly dilation invariant. The relative 1/2 coefficient between the $\Box\pi(\partial\pi)^2$ and $(\partial\pi)^4$ ensures full conformal invariance.[10] Choosing the kinetic term to have the wrong sign, as in (2.15), the theory admits a time-dependent solution

$$e^{\pi} = \frac{1}{H_0(-t)} \ ; \qquad H_0^2 = \frac{2}{3}\frac{\Lambda^3}{f} \ , \tag{2.17}$$

where $-\infty < t < 0$. For consistency of the effective field theory, the scale H_0 should lie below the strong coupling scale Λ, which requires

$$f \gg \Lambda \, . \tag{2.18}$$

This background spontaneously breaks the original SO(4, 2) symmetry down to its SO(4, 1) subgroup. The stress-energy violates the NEC [45, 53, 116]: $\rho + P = -\frac{2f^2}{H_0^2 t^2}$. Perturbations around this solution are stable, and propagate exactly luminally by SO(4, 1) invariance. However, the sound speed can be pushed to superluminal values on slight deformations of this background.[11] A cure to this pathology [53] is to reduce the symmetry by detuning the relative coefficient of the cubic and quartic terms

$$\mathcal{L} = f^2 e^{2\pi}(\partial\pi)^2 + \frac{f^3}{\Lambda^3}\Box\pi(\partial\pi)^2 + \frac{f^3}{2\Lambda^3}(1+\alpha)(\partial\pi)^4 \ , \tag{2.19}$$

[10] Under the dilation and conformal symmetries, the field π transforms as:

$$\delta_D\pi = -1 - x^\mu\partial_\mu\pi \ ; \qquad \delta_{K^\mu}\pi = -2x^\mu - (2x^\mu x^\nu\partial_\nu - x^2\partial^\mu)\pi \ . \tag{2.16}$$

[11] It was shown in [189] that such deformations must break homogeneity/isotropy.

where α is a constant. For $\alpha \neq 0$, this explicitly breaks the special conformal symmetry, leaving dilation and Poincaré transformations as the only symmetries (which conveniently close to form a subgroup). This still allows a $1/t$ background of the form (2.17), with $H_0 = \frac{2}{3}\frac{1}{(1+\alpha)}\frac{\Lambda^3}{f}$ depending on α. For $-1 < \alpha < 3$, this background violates the NEC and has stable perturbations. As a result of the fewer residual symmetries, perturbations propagate with a sound speed different from unity:

$$c_s^2 = \frac{3-\alpha}{3(1+\alpha)}\,. \tag{2.20}$$

This is subluminal for $\alpha > 0$. In other words, for the range

$$0 < \alpha < 3\,, \tag{2.21}$$

the system violates the NEC, is stable against small perturbations, and these perturbations propagate at subluminal speeds. Moreover, the theory is stable against quantum corrections.

The main drawback of the galileon NEC violation is — just like the ghost condensate — the absence of a Lorentz-invariant vacuum. Indeed, the existence and stability of a $1/t$ background requires a wrong-sign kinetic term, as in (2.15) and (2.19). As shown in [53], including the higher-order conformal galileon terms does not help: only the kinetic term contributes to $\rho + P$ for the $1/t$ solution, and it must have the wrong sign to violate NEC. An improvement over the ghost condensate, however, is that perturbations are stable on all scales, whereas perturbations of the ghost condensate in the NEC-violating phase are unstable on large scales (but are stabilized on small scales, thanks to the higher-

derivative contribution to the dispersion relation).

A NEC-violating galileon phase is the hallmark of the Galilean Genesis scenario [45, 53], in which the universe expands from an asymptotically static past. Because of the residual dilation symmetry, nearly massless fields acquire a scale invariant spectrum. The $\mathrm{SO}(4,2) \to \mathrm{SO}(4,1)$ spontaneous breaking is also used in the NEC-satisfying rolling scenario of [46, 167, 168]. More generally, this symmetry breaking pattern arises whenever a number of scalar operators $\mathcal{O}_I$ with weight Δ_I in a conformal field theory acquire a time-dependent profile $\mathcal{O}_I(t) \sim (-t)^{-\Delta_I}$. The general effective action was constructed in [50] utilizing the coset construction, and the consistency relations were derived in [193].

- **DBI Galileons:** An alternative way to avoid superluminality while preserving the full $\mathrm{SO}(4,2)$ symmetry is to consider the DBI conformal galileons [179]. These are the "relativistic" extension of the ordinary conformal galileons, and describe the motion of a 3-brane in an AdS_5 geometry. The DBI conformal galileon action is a sum of five geometric invariants, with 5 free coefficients $c_1, \ldots, c_5$:

$$\mathcal{L} = c_1\mathcal{L}_1 + c_2\mathcal{L}_2 + c_3\mathcal{L}_3 + c_4\mathcal{L}_4 + c_5\mathcal{L}_5 \,, \tag{2.22}$$

where the $\mathcal{L}_i$'s are built out of the induced metric

$$\bar{g}_{\mu\nu} = G_{AB}\partial_\mu X^A \partial_\nu X^B = \phi^2 \left(\eta_{\mu\nu} + \frac{\partial_\mu\phi\partial_\nu\phi}{\phi^4}\right) \,, \tag{2.23}$$

the Ricci tensor $\bar{R}_{\mu\nu}$ and scalar $\bar{R}$, and the extrinsic curvature tensor

$$K_{\mu\nu} = \gamma\phi^2 \left(\eta_{\mu\nu} - \frac{\partial_\mu\partial_\nu\phi}{\phi^3} + 3\frac{\partial_\mu\phi\partial_\nu\phi}{\phi^4}\right) \,. \tag{2.24}$$

Each $\mathcal{L}_i$ is invariant up to a total derivative under SO(4, 2) transformations, inherited from the isometries of AdS_5. The relevant terms come from considering brane Lovelock invariants [194] and the boundary terms associated to bulk Lovelock invariants:

$$
\begin{aligned}
\mathcal{L}_1 &= -\frac{1}{4}\phi^4\,; \\
\mathcal{L}_2 &= -\sqrt{-\bar{g}} = -\frac{\phi^4}{\gamma}\,; \\
\mathcal{L}_3 &= \sqrt{-\bar{g}}K = -6\phi^4 + \phi[\Phi] + \frac{\gamma^2}{\phi^3}\Big(-[\phi^3] + 2\phi^7\Big)\,; \\
\mathcal{L}_4 &= -\sqrt{-\bar{g}}\bar{R} \\
&= 12\frac{\phi^4}{\gamma} + \frac{\gamma}{\phi^2}\Big([\Phi^2] - \big([\Phi] - 6\phi^3\big)\big([\Phi] - 4\phi^3\big)\Big) \\
&\quad + 2\frac{\gamma^3}{\phi^6}\Big(-[\phi^4] + [\phi^3]\big([\Phi] - 5\phi^3\big) - 2[\Phi]\phi^7 + 6\phi^{10}\Big)\,; \\
\mathcal{L}_5 &= \frac{3}{2}\sqrt{-\bar{g}}\left(-\frac{K^3}{3} + K^2_{\mu\nu}K - \frac{2}{3}K^3_{\mu\nu} - 2\left(\bar{R}_{\mu\nu} - \frac{1}{2}\bar{R}\bar{g}_{\mu\nu}\right)K^{\mu\nu}\right) \\
&= 54\phi^4 - 9\phi[\Phi] \\
&\quad + \frac{\gamma^2}{\phi^5}\Big(9[\phi^3]\phi^2 + 2[\Phi^3] - 3[\Phi^2][\Phi] + 12[\Phi^2]\phi^3 \\
&\qquad\qquad + [\Phi]^3 - 12[\Phi]^2\phi^3 + 42[\Phi]\phi^6 - 78\phi^4\Big) \\
&\quad + 3\frac{\gamma^4}{\phi^9}\Big(-2[\phi^5] + 2[\phi^4]\big([\Phi] - 4\phi^3\big) + [\phi^3]\big([\Phi^2] - [\Phi]^2 + 8[\Phi]\phi^3 - 14\phi^6\big) \\
&\qquad\qquad + 2\phi^7\big([\Phi]^2 - [\Phi^2]\big) - 8[\Phi]\phi^{10} + 12\phi^{13}\Big)\,,
\end{aligned}
$$

where $\gamma \equiv 1/\sqrt{1 + (\partial\phi)^2/\phi^4}$ is the Lorentz factor for the brane motion, $\mathcal{L}_1$ measures the proper 5-volume between the brane and some fixed reference brane $\mathcal{L}_2$ is the world-volume action [195], *i.e.*, the brane tension, and the higher-order terms $\mathcal{L}_3$, $\mathcal{L}_4$ and $\mathcal{L}_5$ are various functions of curvature. Moreover, Φ denotes the matrix of second derivatives $\partial_\mu\partial_\nu\phi$, $[\Phi^n] \equiv \mathrm{Tr}(\Phi^n)$, and $[\phi^n] \equiv \partial\phi\cdot\Phi^{n-2}\cdot\partial\phi$,

with indices raised by $\eta^{\mu\nu}$. The motivation for considering Lovelock terms is that they lead to second-order equations of motion for the scalar field ϕ [179].

For suitable choices of the coefficients $c_1, \ldots, c_5$, the theory admits a $1/t$ solution of the form (2.17), which violates the NEC in a stable manner [52]. This was dubbed the *DBI Genesis* phase in [52]. Analogous to DBI inflation [196], the sound speed of fluctuations for relativistic brane motion $\gamma \gg 1$ is highly subluminal. This is an improvement over the galileon examples, since subluminality is achieved while keeping the full conformal symmetries. Moreover, this solution is stable against radiative corrections: terms not of the conformal DBI form are generated radiatively but with coefficients suppressed by inverse powers of γ.

More importantly, the theory also admits a stable, Poincaré-invariant vacuum. As such, DBI Genesis is the first example of a theory possessing both stable NEC-violating and stable Poincaré-invariant vacua. In [52] it was shown that the $2 \to 2$ scattering amplitude satisfies the known analyticity properties required by locality. Unfortunately, like ordinary galileons weak-field deformations of the Poincaré-invariant vacuum allow superluminal propagation of perturbations. Hence we naively do not expect the full scattering S-matrix to be analytic, though as mentioned earlier it is not clear to what extent the apparent superluminality is truly a pathology [183, 184].

Additionally, one would like the theory to be consistent with the second law of black hole thermodynamics. There appears to be great tension between this and the NEC, for instance in the ghost condensate violation of the NEC allows for the formation of perpertuum mobile [180].[12] The story is potentially more subtle for DBI galileons,

[12]For a contrary viewpoint, see [197].

	Ghost condensate	Galilean Genesis	DBI Genesis	This theory
~~NEC~~ vacuum	✓	✓	✓	✓
No ghosts	✓	✓	✓	✓
Sub-luminality	✓	✓	✓	✓
Poincaré vacuum	✗	✗	✓	✓
No ghosts			✓	✓
S-Matrix analyticity ($2 \to 2$)			✓	✓
Sub-luminality			✗	✓
Interpolating solution			✗	✓
Radiative stability	✓	✓	✓	✗
BH Thermodynamics	✗	?	?	?

Table 2.1: Checklist of properties of various theories which possess null energy condition-violating solutions. See Section 1.2 for a discussion of the pathologies in this Table.

thanks to the non-minimal terms required for their covariantization [79, 179].

Ideally, one would like to be able to start from the Poincaré-invariant vacuum and evolve smoothly into the NEC-violating phase. As pointed out recently [128], however, this is impossible in any single-field theory with dilation invariance. This is particularly constraining because many of the attempts to violate the NEC utilize dilation-invariant theories (for example the Galilean Genesis scenarios and the DBI conformal galileons). The argument, reviewed below, shows that any solution that attempts to interpolate between the two vacua inevitably hits a strong coupling point. One way out is to invoke multiple scalar fields. Another way out, which we will explore here, is to break the dilation symmetry explicitly. In doing so, we will be able to construct a theory with the following properties:

- A Poincaré-invariant vacuum with stable and sub-luminal fluctuations about this vacuum.

- A solution which interpolates between a non-NEC-violating phase and a phase of NEC violation with stability and sub-luminality for perturbations about this solution.

2.2 A no-go argument for interpolating solutions

In this Section we review the no-go argument of Rubakov [128], which forbids the existence of a well-behaved solution interpolating between *dilation-invariant* vacua. The argument is very general and applies to any single scalar field theory that enjoys (at the classical level) dilation invariance, and admits both a Poincaré invariant solution and a dilation-preserving, NEC-violating background.

First note that conservation of the energy-momentum tensor is equivalent to the equation of motion via

$$\partial_\mu T^\mu_{\ \nu} = -\frac{\delta S}{\delta \pi}\partial_\nu \pi \ , \tag{2.25}$$

where $\delta S/\delta\pi$ is the Euler–Lagrange derivative. Specializing to $\pi = \pi(t)$, it follows the equation of motion is equivalent to energy conservation:

$$\dot{\rho} = -\dot{\pi}\frac{\delta S}{\delta \pi} \ . \tag{2.26}$$

Now we assume that the equation of motion is second-order, that is, $\delta S/\delta\pi$ contains at most $\ddot{\pi}$ but no higher-derivatives.[13] It then follows that ρ must be a function only of π and $\dot{\pi}$, for otherwise $\dot{\rho}$ would contribute higher-derivative terms in (2.26). Since the theory is dilation invariant, we can deduce the form of ρ:[14]

$$\rho = e^{4\pi} Z\left(e^{-2\pi}\dot{\pi}^2\right) \ , \tag{2.27}$$

where Z is a theory-dependent function.

[13] Note that violating this assumption would lead to Ostrogradski-type instabilities [25, 198].

[14] Under a finite dilation, $x^\mu \mapsto \lambda x^\mu$, the field π transforms as $\pi(x) \mapsto \pi(\lambda x) + \log\lambda$. One can then check that (2.27) is the most general object depending only on π and $\dot{\pi}$ invariant under this symmetry.

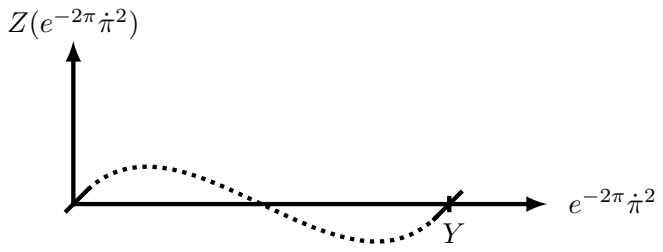

Figure 2.1: In a dilation invariant theory, we must have $Z = 0$ at both $e^{-2\pi}\dot{\pi}^2 = 0$ and $e^{-2\pi}\dot{\pi}^2 = Y$, as well as $Z' > 0$ at both of these points. It is impossible to connect these two solutions without having a region where $Z' < 0$, as is clear from the plot.

If the theory admits a Poincaré-invariant solution, $\pi =$ constant, it will have vanishing energy density:

$$Z(0) = 0\,. \tag{2.28}$$

Additionally, if the theory admits a NEC-violating background which preserves homogeneity and isotropy, then π can only depend on time. If this background is also dilation invariant, then it must take the form $e^{\pi} \sim t^{-1}$, and hence $e^{-2\bar{\pi}}\dot{\bar{\pi}}^2 \equiv Y =$ constant on this solution. Moreover, the assumed symmetries imply $\rho = \beta t^{-4}$ on the time-dependent solution, while energy conservation requires $\dot{\rho} = 0$, and thus $\beta = 0$. It follows that

$$Z(Y) = 0\,. \tag{2.29}$$

In other words, the energy density vanishes on any background that preserves homogeneity, isotropy and dilation symmetry. This of course includes the Poincaré-invariant vacuum and (by assumption) the NEC-violating background.

Next consider the stability of these solutions. We can expand (2.26) about some time-dependent background, $\pi = \bar{\pi}(t) + \varphi$, and use the form (2.27) for ρ to derive an equation of motion for φ. For the diagnosis of ghost instabilities, we only explicitly

need the $\ddot{\varphi}$ term:

$$-2e^{2\bar{\pi}}\bar{Z}'\ddot{\varphi}+\cdots=0\,. \tag{2.30}$$

This clearly derives from the quadratic Lagrangian $\mathcal{L}=e^{2\bar{\pi}}\bar{Z}'\dot{\varphi}^2+\cdots$. In order for φ to be healthy, we must have

$$\bar{Z}'>0\,. \tag{2.31}$$

The problem is now clear: we have two backgrounds, each with $Z=0$. In order for them to both be healthy, we must have $Z'>0$ around each solution. It is impossible to connect these two solutions without having $Z'<0$ — and hence developing a ghost — somewhere in between. More physically, in trying to connect these solutions one must inevitably hit $Z=0$, which corresponds to strong coupling. It is therefore impossible to connect the two backgrounds with a solution which is perturbative. See Fig. 2.1 for a graphical representation of this result.

This no-go argument is very general, but we can get some inspiration for how to avoid it by examining its assumptions. The most natural ones to consider breaking are the assumption of a single degree of freedom and that of dilation invariance. Indeed, Rubakov considers a model which introduces additional degrees of freedom to construct an interpolating solution [128]. Here, we will focus on theories that are not dilation invariant.

2.3 Construction of the theory

To circumvent the no-go argument of Sec. 2.2, we stick to a single-field theory but relax the assumption of dilation invariance. We consider a deformation of the conformal galileon lagranagian (2.15) (used in Galilean Genesis [45, 116]) by introducing

functions $\mathcal{Z}(\pi), \mathcal{J}(\pi)$ which explicitly break scale invariance:

$$\mathcal{L} = \mathcal{Z}(\pi) e^{2\pi} (\partial\pi)^2 + \frac{f_0^3}{\Lambda^3} (\partial\pi)^2 \Box\pi + \frac{1}{\mathcal{J}(\pi)} \frac{f_0^3}{2\Lambda^3} (\partial\pi)^4 \ . \tag{2.32}$$

Our goal is to find suitable functional forms for $\mathcal{Z}(\pi)$ and $\mathcal{J}(\pi)$ such that the theory admits a smooth solution which is NEC-satisfying at early times ($t \ll t_*$), and NEC-violating at late times ($t \gg t_*$). The transition time will be denoted by t_*.

Late time behavior

To achieve NEC violation with strictly subluminal propagation of perturbations at late times ($t \gg t_*$), the theory should approximate the form (2.19), used in subluminal genesis [53]. This requires

$$\mathcal{Z}(\pi) \to f_0^2 \, ; \quad \mathcal{J}(\pi) \to \mathcal{J}_0 \qquad \text{for} \quad t \gg t_* \, , \tag{2.33}$$

where $f_0 \gg \Lambda$ and $\mathcal{J}_0$ is an $\mathcal{O}(1)$ constant. Thus, the theory reduces at late times to

$$\mathcal{L}_{\text{late}} \simeq f_0^2 e^{2\pi} (\partial\pi)^2 + \frac{f_0^3}{\Lambda^3} (\partial\pi)^2 \Box\pi + \frac{1}{\mathcal{J}_0} \frac{f_0^3}{2\Lambda^3} (\partial\pi)^4 \ . \tag{2.34}$$

Comparison with (2.19) gives the translation

$$\mathcal{J}_0 = \frac{1}{1+\alpha} \, , \tag{2.35}$$

hence we anticipate that we will need $\mathcal{J}_0 \lesssim \mathcal{O}(1)$ to have subluminality [53]. At late times, the solution should therefore asymptote to the Genesis background

$$e^{\pi} = \frac{1}{H_0(-t)} \ ; \qquad H_0^2 = \frac{2\mathcal{J}_0}{3} \frac{\Lambda^3}{f_0} \qquad \text{for} \quad t \gg t_* \, . \tag{2.36}$$

The energy scale of this solution is H_0. We demand that it lie below the strong coupling scale of the effective theory, $H_0 \ll \Lambda$, which will be the case if

$$f_0 \gg \Lambda \,. \tag{2.37}$$

The background (2.36) is a solution on flat, Minkowski space. With gravity turned on, it remains an approximate solution at early enough times in the Genesis phase. Gravity eventually becomes important at a time $t_{\rm end}$, which will be computed in Sec. 2.5.

Early time behavior

At early times ($t \ll t_*$), the solution should asymptote to a constant field profile:

$$\pi \simeq \pi_\infty \qquad \text{for} \qquad t \ll t_* \,. \tag{2.38}$$

In order for this constant background to be ghost-free, the sign of the kinetic term should be the usual (negative) one:

$$\mathcal{Z}(\pi) < 0 \qquad \text{for} \qquad t \ll t_* \,. \tag{2.39}$$

We will see that this gives rise to a NEC-satisfying phase, with $\rho \sim P$. In this regime, clearly gravity cannot be ignored arbitrarily far in the past, since the universe must emerge from a big bang singularity. We will come back to this point in Sec. 2.5 and show that the time $t_{\rm beg}$ where gravity becomes important is parametrically larger in magnitude than t_*. In other words, there is a parametrically large window $t_{\rm beg} \ll t \ll t_*$ within which gravity is negligible and the early-time expressions above hold. In particular, π can be approximated as constant over this regime, in the sense that

it varies slowly compared to the Hubble parameter at the transition.

From (2.33) and (2.39), note that $\mathcal{Z}(\pi)$ has the correct sign at early times, and the wrong (*i.e.*, ghost-like) sign at late times (as required for the Genesis solution). Nevertheless, we will see that the kinetic term of fluctuations around the time-dependent solution is healthy during the entire evolution. This does imply, however, that stable, Lorentz-invariant vacua only exist for a finite range in field space.

Interpolating functions

We engineer the desired $\mathcal{Z}(\pi)$ and $\mathcal{J}(\pi)$ by demanding that they give rise to a suitable time-dependent background solution, which interpolates between $\pi \simeq \pi_\infty$ at early times and $e^\pi \sim 1/t$ at late times. A simple ansatz for the background which satisfies these asymptotic conditions is

$$e^{\bar{\pi}(t)} = e^{\pi_\infty}\left(1 + \frac{t_*}{t}\right) , \tag{2.40}$$

where t_* sets the transition time.

Assuming spatial homogeneity, the equation of motion for $\pi = \bar{\pi}(t)$ following from (2.32) is

$$\ddot{\bar{\pi}}\left(-\mathcal{Z}(\bar{\pi})e^{2\bar{\pi}} + \frac{3}{\mathcal{J}(\bar{\pi})}\frac{f_0^3}{\Lambda^3}\dot{\bar{\pi}}^2\right) = \frac{\dot{\bar{\pi}}^2}{2}\left(\left(2\mathcal{Z}(\bar{\pi}) + \mathcal{Z}'(\bar{\pi})\right)e^{2\bar{\pi}} + \frac{3\mathcal{J}'(\bar{\pi})}{2\mathcal{J}^2(\bar{\pi})}\frac{f_0^3}{\Lambda^3}\dot{\bar{\pi}}^2\right) . \tag{2.41}$$

This admits a first integral of motion enforcing energy conservation:

$$\begin{aligned}\rho &= -\mathcal{Z}(\bar{\pi})e^{2\bar{\pi}}\dot{\bar{\pi}}^2 + \frac{3}{2\mathcal{J}(\bar{\pi})}\frac{f_0^3}{\Lambda^3}\dot{\bar{\pi}}^4 \\ &= -\mathcal{Z}(t)e^{2\pi_\infty}\frac{t_*^2}{t^4} + \frac{3}{2\mathcal{J}(t)}\frac{f_0^3}{\Lambda^3}\frac{t_*^4}{t^4(t+t_*)^4} = \text{constant} ,\end{aligned} \tag{2.42}$$

where in the second line we have substituted in the background solution (2.40). At early times ($t \ll t_*$), the two contributions scale differently: $\sim t^{-4}$ for the first term; $\sim t^{-8}$ for the second. The simplest option is for each term to be separately constant, from which we can deduce the scaling $\mathcal{Z}(t) \approx t^4$ and $\mathcal{J}(t) \approx t^{-8}$ for $t \ll t_*$. A nice choice for $\mathcal{J}(t)$ with this property (and satisfying $\mathcal{J} \simeq \mathcal{J}_0$ for $t \ll t_*$) is

$$\mathcal{J}(t) = \frac{\mathcal{J}_0}{(1+\frac{t}{t_*})^8}\,. \tag{2.43}$$

Equivalently, using (2.40),

$$\mathcal{J}(\pi) = \left(1 - e^{-(\pi-\pi_\infty)}\right)^8 \mathcal{J}_0\,. \tag{2.44}$$

Substituting $\mathcal{J}(t)$ into the integrated equation of motion (2.42) yields

$$\mathcal{Z}(t) = -\left(f_\infty^2 + f_0^2\right)\frac{t^4}{t_*^4} + \left(1+\frac{t}{t_*}\right)^4 f_0^2\,, \tag{2.45}$$

where f_∞, introduced for reasons that will soon become obvious, is related to the energy density by

$$\rho = \frac{3}{2t_*^4}\left(1+\frac{f_\infty^2}{f_0^2}\right)\frac{f_0^3}{\mathcal{J}_0\Lambda^3}\,. \tag{2.46}$$

Moreover, we can obtain an expression for π_∞ and the transition time:

$$e^{\pi_\infty} = \sqrt{\frac{3f_0}{2\mathcal{J}_0\Lambda^3}}\frac{1}{|t_*|}\,. \tag{2.47}$$

In terms of π, the function $\mathcal{Z}$ can be expressed as

$$\mathcal{Z}(\pi) = \frac{f_0^2}{\left(e^{\pi-\pi_\infty}-1\right)^4}\left(e^{4(\pi-\pi_\infty)} - \left(1+\frac{f_\infty^2}{f_0^2}\right)\right)\,. \tag{2.48}$$

Hence we have 5 parameters defining the theory: f_0, f_∞, Λ, $\mathcal{J}_0$ and π_∞. The transition time t_* is not a free parameter, as it is set by the other parameters in the Lagrangian. By construction, the Lagrangian (2.32) with the functions (2.44) and (2.48) admits the interpolating solution (2.40) as a solution to its equations of motion.

Early times revisited

With the expressions above for $\mathcal{Z}(\pi)$ and $\mathcal{J}(\pi)$, we can investigate the action at large, constant field values, where it takes the approximate form (note that this limit is essentially the early time limit on the solution (2.40)):

$$\mathcal{L}_{\rm early} \simeq -\frac{f_\infty^2 e^{2\pi_\infty}}{\left(e^{\pi-\pi_\infty}-1\right)^4}(\partial\pi)^2 + \frac{1}{\mathcal{J}_0}\frac{f_0^3}{2\Lambda^3}\frac{(\partial\pi)^4}{\left(1-e^{-(\pi-\pi_\infty)}\right)^8}\,, \tag{2.49}$$

It is convenient to define the almost-canonically-normalized variable,

$$\phi = \frac{1}{1-e^{-(\pi-\pi_\infty)}}\,. \tag{2.50}$$

The virtue of this redefinition is that in terms of ϕ, the background solution (2.40) reduces to a linear form

$$\bar{\phi}(t) = 1 + \frac{t}{t_*}\,. \tag{2.51}$$

Another benefit is that the functions $\mathcal{Z}(\pi)$ and $\mathcal{J}(\pi)$ simplify to

$$\begin{aligned} \mathcal{Z}(\phi) &= f_0^2\phi^4 - \left(f_0^2+f_\infty^2\right)(\phi-1)^4\,; \\ \mathcal{J}(\phi) &= \frac{\mathcal{J}_0}{\phi^8}\,. \end{aligned} \tag{2.52}$$

Furthermore, the early-time action in terms of ϕ reduces to

$$\mathcal{L}_{\rm early} \simeq -f_\infty^2 e^{2\pi_\infty}(\partial\phi)^2 + \frac{f_0^3}{2\mathcal{J}_0\Lambda^3}(\partial\phi)^4 \,. \tag{2.53}$$

The kinetic term is healthy, as it should be, hence the theory admits Poincaré-invariant solutions. Further, the quartic term is manifestly *positive*: this ensures both a lack of superluminality about these Poincaré-invariant vacua and that the simplest dispersion relations following from S-matrix analyticity [110] are satisfied.

2.4 Radiative stability

The reduced symmetry of the action due to the presence of the arbitrary functions $\mathcal{Z}(\pi)$ and $\mathcal{J}(\pi)$ makes it unlikely that the theory will be stable under quantum corrections. However, all is not lost. Recall that for large constant field values the action (2.32) can be cast as

$$\mathcal{L}_{\rm early} \simeq f_\infty^2 \left(-e^{2\pi_\infty}(\partial\phi)^2 + \frac{f_0^3}{2f_\infty^2\mathcal{J}_0\Lambda^3}(\partial\phi)^4 \right) \,. \tag{2.54}$$

In this way, f_∞^2 plays a role analogous to $1/\hbar$; for sufficiently large f_∞, quantum effects can be made negligible and the theory will be radiatively stable [116].[15]

Similarly, at late times (or, as $\pi \to \infty$), the theory can be cast as

$$\mathcal{L}_{\rm late} \simeq f_0^2 e^{2\pi}(\partial\pi)^2 + \frac{f_0^3}{\Lambda^3}(\partial\pi)^2\Box\pi + \frac{1}{\mathcal{J}_0}\frac{f_0^3}{2\Lambda^3}(\partial\pi)^4 \,, \tag{2.55}$$

which is precisely of the form considered in [53], where it was shown to be radiatively stable. Therefore, we see that the functional forms of $\mathcal{Z}(\pi)$ and $\mathcal{J}(\pi)$ are stable at

[15] Another way of saying this is that terms radiatively generated in the Lagrangian (2.54) will be suppressed by powers of f_∞, and can be ignored for sufficiently large values of f_∞.

both ends of the evolution. In between, most likely they will be greatly affected by quantum corrections. However, the fact that their asymptotic forms are preserved makes it plausible that a solution which interpolates between NEC-violating and NEC-satisfying regions will continue to exist. Although the detailed form of the solution will surely be modified, we do not expect its stability properties to be greatly affected, as we are able to satisfy the stability requirements for a wide range of parameters. In this sense the explicit interpolating form for $\mathcal{Z}(\pi)$ and $\mathcal{J}(\pi)$ constructed above is a proof of principle.

2.5 NEC violation and neglecting gravity

It is straightforward to calculate the stress-energy tensor for the Lagrangian (2.32), in the approximation that the gravitational background is Minkowski space. The energy density is constant and has already been given in (2.42) and (2.46). The pressure is given by

$$P = -\mathcal{Z}(\bar{\pi})e^{2\bar{\pi}}\dot{\bar{\pi}}^2 + \frac{1}{2\mathcal{J}(\bar{\pi})}\frac{f_0^3}{\Lambda^3}\dot{\bar{\pi}}^4 - 2\frac{f_0^3}{\Lambda^3}\dot{\bar{\pi}}^2\ddot{\bar{\pi}}\,. \tag{2.56}$$

On the solution (2.40), at late times this reduces to[16]

$$P_{\rm late} \simeq -\left(\frac{1}{\mathcal{J}_0}+2\right)\frac{f_0^3}{\Lambda^3}\frac{1}{t^4}\,. \tag{2.57}$$

Since the late-time pressure grows as $1/t^4$ while the energy density remains constant, the NEC will violated at late times if $P_{\rm late} < 0$. This requires

$$\frac{1}{\mathcal{J}_0} > -2 \qquad\qquad \text{(NEC violation)}\,. \tag{2.58}$$

This is the NEC-violating genesis phase.

[16] As a check, translating to the α parameter of Subluminal Genesis via (2.35), this matches the pressure computed in [53].

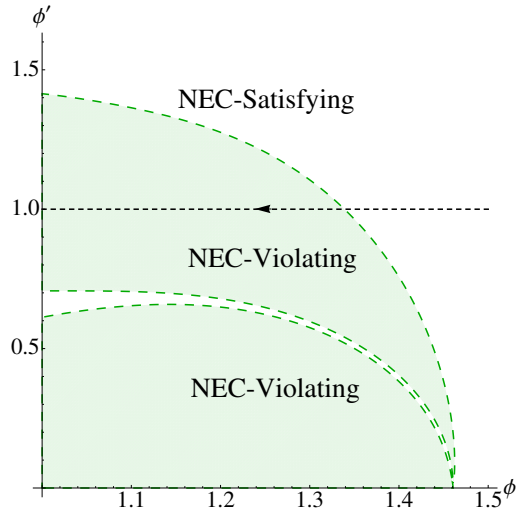

Figure 2.2: NEC-satisfying and NEC-violating regions in the (ϕ, ϕ') phase space, for the parameter values $\frac{f_\infty}{f_0} = 10$ and $\mathcal{J}_0 = 0.75$. The solution of interest, $\phi = 1 + t/t_*$, corresponding to $\phi' = 1$, is plotted as a black dashed line. It first obeys the NEC for a period of time, and then crosses into the NEC-violating regime.

At early times, meanwhile, the pressure is constant and positive:

$$P_{\text{early}} \simeq \frac{1}{2t_*^4}\left(1 + 3\frac{f_\infty^2}{f_0^2}\right)\frac{f_0^3}{\mathcal{J}_0\Lambda^3}\,. \tag{2.59}$$

Hence the early-time regime is NEC-satisfying.

More generally, by combining (2.42) and (2.56) we see that the NEC is violated whenever

$$\rho + P = 2\left(-\mathcal{Z}(\pi)e^{2\pi}\dot{\bar{\pi}}^2 + \frac{1}{\mathcal{J}(\pi)}\frac{f_0^3}{\Lambda^3}\dot{\bar{\pi}}^4 - \frac{f_0^3}{\Lambda^3}\dot{\bar{\pi}}^2\ddot{\bar{\pi}}\right) < 0\,. \tag{2.60}$$

where we have dropped the bars for simplicity. This condition can be studied numerically. For this purpose, we will focus on "on-shell" solutions, that is, on profiles $\bar{\pi}(t)$ that are solutions to the equation of motion (2.41). This allows us to rewrite $\ddot{\bar{\pi}}$ as a function of π and $\dot{\pi}$. Moreover, it is convenient to express the result in terms of the ϕ variable introduced in (2.50), since its background evolution is particularly simple.

The NEC-violating region in phase space corresponds to

$$0 > -\frac{3}{2}\frac{1}{f_0^2\mathcal{J}_0}\mathcal{Z}(\phi)\phi^4 + \left(\frac{1}{\mathcal{J}(\phi)} - 2\phi + 1\right)\phi'^2 - 2\frac{\phi'^2(\phi'^2-1)}{1-2\phi'^2-\left(1+\frac{f_\infty^2}{f_0^2}\right)(1-\phi^{-1})^4}\,,$$

where we have defined $\phi' \equiv t_*\dot{\phi}$. The result is plotted in the (ϕ, ϕ') plane in Fig. 2.2 for a fiducial choice of parameters.

All of the results up to this point have been derived under the approximation that gravitational backreaction can be neglected. We will now quantify the time interval over which this assumption is justified. Consider first the early-time regime. Since pressure and energy density are comparable (and constant) in this epoch, gravitational backreaction can only be neglected for at most a Hubble time $H^{-1} = \sqrt{3M_{\rm Pl}^2/\rho}$. Our approximation is therefore justified for $t \gg t_{\rm beg}$, where (ignoring $\mathcal{O}(1)$ coefficients)

$$\frac{t_{\rm beg}}{t_*} \sim \frac{1}{\sqrt{1+\frac{f_\infty^2}{f_0^2}}}\sqrt{\frac{\Lambda^3}{f_0^3}}|t_*|M_{\rm Pl}\,. \tag{2.61}$$

For consistency, we must have $|t_{\rm beg}| \gg |t_*|$, that is,

$$|t_*| \gg \frac{1}{M_{\rm Pl}}\sqrt{1+\frac{f_\infty^2}{f_0^2}}\sqrt{\frac{f_0^3}{\Lambda^3}}\,. \tag{2.62}$$

Determining the evolution before $t_{\rm beg}$, including gravity, would require a detailed calculation. But since the NEC is preserved, the answer is qualitatively simple: within a time of order $t_{\rm beg}$, the evolution must trace back to a big bang singularity.

During the Genesis phase, on the other hand, the gravitational dynamics are domi-

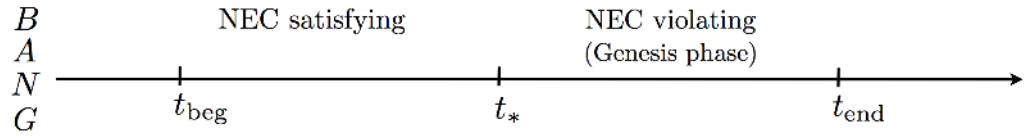

Figure 2.3: Timeline for the evolution. Our approximation of neglecting gravity is valid for the range $t_{\rm beg} \leq t \leq t_{\rm end}$. For $t < t_{\rm beg}$, the universe asymptotes to a big bang singularity (since the NEC is satisfied in this regime). At approximately t_*, the universe transitions from a NEC-satisfying phase to a NEC-violating one. For $t > t_{\rm end}$, cosmological expansion is important, and the universe must transition from the NEC-violating phase to a standard, radiation-dominated phase.

nated by the pressure (2.57). Integrating $M_{\rm Pl}^2 \dot{H} \simeq -\frac{1}{2}P$, we have

$$H_{\rm late} \simeq \frac{1}{6M_{\rm Pl}^2|t|^3}(1+2\mathcal{J}_0)\frac{f_0^3}{\mathcal{J}_0\Lambda^3}\,, \tag{2.63}$$

corresponding to a time-dependent contribution to the energy density:

$$\rho_{\rm late} = \frac{1}{12M_{\rm Pl}^2 t^6}(1+2\mathcal{J}_0)^2\left(\frac{f_0^3}{\mathcal{J}_0\Lambda^3}\right)^2\,. \tag{2.64}$$

This dominates over the constant piece (2.46). Gravitational backreaction can be neglected as long as $P_{\rm late} \gg \rho_{\rm late}$. This breaks down at a time $t_{\rm end}$ obtained by setting $P_{\rm late} \sim \rho_{\rm late}$:

$$|t_{\rm end}| \sim \frac{1}{M_{\rm Pl}}\sqrt{\frac{f_0^3}{\Lambda^3}}\,. \tag{2.65}$$

The condition $f_0 \gg \Lambda$ mentioned in (2.37) ensures that $|t_{\rm end}| \gg M_{\rm Pl}^{-1}$. Moreover, the condition (2.62) automatically implies that $|t_{\rm end}| \ll |t_*|$, which is obviously required for consistency.

To summarize, our approximation of neglecting gravity is valid over the interval

$$t_{\rm beg} \ll t \ll t_{\rm end}\,. \tag{2.66}$$

In order for the transition time to lie within this interval, t_* must satisfy the condition (2.62). The time-line for the entire evolution is sketched in Fig. 2.3.

2.6 Cosmological Evolution

With expressions for P, ρ, $t_{\rm beg}$, and $t_{\rm end}$, it is possible to show how the scale factor may smoothly transition from a decreasing phase to and increasing one. Recall that the Hubble parameter obeys (2.4):

$$M_{\rm Pl}^2 \dot{H} = -\frac{1}{2}(\rho + P) \ . \tag{2.67}$$

Combined with the expressions for $(\rho + P)$ (2.60) and $e^{\pi(t)}$ (2.40), we obtain the following expression for $\dot{H}(t)$:

$$\dot{H}(t) = \frac{-f_0^3}{M_{\rm Pl}^2 J_0 \Lambda^3 t_*^4} \left(\frac{3}{2}\left(1 + \frac{f_\infty^2}{f_0^2}\right) - \frac{1}{2}\left(1 + \frac{t_*}{t}\right)^4 - J_0 \frac{t_*^4}{t^4} \frac{2\frac{t}{t_*} + 1}{(1 + \frac{t}{t_*})^4} \right). \tag{2.68}$$

This expression is valid in the range $t_{\rm end} \ll t \ll t_{\rm beg}$. It may be integrated to give H in this range:

$$\begin{aligned} H(t) = \frac{-f_0^3}{M_{\rm Pl}^2 J_0 \Lambda^3 t_*^3} \Bigg(& \frac{3}{2}\left(1 + \frac{f_\infty^2}{f_0^2}\right)\frac{t}{t_*} + \frac{t_*^3}{6t^3} + \frac{t_*^2}{t^2} + \frac{3t_*}{t} \\ & - 2\log\frac{t}{t_*} - \frac{t}{2t_*} + \frac{J_0}{3}\frac{t_*^3}{t^3}\frac{1}{(1 + \frac{t}{t_*})^3} \Bigg) + C + H_i \ , \end{aligned} \tag{2.69}$$

where C and H_i are both integration constants, but C is chosen to ensure that $H(t_{\rm beg}) = H_i$. This is plotted over the range of validity in Fig. 2.4 for two different values of H_i. The dashed line solution represents an expanding universe that originated in a big bang, and the solid line is a contracting universe that might have originated from Minkowski space or a big bang singularity in the asymptotic past.

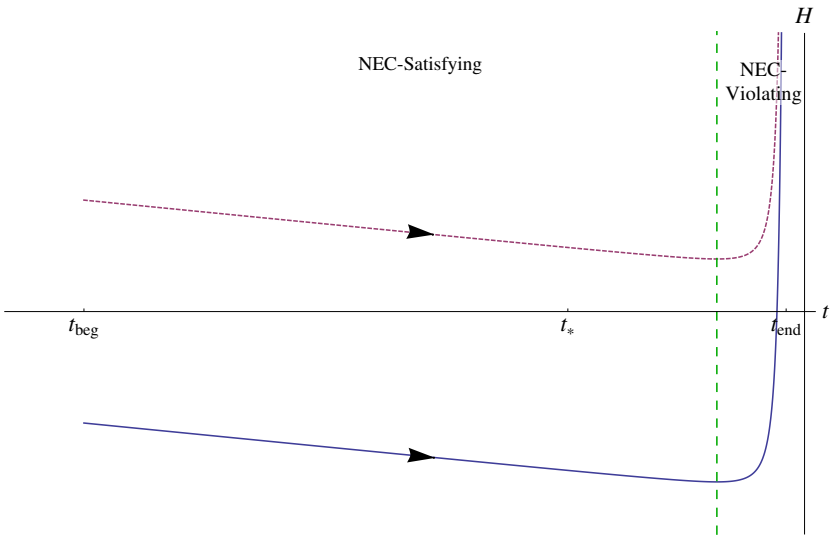

Figure 2.4: The Hubble parameter is plotted for two values of H_i with the fiducial parameters $\mathcal{J}_0 = 0.75$, $f_\infty/f_0 = 10$, $\Lambda = 0.1$, $t_* = -1$, and $C = -6.3 \times 10^{-4} M_{\rm Pl}$. The vertical dashed line marks the boundary between the NEC-satisfying and NEC-violating phases. As we would expect, $\dot{H} < 0$ when the NEC holds, and $\dot{H} > 0$ when it is violated. The dashed solution (corresponding to $H_i = 0.001 M_{\rm Pl}$) always has $H > 0$. It represents an initially expanding universe with decelerating expansion, and could match onto a big-bang type solution for $t < t_{\rm beg}$. The solid line (with $H_i = -0.001 M_{\rm Pl}$) represents an initially contracting universe ($H < 0$) which enters the phase of NEC-violation and undergoes a cosmological bounce to an accelerating phase ($H > 0$), all within the regime of validity of our effective theory.

Although both solutions demonstrate the transition from $\dot{H} < 0$ to $\dot{H} > 0$, the solid line also shows that a solution can smoothly go from $H < 0$ to $H > 0$ — *i.e.*, a bounce. Notice that this bounce occurs before $t_{\rm end}$, our estimate for when gravitational back-reaction can no longer be ignored in the solution for π. This indicates that we can trust the existence of the bounce within our effective theory.

2.7 Stability of perturbations

We now turn to the study of perturbations around background solutions. Expanding the Lagrangian (2.32) to quadratic order in perturbations $\varphi = \pi - \bar{\pi}$, we find

$$\mathcal{L}_{\rm quad} = \mathcal{Z}_\varphi(t)\dot{\varphi}^2 - \mathcal{K}_\varphi(t)(\nabla\varphi)^2 \,, \tag{2.70}$$

where we have defined the functions

$$\begin{aligned}\mathcal{Z}_\varphi(t) &\equiv \left(-\mathcal{Z}(\bar{\pi})e^{2\bar{\pi}} + \frac{3}{\mathcal{J}(\bar{\pi})}\frac{f_0^3}{\Lambda^3}\dot{\bar{\pi}}^2\right) ; \\ \mathcal{K}_\varphi(t) &\equiv \left(-\mathcal{Z}(\bar{\pi})e^{2\bar{\pi}} + 2\frac{f_0^3}{\Lambda^3}\ddot{\bar{\pi}} + \frac{1}{\mathcal{J}(\bar{\pi})}\frac{f_0^3}{\Lambda^3}\dot{\bar{\pi}}^2\right) . \end{aligned} \tag{2.71}$$

The constraints on the quadratic theory are the following:

- **Absence of ghosts**: To avoid ghosts, the kinetic term should be positive: $\mathcal{Z}_\varphi > 0$. It is straightforward to show that will be the case if

$$\mathcal{J}_0 > 0 \qquad\qquad \text{(No ghosts)} . \tag{2.72}$$

  In particular, the NEC-violating condition (2.58) follows automatically.

- **Absence of gradient instabilities**: Similarly, the spatial gradient term should be positive: $\mathcal{K}_\varphi > 0$. Expressing this condition in terms of ϕ, and dropping the bars for simplicity, we obtain

$$\begin{aligned} 0 < -\frac{3}{2}\frac{1}{f_0^2\mathcal{J}_0}Z(\phi)\phi^4 + \left(2(2\phi-1) + \frac{1}{\mathcal{J}(\phi)}\right)\phi'^2 \\ + 4\frac{\phi'^2(\phi'^2-1)}{1-2\phi'^2-\left(1+\frac{f_\infty^2}{f_0^2}\right)(1-\phi^{-1})^4} , \end{aligned} \tag{2.73}$$

  where we recall that $\phi' \equiv \dot{\phi}t_*$.

- **Subluminality**: The final constraint at the quadratic level is to demand subluminal propagation: $\mathcal{K}_\varphi/\mathcal{Z}_\varphi < 1$. Assuming that both (2.72) and (2.73) are satisfied, subluminality follows by definition if the kinetic term is larger than

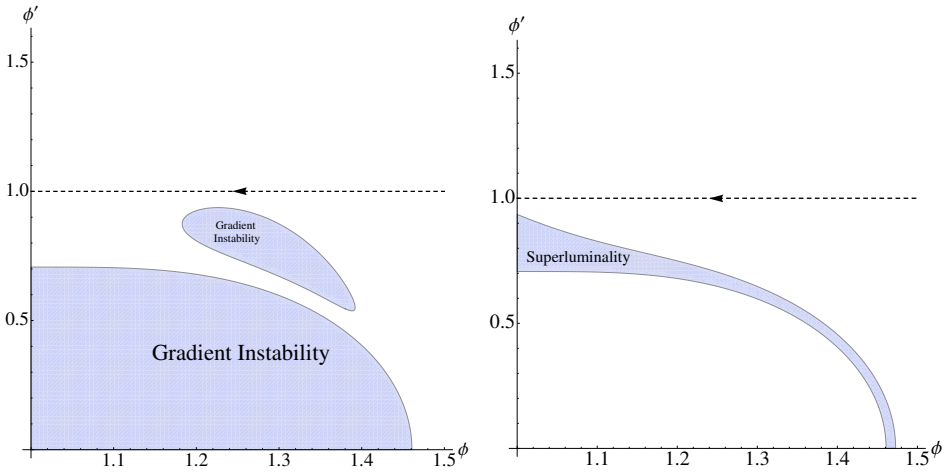

(a) Gradient Instability

(b) Superluminality

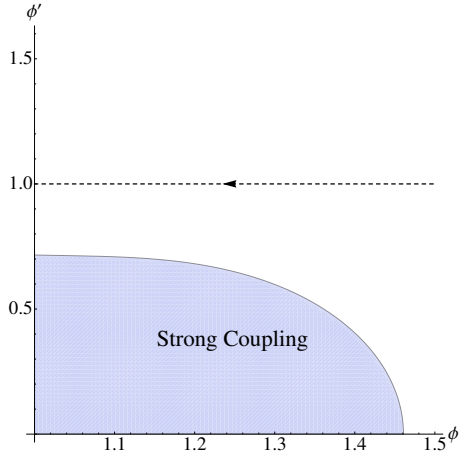

(c) Strong Coupling

Figure 2.5: The shaded regions represent parts of the (ϕ, ϕ') phase space where perturbations (a) suffer from gradient instabilities; (b) propagate superluminally; (c) are strongly coupled. The parameter values are $\frac{f_\infty}{f_0} = 10$ and $\mathcal{J}_0 = 0.75$. The solution of interest, $\phi = 1 + t/t_*$, corresponding to $\phi' = 1$, is plotted as a black dashed line. It avoids all pathological regions.

the gradient term. It is straightforward to show that this will be the case if

$$\left(\frac{1}{\mathcal{J}(\phi)} - 2\phi + 1\right)\phi'^2 - 2\frac{\phi'^2(\phi'^2-1)}{1-2\phi'^2-\left(1+\frac{f_\infty^2}{f_0^2}\right)(1-\phi^{-1})^4} > 0\ . \tag{2.74}$$

In the genesis regime (corresponding to $\phi \to 1$ and $\phi' \to 1$), in particular, this gives a constraint on the constant $\mathcal{J}_0$:

$$\mathcal{J}_0 < 1\,. \tag{2.75}$$

Beyond the quadratic theory, we should also check that the interactions are perturbative. Consider the cubic vertex for the perturbations:

$$\mathcal{L}_3 = \frac{f_0^3}{\Lambda^3}(\partial\varphi)^2\Box\varphi\,, \tag{2.76}$$

After canonical normalization of the kinetic term, $\varphi_c \equiv \mathcal{Z}_\varphi^{1/2}\varphi$, the cubic term becomes suppressed by the effective strong coupling scale

$$\Lambda_{\rm eff} = \frac{\Lambda}{f_0}\mathcal{Z}_\varphi^{1/2}\,. \tag{2.77}$$

For consistency of the effective field theory, the characteristic frequency of the background, namely $\dot{\bar{\pi}}$, should lie below this cutoff:

$$\dot{\bar{\pi}} \ll \Lambda_{\rm eff}\,. \tag{2.78}$$

In the Genesis phase, in particular, $\dot{\bar{\pi}} \simeq 1/t$ sets the scale at which perturbations freeze out. Hence (2.78) is necessary to consistently describe the generation of perturbations within the effective theory. A straightforward calculation shows that this condition

implies:

$$2\bar{\phi}'^2\left(\frac{\mathcal{J}_0\Lambda}{3f_0\bar{\phi}^8}-1\right)\ll\left(1+\frac{f_\infty^2}{f_0^2}\right)\left(1-\bar{\phi}^{-1}\right)^4-1\qquad\text{(weak coupling)}\,.\tag{2.79}$$

Note that the left-hand side is negative-definite within the range $0<\mathcal{J}_0<1$ allowed by (2.72) and (2.75). As a check, note that in the genesis regime, (2.79) reduces to $\frac{\mathcal{J}_0\Lambda}{f_0}\ll\frac{3}{2}$, which is another way to confirm the condition $f_0\gg\Lambda$ mentioned in (2.37).

In summary, the allowed range of $\mathcal{J}_0$ values is

$$0<\mathcal{J}_0<1\,.\tag{2.80}$$

The remaining constraints — no gradient instabilities (2.73), subluminality (2.75), and weak coupling (2.79) — are plotted in the (ϕ,ϕ') phase space in Fig. 2.5 for a fiducial choice of parameters.

These constraints are overlaid in Fig. 2.6 with a range of solutions to the equation of motion. On these plots, the background solution (2.51) of interest corresponds to $\phi'=1$. Other background solutions, corresponding to different initial conditions, are also plotted as solid lines. This shows that there is a wide range of trajectories that interpolate between a constant field profile at early times and the Genesis solutions at late times, while avoiding the pathological region at all times. Furthermore, it is clear that the background solution $\phi'=1$ is an attractor at late times.

2.8 Conclusions

It has proven surprisingly difficult to violate the null energy condition with a well-behaved relativistic quantum field theory. In the simplest attempts, violating the NEC generally introduces ghost instabilities, gradient instabilities, superluminality,

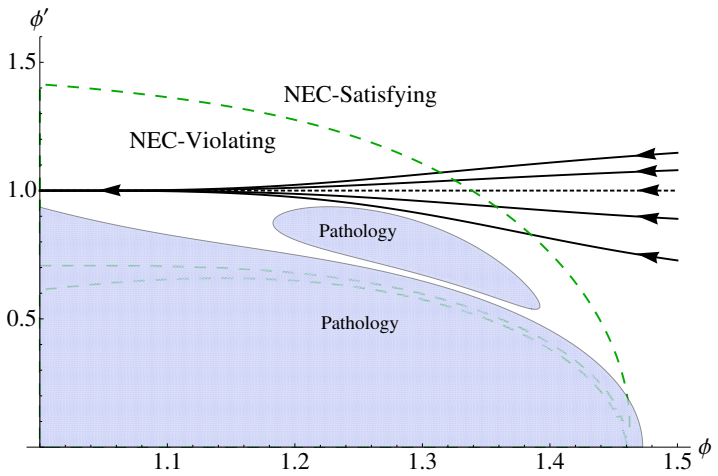

Figure 2.6: Phase portrait with all constraints overlaid, again for the fiducial choice of parameters $\frac{f_\infty}{f_0} = 10$ and $\mathcal{J}_0 = 0.75$. The shaded region represents the union of all pathological regions shown in Fig. 2.5. The green long-dashed line separates the NEC-satisfying and NEC-violating regions. The black short-dashed line corresponds to the background solution of interest, given by (2.51). The solid lines represent other background solutions (with different initial conditions).

or absence of a Lorentz-invariant vacuum. Progress has been made in avoiding some of these shortcomings, but a fully satisfactory example remains to be found. The null energy condition appears to be connected to some fundamental physics principles, such as black hole thermodynamics and the (non)-existence of cosmological bounces. Therefore, if it turns out that violating the NEC is impossible, pinpointing which of the aforementioned pathologies is the real roadblock will tell us something fundamental.

The recently-proposed DBI Genesis scenario is the first example of a theory admitting both a Poincaré-invariant vacuum and NEC-violating solutions. As argued by Rubakov, however, these two backgrounds lie on different branches of solutions and cannot be connected by a smooth solution without strong coupling occurring. This is an immediate consequence of dilation invariance.

Here, we have abandoned dilation symmetry in order to circumvent Rubakov's no-go

argument. We have constructed a theory which admits a time-dependent solution that smoothly interpolates between a NEC-satisfying phase at early times and a NEC-violating phase at late times. There exists a wide range of parameters for which perturbations around the background are stable, comfortably subluminal and weakly-coupled at all times.

The main drawback of the construction is the presence of suitably-engineered interpolating functions in the action. It is highly unlikely that the detailed form of these functions will be preserved by quantum corrections. However, we argued that their asymptotic forms both in the past and in the future are radiatively stable. Moreover, our analysis did not depend sensitively on the details of the interpolation. Therefore, all we need is for the quantum-corrected action to still allow an interpolation between NEC-satisfying and NEC-violating solutions. We leave a detailed analysis of radiative stability to future work.

Another drawback of the explicit example presented here is that the kinetic term flips sign as we adiabatically vary ϕ. It is healthy at early times, consistent with Poincaré invariance, but becomes ghost-like at late times, which is necessary to obtain a NEC-violating solution with the cubic Galilean Genesis action. Of course, as mentioned earlier, perturbations around the time-dependent background are always healthy. However, it would be aesthetically desirable if the perturbations around ϕ = constant backgrounds were also healthy for all field values of interest. This should be achievable by deforming the DBI Genesis Lagrangian, since this theory precisely satisfies this property while allowing a NEC-violating background. We plan to study the DBI Genesis generalization in the future. It is also possible that the DBI extension will alleviate the quantum stability issues discussed above.

Chapter 3

A Positive Energy Theorem for $P(X)$ Theories

In the previous Chapter we were concerned with energy conditions, which are local statements about the energy of a theory. In particular, we showed that scalar field theories may violate the null energy condition while still avoiding pathologies. In this Chapter we ask if there are any other desirable properties for a well-behaved theory to have.

One property we might demand from a theory is is that the vacuum be classically stable in the presence of gravity. This will be the case if the total energy of the system (matter energy plus gravitational energy) is bounded from below, and is minimized only by empty Minkowski space. This property is known as *positive energy*. Unlike the energy conditions of the previous Chapter, which were local requirements on $T_{\mu\nu}$ at each point in space-time, positive energy is a global condition that constraints the total mass/energy of the spacetime.

Positive energy was first proved for matter that obeyed the dominant energy condition [81, 82], and then more generally for canonical scalar fields [85, 86], as will be reviewed in Section 3.2. In this Chapter we present a further generalization of these arguments to derivatively-coupled scalar fields, culminating in a positive energy theorem for $P(X)$ theories. It is based on work that originally appeared in [2].

Energy can be a difficult quantity to define in general relativity. First of all, energy is the conserved quantity associated with time translation symmetry, so it will only be conserved if the space-time admits a timelike Killing vector k^μ.

Let us assume for the moment that a space-time does have a timelike Killing vector. Then perhaps the most straightforward way to define the total energy is first define the current [199] $J^\mu \equiv k_\nu T^{\mu\nu}$. This current is covariantly conserved by the conservation of $T_{\mu\nu}$ and the facts that $T_{\mu\nu}$ is symmetric while $\nabla_\mu k_\nu$ is antisymmetric by the Killing equation. We might then identify the integral of J^μ over a spacelike surface and identify this with the total energy:

$$E = \int_\Sigma d^3x \sqrt{\gamma} n_\mu J^\mu \ , \tag{3.1}$$

where Σ is a spacelike hypersurface, γ is the induced metric on the surface, and n^μ is a unit vector normal to Σ.

However, this approach is somewhat lacking. For example, consider a cloud of gas with energy/mass m that collapses to a singularity. After the collapse, $T_{\mu\nu}$ vanishes everywhere except (perhaps) the singularity, making the above integral difficult to evaluate. We expect that the total energy should be unchanged, yet after the gravitational collapse the situation has become unclear.

We can improve matters by using a different conserved current in Eq. (3.1). Consider instead [199, 200]

$$J^\mu = k_\nu R^{\mu\nu} \ . \tag{3.2}$$

This current is still covariantly conserved: $\nabla_\mu k_\nu R^{\mu\nu} = 0$ by the symmetry/antisymmetry of its components, and $k_\nu \nabla_\mu R^{\mu\nu} = \frac{1}{2} k_\nu \nabla^\nu R = 0$ by the Killing equation and the Bianchi identity.

This definition carries a significant advantage in that it may be cast as a total derivative: $k^\nu R_{\mu\nu} = \nabla_\mu \nabla_\nu k^\mu$, allowing us to rewrite the above volume integral as a surface integral at spatial infinity:

$$E_{\text{Komar}} = \oint_{\partial\Sigma} d^2x \sqrt{\gamma^{(2)}} n_\mu \sigma_\nu \nabla^\mu k^\nu \ , \tag{3.3}$$

where we integrate over the boundary of the spacelike hypersurface $\partial\Sigma$ which has an induced metric $\gamma^{(2)}$ and normal vector σ_ν. This expression known as the Komar energy, and it gives the total energy for a space-time with a timelike Killing vector k^μ. Since it is evaluated at spacelike infinity, where fields are presumably very weak, it avoids one having to compute integrals over singularities.

A second approach, due to Abbott, Deser, and Misner [80], is to identify the total energy with the Hamiltonian of the system. The first step is to foliate space-time into spacelike hypersurfaces with metric h_{ij}:

$$ds^2 = -N^2 dt^2 + h_{ij} \left(dx^i + N^i dt\right) \left(dx^j + N^j dt\right) \ , \tag{3.4}$$

We have introduced the *lapse function* N, which measures the passage of proper time orthogonal to the spatial slices, and the *shift vector* N^i, which measures movement tangential to the spatial slices with the passage of coordinate time.

The conjugate momentum to the spatial metric h_{ij} is

$$\pi^{ij} = \sqrt{h} \left(K^{ij} - K h^{ij}\right) \ , \tag{3.5}$$

where the extrinsic curvature of the spatial slices is $K_{ij} = \frac{1}{2N} \left(\dot{h}_{ij} - D_i N_j - D_j N_i\right)$, where D_i is the derivative associated with h_{ij}.

The Hamiltonian following from the Einstein-Hilbert action is then

$$H = \frac{M_{\rm Pl}^2}{2} \int d^3x N^\mu \mathcal{H}_\mu \ , \tag{3.6}$$

where we have defined $N^\mu = (N, N^i)$ and the Hamiltonian density

$$\begin{aligned} \mathcal{H}_0 &= -\sqrt{h}R^{(3)} + \frac{1}{\sqrt{h}}\left(\pi^{ij}\pi_{ij} - \frac{1}{2}(\pi^i{}_i)^2\right) \ , \\ \mathcal{H}_i &= -2h_{ij}D_k\pi^{jk} \ . \end{aligned} \tag{3.7}$$

Assuming the space-time is asymptotically flat, so that $g_{\mu\nu} = \eta_{\mu\nu} + h_{\mu\nu}$ for small h at spatial infinity, this Hamiltonian simplifies considerably and may be written as a boundary integral at spatial infinity. This quantity is henceforth referred to as the ADM mass:

$$M_{\rm ADM} = \frac{M_{\rm Pl}^2}{2} \oint_{\partial\Sigma} d^2x \sqrt{\gamma^{(2)}}\sigma^i \left(\partial^j h_{ij} - \partial_i h\right) \ . \tag{3.8}$$

The ADM mass is the generator of time translations in asymptotically flat space-times, while the Komar energy is the total energy of a stationary space-time. If $h_{\mu\nu}$ is time independent at spatial infinity, then the two quantities are the same.

We may now formulate the positive energy theorem in a more precise way: a theory has positive energy for asymptotically flat solutions if the ADM mass is non-negative and is zero for Minkowski space only.[17]

It was originally shown [81] that Einstein gravity plus matter has positive energy if the matter obeys the dominant energy condition (DEC)[18]. This proof was later

[17]Note that we are focusing on flat (or AdS) asymptotics, where the matter fields (in our case, a scalar field) become constant at spatial infinity. This immediately rules out time-dependent asymptotics, which may be more realistic for cosmology.

[18]The DEC states that: *i*) for any time-like u, $T_{\mu\nu}u^\mu u^\nu \geq 0$; and *ii*) for any future-pointing and causal u, $-T^\mu_\nu u^\nu$ is also future-pointing and causal. Roughly, these correspond respectively to the

simplified using a spinor technique due to Witten [82–84]. (Similar proofs exist for asymptotically anti-de Sitter [201–204] and de Sitter [205, 206] space-times.) The result was extended by Boucher and Townsend, who showed that the DEC is not necessary to ensure positive energy [85, 86]. See also [207]. This proof will be reviewed in Sec. 3.2. For a nonlinear σ-model with N scalars,

$$\mathcal{L} = -\frac{1}{2} f_{IJ}(\phi) \partial_\mu \phi^I \partial^\mu \phi^J - V(\phi^I) \ , \tag{3.9}$$

where f_{IJ} is positive-definite, positive energy is guaranteed so long as $V(\phi^I)$ is derivable from a "superpotential" $W(\phi^I)$ obeying the equation[19]:

$$V(\phi^I) = 8 f^{IJ} W_{,\phi^I} W_{,\phi^J} - 12 W^2 \ , \tag{3.10}$$

assuming that $V(\phi^I)$ admits a minimum with $V(\bar{\phi}^I) \leq 0$.

In this Chapter, we further extend this result and derive a positive energy theorem for scalar theories of the form

$$\mathcal{L} = P(X, \phi) \ , \tag{3.11}$$

by similarly constraining the functional form that $P(X, \phi)$ can take. Here X is the canonical kinetic term: $X = -\frac{1}{2}(\partial\phi)^2$. This class of theories has a long history, especially in cosmology. As mentioned earlier, they can be used for inflation [13, 208, 209], dark energy [14, 210], bouncing cosmologies [150, 153, 166], and display screening around heavy sources [15, 16, 105, 114, 211]. Furthermore, $P(X)$ theories describe the low energy dynamics of superfluids [17].

We establish the positive energy result in two different ways. First, at the classical

statements that the energy density is positive, and the energy-momentum flow is subluminal.

[19] In fact, $V(\phi^I)$ must only satisfy the weaker inequality $V(\phi^I) \geq 8 f^{IJ} W_{,\phi^I} W_{,\phi^J} - 12 W^2$.

level we map (3.11) to an equivalent two-derivative theory via an auxiliary field [212]. Turning on a small kinetic term for this second field, the action takes the form (3.9). We can then apply the result (3.10), which is translated to a statement about $P(X, \phi)$ upon integrating out the auxiliary field.

Second, we will reproduce this result directly at the $P(X, \phi)$ level using Witten's spinor arguments [82]. This approach was taken in [213], although we will see that their result was too restrictive. We will show that relaxing a small technical assumption in their argument allows for greater flexibility in choosing the functional form of $P(X, \phi)$.

This broader assortment of $P(X, \phi)$ theories consistent with positive energy allows for interesting phenomena. In particular, consider $P(X) = X + \alpha X^2$, arguably the simplest $P(X, \phi)$ example. With $\alpha > 0$, this theory obeys the DEC and hence has positive energy. Even with $\alpha < 0$, however, we will show that the theory allows positive energy, as long as we restrict to the region $P_{,X} > 0$. This is remarkable since this theory with $\alpha < 0$ both exhibits a screening mechanism and violates some of the S-matrix analyticity requirements for a local theory [110].

3.1 Two-Field Description

A $P(X, \phi)$ theory can be mapped to a 2-derivative action by introducing an auxiliary field χ [212] so that the Lagrangian takes the form

$$\mathcal{L} = -\frac{1}{2} P_{,\chi} (\partial\phi)^2 - \chi P_{,\chi} + P \,, \tag{3.12}$$

where $P = P(\chi, \phi)$. Indeed, the equation of motion for χ is $P_{,\chi\chi}(X - \chi) = 0$, which sets $\chi = X$, as long as $P_{,\chi\chi} \neq 0$. Substituting $\chi = X$ in (3.12) gives $\mathcal{L} =$

$P(X,\phi)$, establishing the classical equivalence of the two descriptions. To put it in the form (3.9), we simply turn on a small kinetic term for χ:

$$\mathcal{L} = -\frac{1}{2}P_{,\chi}(\partial\phi)^2 - \frac{1}{2}Z^2(\partial\chi)^2 - \chi P_{,\chi} + P \ . \tag{3.13}$$

At this level, this is just a technical trick — at the end we will take $Z \to 0$. Upon making the identifications

$$f_{\chi\chi} = Z^2 \ ; \qquad f_{\phi\phi} = P_{,\chi} \ ; \qquad V(\chi,\phi) = \chi P_{,\chi} - P \, , \tag{3.14}$$

this is of form (3.9). Note f_{IJ} must be positive-definite, imposing $P_{,\chi} > 0$. After integrating out χ, this translates to $P_{,X} > 0$, which is equivalent to the NEC [20]. In some cases this will restrict the range of X, but this is acceptable because it is a *Lorentz-invariant* restriction on the space of allowed solutions. The condition $P_{,X} > 0$ is required for the validity of the single-field EFT which is partially UV completed by the two-field system (3.13) [212].

Substituting (3.14), the condition (3.10) yields

$$\chi P_{,\chi} - P = 8\frac{W_{,\phi}^2}{P_{,\chi}} + 8\frac{W_{,\chi}^2}{Z^2} - 12W^2 \ . \tag{3.15}$$

To have a smooth $Z \to 0$ limit, the superpotential must take the form $W(\chi,\phi) = \mathcal{W}(\phi) + \frac{Z}{2\sqrt{2}}\mathcal{G}(\chi,\phi) + \mathcal{O}(Z^2)$, where the factor of $2\sqrt{2}$ is introduced to simplify later expressions. Substituting this into (3.15) and taking $\chi \to X$, the positive energy

[20] The stress tensor for $P(X,\phi)$ is $T_{\mu\nu} = P_{,X}\partial_\mu\phi\partial_\nu\phi + g_{\mu\nu}P$. Contracting with a null vector n^μ, the NEC boils down to $0 \leq T_{\mu\nu}n^\mu n^\nu = P_{,X}(n^\mu\partial_\mu\phi)^2$, which requires $P_{,X} > 0$.

condition becomes

$$P - XP_{,X} + 8\frac{\mathcal{W}_{,\phi}^2}{P_{,X}} + \mathcal{G}_{,X}^2 - 12\mathcal{W}^2 = 0 \ . \tag{3.16}$$

This is our main result. It is the analogue of (3.10) for theories of the $P(\phi, X)$ type. Positivity of the energy requires the existence of two functions, $\mathcal{W}(\phi)$ and $\mathcal{G}(\phi, X)$, related to $P(\phi, X)$ through (3.16). Asymptotically, we assume $X \to 0$ and $\phi \to \phi_0$ such that $P_{,\phi}(\phi_0) = 0$.

The proof generalizes to N scalar fields with $P(X^{IJ}, \phi^K)$, where following [213] we have defined the tensor $X^{IJ} = -\frac{1}{2}\partial_\mu\phi^I\partial^\mu\phi^J$. This generalization is particularly interesting because the EFT of fluids [214] is a theory of this type (to be precise, fluids are described by pure $P(X^{IJ})$, with no ϕ^K terms appearing without derivatives). We introduce a matrix of scalar fields χ^{IJ}, and the generalization of (3.13) becomes

$$\begin{aligned} \mathcal{L} = -\frac{1}{2}P_{MN}\partial^\mu\phi^M\partial_\nu\phi^N \ &- \ \frac{1}{2}Z^2P_{KM}P_{LN}\partial_\mu\chi^{KL}\partial_\nu\chi^{MN} \\ &+ \ P - \chi^{MN}P_{MN} \ , \end{aligned} \tag{3.17}$$

where $P_{IJ} \equiv \partial P/\partial\chi^{IJ}$ is positive definite and invertible. Again, integrating out χ and setting $Z \to 0$ gives $X^{IJ} = \chi^{IJ}$. Following the same steps as before, we find that the superpotential must take the form $W = \mathcal{W}(\phi^I) + \frac{Z}{2\sqrt{2}}\mathcal{G}(\phi^I, \chi^{MN}) + \mathcal{O}(Z^2)$. Writing the inverse of P_{IJ} as P^{IJ}, we arrive at the positivity condition

$$\begin{aligned} P \ &- \ X^{MN}P_{MN} + 8P^{MN}\mathcal{W}_{,\phi^M}\mathcal{W}_{,\phi^N} \\ &+ \ P^{KM}P^{LN}\mathcal{G}_{KL}\mathcal{G}_{MN} - 12\mathcal{W}^2 = 0 \ . \end{aligned} \tag{3.18}$$

3.2 Direct derivation

We now re-derive the positive energy condition (3.16) directly at the level of $P(X,\phi)$. This method generally follows the presentation of Witten's proof of the positive energy theorem in [82, 84–86], but with a crucial difference. We begin with a review of the proof for canonical scalar fields, and then generalize this approach to $P(X,\phi)$ theories.

The starting point is the Nester 2-form [82, 84]:

$$N^{\mu\nu} = -i\left(\bar{\epsilon}\gamma^{\mu\nu\rho}\hat{\nabla}_\rho\epsilon - \overline{\hat{\nabla}_\rho\epsilon}\gamma^{\mu\nu\rho}\epsilon\right) \ . \tag{3.19}$$

where we have defined the super-covariant derivative

$$\hat{\nabla}_\mu\epsilon = \left(\nabla_\mu + \mathcal{A}_\mu\right)\epsilon \ . \tag{3.20}$$

Some words on notation: ϵ is a *commuting* Dirac spinor [85], with conjugate $\bar{\epsilon} = i\epsilon^\dagger\gamma^0$; the Dirac matrices obey the Clifford algebra $\{\gamma_\mu,\gamma_\nu\} = 2g_{\mu\nu}$, and we have defined the anti-symmetric product $\gamma^{\mu\nu\rho} \equiv \gamma^{[\mu}\gamma^\nu\gamma^{\rho]}$.

The virtue of $N^{\mu\nu}$ is that its integral is simply related to the energy of a gravitating system [82, 84, 85]

$$E = \int_{\partial\Sigma} \mathrm{d}\Sigma_{\mu\nu}N^{\mu\nu} = \int_\Sigma \mathrm{d}\Sigma_\nu\nabla_\mu N^{\mu\nu} \ , \tag{3.21}$$

where Σ is an arbitrary space-like surface, with $\mathrm{d}\Sigma_\nu$ denoting the normal-pointing volume form. The divergence of $N^{\mu\nu}$ is given by [86]

$$\nabla_\nu N^{\mu\nu} = 2i\overline{\hat{\nabla}_\nu\epsilon}\gamma^{\mu\nu\rho}\hat{\nabla}_\rho\epsilon - \frac{T^\mu_{\ \nu}}{M_{\rm Pl}^2}\, i\bar{\epsilon}\gamma^\nu\epsilon - i\bar{\epsilon}\gamma^{\mu\nu\rho}\mathcal{F}_{\nu\rho}\epsilon \ , \tag{3.22}$$

where $\mathcal{F}_{\nu\rho} = \nabla_\nu\mathcal{A}_\rho - \nabla_\rho\mathcal{A}_\nu + [\mathcal{A}_\nu,\mathcal{A}_\rho]$ is the curvature of the connection $\mathcal{A}_\mu$.

The term $2i\overline{\hat{\nabla}_\nu \epsilon}\gamma^{\mu\nu\rho}\hat{\nabla}_\rho\epsilon$ gives a positive contribution to the energy after imposing the Witten condition $\gamma^i\hat{\nabla}_i\epsilon = 0$ [82]. The other two terms are not manifestly positive.

Let us briefly consider the special case $\mathcal{A}_\mu = 0$, so that the third term of Eq. (3.22) then vanishes. This is the case originally considered by Witten. The second term is guaranteed positive if the stress-energy tensor obeys the dominant energy condition. This was the bottom line of the proof of Witten: positive energy is guaranteed if the matter fields obey the DEC [82].

We can relax this condition by including $\mathcal{A}_\mu \neq 0$. The stress tensor for (3.11) is

$$T_{\mu\nu} = P_{,X}\partial_\mu\phi\partial_\nu\phi + Pg_{\mu\nu} \ . \tag{3.23}$$

Following [85, 86], we will temporarily specialize to a canonical scalar field, $P(X,\phi) = X - V(\phi)$.

To proceed, we make the ansatz [86]

$$\mathcal{A}_\mu = \mathcal{W}(\phi)\gamma_\mu \, , \tag{3.24}$$

for some $\mathcal{W}(\phi)$. The last term in (3.22) becomes

$$-i\bar{\epsilon}\gamma^{\mu\nu\rho}\mathcal{F}_{\nu\rho}\epsilon = -4i\bar{\epsilon}\gamma^{\mu\nu}\epsilon\mathcal{W}_{,\phi}\partial_\nu\phi + 12i\bar{\epsilon}\gamma^\mu\epsilon\mathcal{W}^2 \ . \tag{3.25}$$

Our goal is to write this as a sum of squares of spinors, plus a remainder piece. To do this, we define

$$\delta\lambda = \frac{1}{\sqrt{2}}\left(\gamma^\mu\partial_\mu\phi - 4\mathcal{W}_{,\phi}\right)\epsilon \ , \tag{3.26}$$

so that

$$-i\bar{\epsilon}\gamma^{\mu\nu\rho}\mathcal{F}_{\nu\rho}\epsilon = i\overline{\delta\lambda}\gamma^{\mu}\delta\lambda + i\bar{\epsilon}\gamma^{\nu}\epsilon P_{,X}\partial^{\mu}\phi\partial_{\nu}\phi + i\bar{\epsilon}\gamma^{\mu}\epsilon\Big(V(\phi) - 8\mathcal{W}_{,\phi}^{2} + 12\mathcal{W}^{2}\Big) \ . \tag{3.27}$$

Combining (3.22), (3.23) and (3.31), we obtain

$$\nabla_{\nu}N^{\mu\nu} = 2i\overline{\hat{\nabla}_{\nu}\epsilon}\gamma^{\mu\nu\rho}\hat{\nabla}_{\rho}\epsilon + i\overline{\delta\lambda}\gamma^{\mu}\delta\lambda + i\bar{\epsilon}\gamma^{\mu}\epsilon\Big(V(\phi) - 8\mathcal{W}_{,\phi}^{2} + 12\mathcal{W}^{2}\Big) \ . \tag{3.28}$$

The first line is positive-definite, whereas the second line is not. To ensure positivity of E, it is sufficient to set the second line to zero. The theory is therefore guaranteed to have positive energy if the potential can be be written in terms of $\mathcal{W}(\phi)$:

$$V(\phi) = 8\mathcal{W}_{,\phi}^{2} - 12\mathcal{W}^{2} \ . \tag{3.29}$$

Now we return to the full $P(X,\phi)$ case. This time we define *two* spinor fields

$$\begin{aligned}\delta\lambda_{1} &= \frac{1}{\sqrt{2}}\left(\sqrt{P_{,X}}\gamma^{\mu}\partial_{\mu}\phi - 4\frac{\mathcal{W}_{,\phi}}{\sqrt{P_{,X}}}\right)\epsilon \ ; \\ \delta\lambda_{2} &= \mathcal{G}_{,X}\epsilon \ ,\end{aligned} \tag{3.30}$$

so that

$$-i\bar{\epsilon}\gamma^{\mu\nu\rho}\mathcal{F}_{\nu\rho}\epsilon = i\sum_{i=1}^{2}\overline{\delta\lambda}_{i}\gamma^{\mu}\delta\lambda_{i} + i\bar{\epsilon}\gamma^{\nu}\epsilon P_{,X}\partial^{\mu}\phi\partial_{\nu}\phi + i\bar{\epsilon}\gamma^{\mu}\epsilon\left(XP_{,X} - P - 8\frac{\mathcal{W}_{,\phi}^{2}}{P_{,X}} - \mathcal{G}_{,X}^{2} + 12\mathcal{W}^{2}\right) \ . \tag{3.31}$$

This is the key difference from the derivation in [213]. In that calculation, the authors only used one $\delta\lambda$ spinor field, which led to a restricted class of solutions. Instead we expressed $-i\bar{\epsilon}\gamma^{\mu\nu\rho}\mathcal{F}_{\nu\rho}\epsilon$ as the sum of *two* squares of spinors. The second spinor introduces a new function $\mathcal{G} = \mathcal{G}(X,\phi)$, which allows us to derive a more general positivity constraint than [213].

Combining (3.22), (3.23) and (3.31), we obtain

$$\begin{aligned}\nabla_\nu N^{\mu\nu} &= 2i\overline{\hat{\nabla}_\nu\epsilon}\gamma^{\mu\nu\rho}\hat{\nabla}_\rho\epsilon + i\sum_{i=1}^{2}\overline{\delta\lambda}_i\gamma^\mu\delta\lambda_i \\ &+ i\bar{\epsilon}\gamma^\mu\epsilon\left(XP_{,X} - P - 8\frac{\mathcal{W}_{,\phi}^2}{P_{,X}} - \mathcal{G}_{,X}^{\,2} + 12\mathcal{W}^2\right) . \end{aligned} \tag{3.32}$$

Once again we ensure positivity of E by setting the second line to zero. This yields (3.16), which is precisely the energy condition obtained from the 2-field approach. The mass vanishes for $\hat{\nabla}_\mu\epsilon = \delta\lambda_a = 0$, which implies Minkowski or AdS space-time [85]. Having derived this constraint on the functional form of P, we now turn to solving this equation in a few situations of interest[21].

3.3 Special Cases

We now examine some special cases of $P(X,\phi)$ theories which have unique properties.

Pure $P(X)$: One simple but nontrivial case to consider is $P = P(X)$, *i.e.*, a field with purely derivative couplings and no potential. We simply assume that $\mathcal{W} \equiv \mathcal{W}_0$ is constant, and take $\mathcal{G} = \mathcal{G}(X)$. In this case, the positive energy condition (3.16)

[21] An alternative route to (3.16) is to not introduce $\mathcal{G}_{,X}$ through (3.30), but demand that the second line of (3.32) (with $\mathcal{G}_{,X} = 0$) be positive definite. This yields the inequality $XP_{,X} - P - 8\mathcal{W}_{,\phi}^2/P_{,X} + 12\mathcal{W}^2 \geq 0$. Since this is positive-definite, we can write is as the square of some function. Calling this function $\mathcal{G}_{,X}$ yields (3.16).

reduces to an ordinary differential equation for $\mathcal{G}$, which can be integrated:

$$\mathcal{G}(X) = \int \mathrm{d}X \left(XP_{,X} - P + 12\mathcal{W}_0^2 \right)^{1/2} . \tag{3.33}$$

In order for this integral to be real-valued, we must have $XP_{,X} - P \geq -12\mathcal{W}_0^2$. Note that this condition is weaker than the dominant energy condition: $XP_{,X} - P \geq 0$.

As a simple example, consider the function

$$P(X) = X - \beta X^2 \, ; \qquad \beta \geq 0 \, . \tag{3.34}$$

This theory violates the DEC for all X: $XP_{,X} - P = -\beta X^2 < 0$. Recall that our derivation requires $P_{,X} \geq 0$, so we must restrict ourselves to the range $|X| \leq 1/\sqrt{2}\beta$. In this case, (3.33) can be integrated, ensuring the existence of a suitable superpotential, and guaranteeing that the theory has positive energy in the allowed X range.

This theory with "wrong-sign" X^2 term is well-known to violate the standard dispersion relations following from local S-matrix theory [110], at least at tree level. Nevertheless, we have shown that the theory does allow positive energy, at least over the range of X where the NEC is satisfied. This may seem paradoxical from the perspective of the 2-field action discussed earlier; after all, (3.13) describes two healthy scalars with some potential, and therefore should have an analytic S-matrix. The resolution is that the vacuum state $X = 0$ or, equivalently, $\chi = 0$, is tachyonic in the two-field language, hence its S-matrix is ill-defined.

Separable $P(X, \phi)$: A slightly more complicated case is where P is a separable func-

tion:

$$P(X,\phi) = K(\phi)\tilde{P}(X) - V(\phi)\ , \tag{3.35}$$

with $K(\phi) \geq 0$ without loss of generality. This form has been widely-studied in the context of k-essence [13, 14].

It will prove convenient to redefine the arbitary function $\mathcal{G}(X,\phi)$ via

$$\mathcal{G}_{,X}^2 = \mathcal{H}(X,\phi) + 8\frac{\mathcal{W}_{,\phi}^2}{K(\phi)}\left(1 - \frac{1}{\tilde{P}_{,X}}\right). \tag{3.36}$$

Inserting this into (3.16), we find that P must satisfy

$$\tilde{P} - X\tilde{P}_{,X} + \frac{\mathcal{H}(X,\phi)}{K(\phi)} = \frac{1}{K(\phi)}\left(12\mathcal{W}^2 - 8\frac{\mathcal{W}_{,\phi}^2}{K} + V(\phi)\right).$$

For this to be separable, $\mathcal{H}$ must factorize as $\mathcal{H}(X,\phi) = K(\phi)H(X)$. The above then implies two equations

$$\begin{aligned} H(X) &= X\tilde{P}_{,X} - \tilde{P}(X) - E\,; \\ V(\phi) &= 8\frac{\mathcal{W}_{,\phi}^2}{K(\phi)} - 12\mathcal{W}^2 + EK(\phi)\ . \end{aligned} \tag{3.37}$$

We must ensure that through all these redefinitions we maintain $\mathcal{G}_{,X}^2 \geq 0$. Combining (3.36)–(3.37), we find

$$X\tilde{P}_{,X} - \tilde{P}(X) \geq E - 8\frac{\mathcal{W}_{,\phi}^2}{K^2(\phi)}\left(1 - \frac{1}{\tilde{P}_{,X}}\right). \tag{3.38}$$

This allows for DEC-violation through the kinetic part of the action whenever the right-hand side is negative.

A few limiting cases of these results:

- If $\tilde{P} = X$, corresponding to the two-derivative lagrangian $\mathcal{L} = K(\phi)X - V(\phi)$, we can set $E = 0$ and $\mathcal{G} = 0$. The second of (3.37) reduces to the standard result (3.10) for a single scalar field

$$V(\phi) = 8\frac{\mathcal{W}_{,\phi}^{2}}{K(\phi)} - 12\mathcal{W}^{2}\,. \tag{3.39}$$

- For the pure $P(X)$ case, corresponding to $K(\phi) = 1$ and $V(\phi) = 0$, the second of (3.37) allows us to choose $\mathcal{W} = \mathcal{W}_0 =$ constant, with $E = 12\mathcal{W}_0^2$. The first of (3.37), combined with (3.36), then implies

$$\mathcal{G}_{,X}^{2} = \mathcal{H}(X) = XP_{,X} - P + 12\mathcal{W}_0^2\,, \tag{3.40}$$

  whose integral reproduces (3.33).

3.4 Conclusions

In this Chapter we derived, following two different methods, an extension of the positive energy theorem of General Relativity to the class of $P(X, \phi)$ scalar field theories. We found that as long as it is possible to write P in terms of two arbitrary superpotential-like functions, positive energy is guaranteed. This derivation generalizes the result of [85, 86] for two-derivative scalar theories with arbitrary potential, and reduces to the known condition as a particular case. This result allows for more general P than the recent result of [213], and we highlighted the technical step where our derivation deviates from theirs.

By examining a few special classes of P we showed that in the $P(X)$ context it is

possible to have positive energy while violating the DEC. The derivation does however require that the NEC to be satisfied. More interestingly, it is possible to have positive energy in cases where the S-matrix fails to satisfy the usual analyticity requirements for a local theory.

It is worth noting that we have spent some effort to find a similar method for proving a positive energy theorem for galileons, but to no avail. Here we summarize the obstruction.

We look for positive energy in theories that have the general form

$$\mathcal{L} = P(\pi, X, \Box\pi) \ . \tag{3.41}$$

For example, the cubic galileon (Eq. (1.17)) corresponds to $\mathcal{L} = c_2 X + c_3 X \Box\pi$. As in Section 3.1, we define an equivalent three-field action:

$$\mathcal{L} = P(\pi, \chi, \psi) + P_{,\chi}\,(X - \chi) + P_{,\psi}\,(\Box\pi - \psi) \ . \tag{3.42}$$

Varying with respect to χ and ψ gives $\chi = X$ and $\psi = \Box\pi$, respectively. Substituting these equations of motion back into the Lagrangian gives Eq. (3.41).

Our next step is to temporarily include kinetic terms for χ, ψ. We also integrate the $\Box\pi$ term by parts. Furthermore, we specialize to the action $P = F(\pi, \chi) + \psi G(\pi, \chi)$. The Lagrangian now fits the form of Eq. (3.9), with

$$\phi^{\mathrm{I}} = \begin{pmatrix} \pi \\ \chi \\ \psi \end{pmatrix} \ , \qquad f_{\mathrm{IJ}} = \begin{pmatrix} P_{,\chi} + 2G_{,\pi} & G_{,\chi} & 0 \\ G_{,\chi} & Z_\chi^2 & 0 \\ 0 & 0 & Z_\psi^2 \end{pmatrix} \ . \tag{3.43}$$

The problem is now clear: for the positive energy proof to work, the matrix $f_{\rm IJ}$ must be positive definite in the limit $Z_i \to 0$ (see the comment directly following Eq. (3.9)). But this not the case — one of the eigenvalues is negative, indicating that one of the degrees of freedom is ghostlike.

Several ways forward have been attempted. The first approach was to introduce extra spinor fields, hoping to cancel the negative pieces, but this led to the unusual field space restriction $\Box\pi < -1$ for positive energy. Another approach was to consider the proof in 1+1 dimensions. This led to another unusual field space restriction: $\pi'' < (1 + \pi'^2)^{-1}$.

Neither answer is fully satisfactory. One might imagine that positive energy should be a given, at least for certain galileon terms, because a even free scalar field theory (which admits a positive energy theorem) is dual to a galileon [184]. Nevertheless, no way around the complications from the ghostlike degree of freedom have been found to date.

Chapter 4

Constraints on Chameleon Field Theories

The past two chapters have investigated questions of theoretical viability in scalar-tensor theories. Of course, much may also be learned from experimental efforts as well. In this Chapter we derive constraints on chameleon field theories from atom interferometry, a powerful new test of short-range gravitational interactions. It contains work that appeared in [3].

Ordinary scalar-tensor theories are subject to tight experimental bounds from a variety of tests, including cosmology, astrophysics, and laboratory measurements [90, 215]. Theories that include a screening mechanism are much more weakly constrained by virtue of their dynamical suppression of the scalar force. Regions where experimental measurements are performed, such as the solar system or laboratory, are usually quite dense, leading to an effective decoupling and correspondingly weak force.

Theories within the same class of screening (canonical vs. derivative) all lead to similar phenomenology, even though their Lagrangians may look quite different [7]. Theories with potential screening yield the richest phenomenology on small scales, including in the laboratory and in the solar system. On the other hand, the range of the scalar-mediated force can be at most $\sim$ Mpc cosmologically [216, 217]. Theories with derivative screening have the largest impact on scales larger than $\sim$ Mpc, but presently lead to unmeasurably small effects in the laboratory [218].

Theories with a screening mechanism result in a fifth force that depends on its environment, an idea which has spurred a great deal of activity. Astrophysically, chameleon scalars affect the internal dynamics [219, 220] and stellar evolution [221–223] of dwarf galaxies residing in voids or mildly overdense regions. In the laboratory, chameleons have motivated multiple experimental efforts aimed at searching for their signatures, including torsion-balance experiments [224, 225], Bose-Einstein condensates [226], gravity resonance spectroscopy [92, 227] and neutron interferometry [228–231]. Assuming an additional coupling between photons and chameleons, the CHameleon Afterglow SEarch (CHASE) experiment [232, 233] has looked for an afterglow from trapped chameleons converting into photons. Similarly, the Axion Dark Matter eXperiment (ADMX) resonant microwave cavity was used to search for chameleons [234]. Photon-chameleon mixing can occur deep inside the Sun [235] and affect the spectrum of distant astrophysical objects [236]. For a recent review of chameleon constraints, see [215].

In this Chapter we focus on chameleon scalar field theories, though our methods and results can be generalized to other theories with potential screening (indeed, the next Chapter will focus on similar constraints in symmetron theories). In chameleon theories, the mass of chameleon particles depends on the local environmental matter density, which is the result of an interplay between their self-interaction potential and their coupling to ordinary matter. In dense regions, such as in the laboratory, the mass of the chameleon is large, and the resulting force mediated by the chameleon is short-ranged, shielding the chameleon interaction from detection. In regions of low density, such as in space, the mass of chameleon particles can be much smaller, and the resulting force mediated by the chameleon is long-ranged.

The simplest Lagrangian for a chameleon theory is

$$L_{\rm cham} = -\frac{1}{2}(\partial\phi)^2 - V(\phi) - \frac{\phi}{M}\rho_{\rm m}\,, \tag{4.1}$$

where $\rho_{\rm m}$ is the matter density, assumed to be non-relativistic. The chameleon mechanism is achieved for various different potentials. For concreteness, in this Chapter we will focus on the inverse power-law form [237, 238]

$$V(\phi) = \Lambda^4\left(1 + \frac{\Lambda^n}{\phi^n}\right)\,; \qquad n > 0\,. \tag{4.2}$$

The inverse power-law form, considered in the original chameleon papers [239, 240], is motivated by earlier studies of tracker quintessence models [241, 242] and arises generically from non-perturbative effects in supergravity/string theories, *e.g.*, [243–245]. (Potentials with *positive* powers, $V(\phi) \sim \phi^{2s}$ with s an integer ≥ 2, can also realize the chameleon mechanism [246].) The constant piece can drive cosmic acceleration at the present time for $\Lambda = \Lambda_0 \simeq 2.4$ meV. The $1/\phi^n$ term is responsible for the non-linear scalar interactions required for the chameleon mechanism to be operational.

Our primary interest is atom interferometry, as described in Section 1.3. Following the initial theory papers promoting this method [94, 95], an experiment was carried out by collaborators at UC Berkeley to search and constrain the chameleon parameter space [3, 4, 96]. The experiment measures the force between a metal sphere (the "source" mass) and ^{133}Cs atoms (the "test" mass). Because the experiment is performed in vacuum, the chameleon Compton wavelength is comparable to the size of the vacuum chamber and hence relatively long-ranged on the scale of the experiment. Moreover, due to their microscopic size, the Cs atoms are unscreened and hence act

as test particles. The chameleon force they experience is still suppressed by the fact that the source mass is screened, but less so than the force between two macroscopic objects. This set-up places a bound on the anomalous contribution to the acceleration: $a < 5.5\ \mu\mathrm{m/s}^2$ at the 95% confidence level [96], while an updated version of the experiment reported $a < 50\ \mathrm{nm/s}^2$ [4].

To translate this into a constraint on the chameleon parameter space, the authors of [96] used a number of analytical approximations. Specifically, they treated the vacuum chamber as a sphere and ignored the details of chamber walls. The assumption of spherical symmetry reduces the static equation of motion, which is a three-dimensional partial differential equation (PDE), to a one-dimensional ordinary differential equation (ODE) that can easily be integrated numerically. They then calculated the force between source mass and atoms using approximate analytical expressions derived in the early chameleon papers [239, 240]. In the past these methods have proven to do a fairly good job at estimating the chameleon profile in various situations. But if we are to rigorously exclude part of the chameleon theory space, a more accurate treatment is warranted.

In this Chapter we present a scheme to solve the full three-dimensional PDE for the chameleon profile in the vacuum chamber, making it possible to calculate the force due to the chameleon field at any point and along any direction. This allows us to relax the assumption of spherical symmetry, and to therefore accurately model the cylindrical vacuum chamber used in [96]. Furthermore, we can exactly and consistently include the effects of the chamber walls and the source mass, which is offset from the center, without having to resort to approximate analytical expressions.

The motivations for this work are three-fold. Firstly, the exact approach followed here allows us to quantify the validity of the approximations made in [96], as well to

place rigorous constraints on chameleon theories from the experimental bound on a. Secondly, it allows us to check claims in the literature that accounting for the chamber walls leads to a significant effect on the field profile deep inside the chamber [247] or that the thin-shell expression that goes back to [239, 240] gives a poor approximation to the chameleon force [248]. We will see that these claims are wrong. A detailed treatment of the walls has negligible effect inside the chamber, a conclusion that is now shared by the authors of [247] in a revised version of their paper. We will also find that the thin-shell approximation works remarkably well.

Our main findings are at once reassuring and disappointing! The analytical approximations made in [96] work remarkably well and unexpectedly well. Specifically, carefully simulating the vacuum chamber as a cylinder with dimensions matching those of [96], taking into account the backreaction of the source mass, its offset from the center, and the effects of the chamber walls, the acceleration on a test atomic particle is found to differ by only 20% from the simplified analysis of [96]. A 20% difference would be barely visible on the logarithmic exclusion plots, but the actual difference is even smaller, thanks to a fortuitous cancellation. Namely, while the acceleration in [96] is a slight overestimate (by $\sim 20\%$) of the actual answer, this is compensated by an a slight *underestimate* of the vacuum chamber radius (5 cm instead of the actual 6 cm). These two "mistakes" interfere destructively, leaving us with almost identical constraints on the chameleon parameters.

Looking ahead, our code can be used to determine the ideal source mass geometry and position to optimize the sensitivity to scalar forces in future experiments. In fact, it already has played a role in developing more sensitive atom interferometry tests. Early analysis, briefly reported in Section 4.6, found in addition a number of small improvements that a cylindrical source mass was superior to a spherical one for

optimizing the signal from chameleon forces. These findings were used in an updated version of the experiment which, combined with better control of systematic errors, improved the sensitivity by two orders of magnitude [4].

Although our treatment is cast in the context of atom interferometry, the code is quite versatile and can be applied to *any* experiment — atom interferometry, cold neutrons or a torsion pendulum — aimed at constraining the chameleon field inside a vacuum chamber. To illustrate the usefulness of the code, we will apply it in Sec. 4.6 to forecast the signal in an improved version of our experiment, as well as for a proposed interferometry experiment to take place in NASA's Cold Atom Laboratory aboard the International Space Station. The code is also versatile; in Chapter 5 we use it to place similar constraints on symmetrons, which are an entirely separate class of theories.

This Chapter is organized as follows. We give a brief review of the chameleon mechanism in Sec. 4.1, including a discussion of the thin-shell approximate treatment used in [96]. We summarize existing experimental constraints and motivations for the present work in Sec. 4.2. After a brief description of our numerical method in Sec. 4.3, we present the results of 3D integration as a series of refinements, from the crude "spherical cow" approximation made in [96] all the way to the actual experimental set-up with cylindrical chamber and offset source mass in Sec. 4.4. In Sec. 4.5 we simulate the chameleon profile with the experimental set-up [96] for a range of chameleon parameters, and derive realistic constraints on the space of chameleon theories. In Sec. 4.6 we report results on ongoing and upcoming experiments. We summarize our results and discuss future applications in Sec. 4.7. The work presented in this chapter originally appeared in [3], and since that time the experiment has been updated slightly with correspondingly stronger constraints. The chameleon

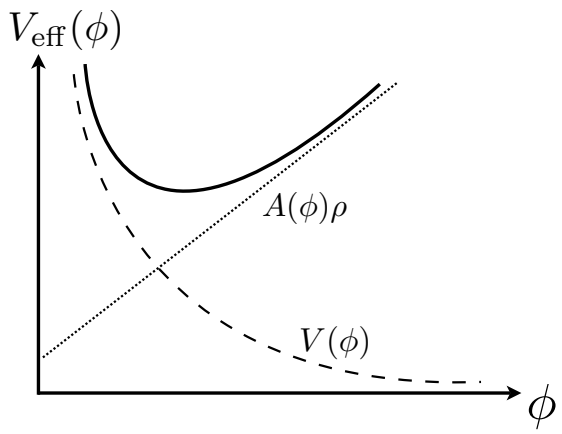

Figure 4.1: Schematic of the effective potential felt by a chameleon field (solid line), given by the sum of the bare potential of runaway form, $V(\phi)$ (dashed line), and a density-dependent piece, from coupling to matter (dotted line).

constraints described here are the latest available [4] at the time of the writing of this Thesis.

4.1 Chameleons: A Brief Review

A chameleon scalar field has the defining property of coupling to matter in such a way that its effective mass increases with increasing local matter density [239, 240, 246, 249–251]. The scalar-mediated force between matter particles can be of gravitational strength (or even stronger), but its range is a decreasing function of ambient matter density, and therefore avoids detection in regions of high density. Deep in space, where the mass density is low, the scalar is light and mediates a fifth force of gravitational strength, but near the Earth, where experiments are performed, and where the local density is high, it acquires a large mass, making its effects short ranged and hence unobservable.

Theoretical set up

In the Newtonian limit where matter is non-relativistic, the Lagrangian for a prototypical chameleon theory is

$$L_{\rm cham} = -\frac{1}{2}(\partial\phi)^2 - V(\phi) - A(\phi)\rho_{\rm m}\,. \tag{4.3}$$

This generalizes (4.1) to include a general coupling function $A(\phi)$ to the matter density $\rho_{\rm m}$. For simplicity, we assume that the chameleon scalar field ϕ couples universally to matter, *i.e.*, via a single function $A(\phi)$. Generalizations involving different coupling functions for different matter species are also possible, resulting in violations of the weak equivalence principle. In the simpler case of interest, the theory is characterized by two functions: the self-interaction potential $V(\phi)$ and the coupling function to matter $A(\phi)$. The coupling function is assumed to be approximately linear,[22]

$$A(\phi) \simeq 1 + \frac{\phi}{M}\,. \tag{4.4}$$

To compare with experiments we will be primarily interested in the range $10^{-5}M_{\rm Pl} \lesssim M \lesssim M_{\rm Pl}$, where $M_{\rm Pl} = (8\pi G_{\rm N})^{-1/2} \simeq 2.4 \times 10^{18}$ GeV is the reduced Planck mass. This range of M is interesting because it has not yet been experimentally ruled out. Over this range, the field excursion is much smaller than M throughout the apparatus, and hence the linear approximation (4.4) is justified.

For the self-interaction potential, as mentioned in the Introduction we specialize to

[22] In the symmetron [252–256] and varying-dilaton [257] mechanisms, on the other hand, a $\phi \to -\phi$ symmetry precludes the linear term in $A(\phi)$. The appropriate form in those classes of theories is $A(\phi) \simeq 1 + \frac{\phi^2}{M^2}$. In practice, however, the phenomenology of symmetrons/varying-dilatons is qualitatively similar to that of the chameleon.

the Ratra–Peebles inverse power-law form [237, 238]

$$V(\phi) = \Lambda^4 \left(1 + \frac{\Lambda^n}{\phi^n}\right) , \tag{4.5}$$

with $n > 0$. The constant piece can drive cosmic acceleration at the present time for $\Lambda = 2.4$ meV, whereas the $1/\phi^n$ piece is responsible for the chameleon mechanism.

It is clear from the action (4.3) that the scalar field is governed by a density-dependent effective potential

$$V_{\rm eff}(\phi) = V(\phi) + A(\phi)\rho_{\rm m} \, . \tag{4.6}$$

This is sketched in Fig. 4.1. In an environment of homogeneous $\rho_{\rm m}$, the effective potential is minimized at

$$\phi_{\rm eq} = \left(\frac{nM\Lambda^{4+n}}{\rho_{\rm m}}\right)^{\frac{1}{n+1}} \, . \tag{4.7}$$

The mass of chameleon particles around this state, defined as usual by $m^2(\phi_{\rm eq}) = \left.\frac{\partial^2 V_{\rm eff}}{\partial\phi^2}\right|_{\phi=\phi_{\rm eq}}$, is

$$m_{\rm eq}^2 = \frac{n(n+1)\Lambda^{4+n}}{\phi_{\rm eq}^{n+2}} \sim \rho_{\rm m}^{\frac{n+2}{n+1}} \, . \tag{4.8}$$

As the value of $\rho_{\rm m}$ increases, we see that $\phi_{\rm eq}$ decreases while $m_{\rm eq}$ increases, as desired. This is sketched in Fig. 4.2.

More generally, to compute the chameleonic acceleration on a test particle due to an arbitrary static distribution of matter, we begin by solving for the ϕ profile:

$$\vec{\nabla}^2\phi = V_{{\rm eff},\phi} \, . \tag{4.9}$$

For general $\rho_{\rm m}(\vec{x})$, we must of course resort to numerical integration. Given the resulting field profile $\phi(\vec{x})$, the acceleration on a test particle due to the chameleon

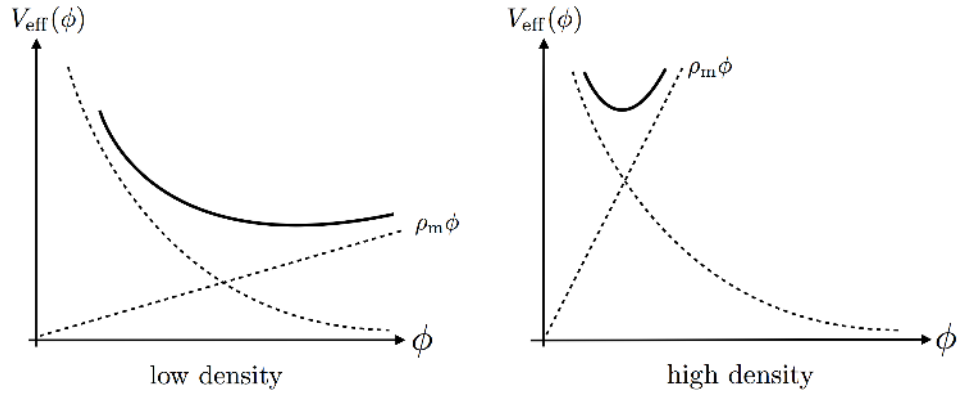

Figure 4.2: Effective potential for low ambient matter density (Left) and high ambient density (Right). As the density increases, the minimum of the effective potential, $\phi_{\rm min}$, shifts to smaller values, while the mass of small fluctuations, m_ϕ, increases.

interaction readily follows from (4.3):

$$\vec{a} = \frac{1}{M}\vec{\nabla}\phi \ . \tag{4.10}$$

For the parameters of interest, we will see that the atoms in the experiment behave as test particles to an excellent approximation. Indeed, this is one of the virtues of using atom-interferometry to test chameleons! More generally, the chameleon force on an extended body can be computed borrowing a method developed by Einstein, Infeld and Hoffmann [258] in the context of General Relativity, as nicely shown in [219] and reviewed in Appendix A.

Thin-shell approximate treatment

Before solving the chameleon equation of motion exactly using numerical integration, it is helpful to gain intuition on how the chameleon force is suppressed in the presence of high ambient density by reviewing the approximate solution first presented in [239, 240]. One of the main goals of this Chapter is to assess to what extent the approximate treatment works.

Consider a static, spherical source with radius R and homogeneous density $\rho_{\rm obj}$. For the moment, we imagine that this object is immersed in a homogeneous medium with density $\rho_{\rm bg}$. (We will come back shortly to the case of the vacuum chamber, where the ambient density is approximately zero.) We denote by $\phi_{\rm obj}$ and $\phi_{\rm bg}$ the minima of the effective potential at the object and ambient density, respectively. The scalar equation of motion reduces to

$$\phi'' + \frac{2}{r}\phi' = V_{,\phi} + \frac{\rho_{\rm m}(r)}{M} \;\; ; \qquad\qquad \rho_{\rm m}(r) = \begin{cases} \rho_{\rm obj} & r < R \\ \rho_{\rm bg} & r > R \end{cases} \;\; . \tag{4.11}$$

The boundary conditions are $\phi'(r=0) = 0$, enforcing regularity at the origin; and $\phi \to \phi_{\rm bg}$ as $r \to \infty$, which minimizes the effective potential far from the source.

For a sufficiently large body — in a sense that will be made precise shortly — the field approaches the minimum of its effective potential deep in its interior:

$$\phi \simeq \phi_{\rm obj} \; ; \qquad\qquad r < R \, . \tag{4.12}$$

Outside of the object, but still within an ambient Compton wavelength away ($r < m_{\rm bg}^{-1}$), the field profile goes approximately as $1/r$: $\phi \simeq \frac{C}{r} + \phi_{\rm bg}$. One integration constant has already been set to fulfill the second boundary condition above. The other constant C is fixed by matching the field value at $r = R$, with the result

$$\phi \simeq -\frac{R}{r}(\phi_{\rm bg} - \phi_{\rm obj}) + \phi_{\rm bg} \, . \tag{4.13}$$

Further intuition on this solution follows from a nice analogy with electrostatics [259, 260]. Since $\nabla^2\phi \simeq 0$ both inside and outside the source, the body acts as a chameleon

analogue of a conducting sphere. Any chameleon "charge" is confined to a thin shell of thickness ΔR near the surface. The surface "charge density" $\frac{\rho_{\rm obj}\Delta R}{M}$ must support the discontinuity in field gradients:

$$\left.\frac{\mathrm{d}\phi}{\mathrm{d}r}\right|_{r=R^+} = \frac{\rho_{\rm obj}\Delta R}{M}\,. \tag{4.14}$$

Substituting (4.13) fixes the shell thickness:

$$\Delta R = \frac{M\phi_{\rm bg}}{\rho_{\rm obj}R}\,, \tag{4.15}$$

where we have assumed $\phi_{\rm bg} \gg \phi_{\rm obj}$ appropriate for large density contrast. For consistency, we should have $\Delta R \ll R$, in other words $\frac{M\phi_{\rm bg}}{\rho_{\rm obj}R^2} \ll 1$. In that case the object is said to be *screened*. The acceleration on a test particle located within $r < m_{\rm bg}^{-1}$ away is

$$a \simeq a_{\rm N}\left(\frac{M_{\rm Pl}}{M}\right)^2\frac{6\Delta R}{R} \qquad \text{(screened)}\,, \tag{4.16}$$

where $a_{\rm N}$ is the Newtonian acceleration. If instead $\frac{M\phi_{\rm bg}}{\rho_{\rm obj}R^2} \gg 1$, the object is said to be *unscreened*, and the exterior acceleration is unsuppressed:

$$a \simeq 2a_{\rm N}\left(\frac{M_{\rm Pl}}{M}\right)^2 \qquad \text{(unscreened)}\,. \tag{4.17}$$

In the case of a vacuum chamber, the background density is so small that the Compton wavelength $m_{\rm bg}^{-1}$ is much larger than the radius of the chamber, hence the field is unable to minimize its effective potential. Instead the scalar field approaches a value about which the Compton wavelength is comparable to the size of the vacuum chamber, $m_{\rm vac}^{-1} \sim R_{\rm vac}$. In other words, from (4.8) the background value is set by the condition $\phi_{\rm vac} \sim (n(n+1)\Lambda^{4+n}R_{\rm vac}^2)^{\frac{1}{n+2}}$. Following [96] it is convenient to introduce

a "fudge" factor ξ, to turn the relation into an equality:

$$\phi_{\rm bg} = \xi\Big(n(n+1)\Lambda^{4+n}R_{\rm vac}^2\Big)^{\frac{1}{n+2}} \ . \tag{4.18}$$

In [96] it was found that ξ is largely insensitive to n, Λ and M, as well as to the assumed chamber geometry. Specifically, for $n = 1$ and the dark energy value $\Lambda = 2.4$ meV, one finds $\xi = 0.55$ for a spherical vacuum chamber and $\xi = 0.68$ for an infinite cylinder.

The field profile for a spherical source inside a spherical chamber follows identically from the earlier derivation, with $\phi_{\rm bg}$ now given by (4.18). In particular the expression for the shell thickness (4.15) becomes $\Delta R = \frac{M\xi}{\rho_{\rm obj}R}\left(n(n+1)\Lambda^{4+n}R_{\rm vac}^2\right)^{\frac{1}{n+2}}$. For the parameter values considered here, it is easily seen that the source mass is always screened, *i.e.*, the resulting acceleration on a test particle is given by (4.16). Similarly, the atoms are unscreened — they do not significantly perturb the chameleon field and therefore behave as test particles to an excellent approximation.

4.2 Existing Constraints and Motivations for this Work

The class of chameleon theories described above are specified by three parameters: the coupling scale M, with $M \sim M_{\rm Pl}$ corresponding to gravitational strength fifth force; the scale of the potential Λ, with $\Lambda = \Lambda_0 \simeq 2.4$ meV corresponding to the value needed to reproduce the observed cosmic acceleration; and the inverse power n specifying the shape of the potential.

Figure 4.3a) shows current experimental constraints in the (Λ, M) plane for $n = 1$, where the solid line indicates $\Lambda = \Lambda_0 \simeq 2.4$ meV. The narrow light blue stripes on the left panel show the influence of varying the fudge parameter over $0.55 \leq \xi \leq 0.68$.

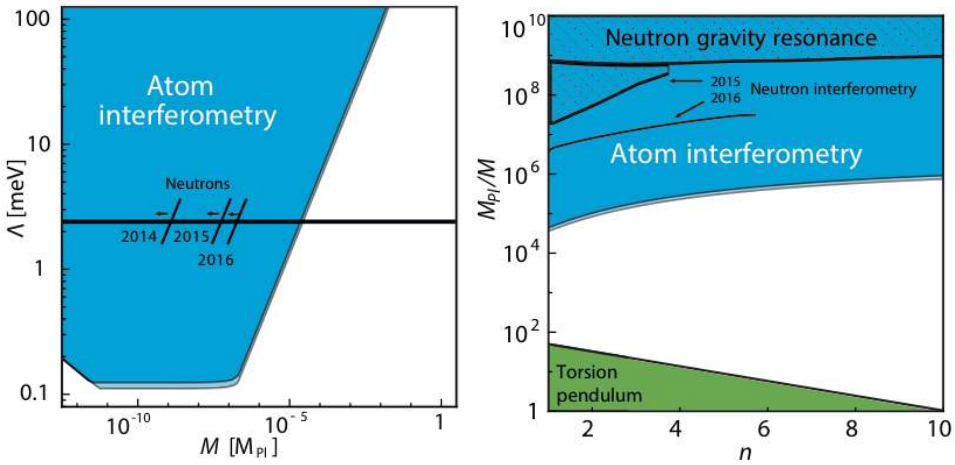

(a) (b)

Figure 4.3: Current constraints due to atom interferometry and torsion pendulum experiments. We are mainly concerned with $\Lambda = \Lambda_0$, indicated by the black line on the first plot, so that the chameleon field can drive the observed accelerated expansion of the universe. The narrow light blue stripes on the left panel show the influence of varying the fudge parameter over $0.55 \leq \xi \leq 0.68$. The second plot shows $M_{\rm Pl}/M$ *vs.* n, and also assumes $\Lambda = \Lambda_0$. The "torsion pendulum" region shown in green has been corrected from [96] to accurately reflect the constraints imposed by that experiment, following [225].

Meanwhile, Fig. 4.3b) plots the excluded region in the (M, n) plane, with Λ fixed to the dark energy value 2.4 meV. Various experiments contribute to these plots. These include measurements of the Casimir-Polder force using an oscillating ^{87}Rb Bose-Einstein condensate [226], gravity resonance spectroscopy using ultracold neutrons [92, 227] and neutron interferometry [228–231]. The Eöt-Wash torsion balance experiment [224] constraint rules out $M \gtrsim 10^{-2}\ M_{\rm Pl}$ with $\Lambda = \Lambda_0 \simeq 2.4$ meV, corresponding to the lower region of Fig. 4.3b).[23]

In this Chapter we focus on the Berkeley atom interferometry experiment [96], which rules out most of the parameter space shown in the figures. At the time the following numerical techniques were developed, for $\Lambda = \Lambda_0 \simeq 2.4$ meV and $n = 1$ (Fig. 4.3a)) atom interferometry excluded the range $M \lesssim 10^{-5}\ M_{\rm Pl}$. (Since that time, sensitivity has improved by over two orders of magnitude, in part due to optimizations made possible by the work developed in this Chapter [4].) The Berkeley experiment, motivated by a theory paper of Burrage *et al.* [94], used atom interferometry to measure the force between ^{133}Cs atoms and an Al sphere. The original experiment constrained an anomalous contribution to the free-fall acceleration as $\Delta a = (0.7 \pm 3.7)\ \mu{\rm m/s}^2$. The excluded regions were then generated using a number of simplifying assumptions:

- The background chameleon field profile $\phi_{\rm bg}$ was computed *i*) without the source mass, *ii*) ignoring the thickness of the chamber walls, and *iii*) assuming a spherical vacuum chamber.

- The chameleon acceleration acting on the atoms was calculated using the thin-shell expression (4.16) described earlier.

The purpose of our Chapter is to check those assumptions. We do so by comput-

[23] As already mentioned in the Introduction, other experiments constrain the electromagnetic coupling $e^{\beta_\gamma \phi} F_{\mu\nu} F^{\mu\nu}$, which induces photon/chameleon oscillations.

ing the chameleon field profile numerically using a 3-dimensional PDE solver that we developed for this purpose. Our numerical method will be described in detail in Section 4.3. We solve for the chameleon field profile inside the source sphere, vacuum chamber, and within the vacuum chamber walls. However, we neglect the backreaction of the atoms, treating them as test particles that do not significantly influence the chameleon field profile. This assumption is justified by the fact that the atoms are small and light enough to be unscreened for the range of parameters considered here. We will perform a battery of checks, described in detail in Sec. 4.4.

For the benefit of the anxious reader, we can summarize our findings succinctly as follows: *the simplifying assumptions made in [96] and listed above work remarkably and surprisingly well.* Specifically, carefully simulating the vacuum chamber as a cylinder with dimensions matching those of [96], taking into account the backreaction of the source mass, its offset from the center, and the effects of the chamber walls, the acceleration on a test atomic particle is found to differ by only 20% from the simplified analysis of [96]. A 20% difference would be barely visible on a logarithmic scale such as in Fig. 4.3, but the actual difference is even smaller, thanks to a fortuitous cancellation. Namely, while the acceleration [96] is a slight overestimate (by $\sim 20\%$) of the actual answer, this is compensated by a slight *underestimate* of the vacuum chamber radius (5 cm instead of the actual 6 cm). These two "mistakes" interfere destructively, leaving us with an identical constraint: $M \lesssim 2.3 \times 10^{-5} M_{\rm Pl}$ is ruled out for $\Lambda = \Lambda_0$. Applying the same methods to the latest experimental constraints [4] gives us a new constraint of $M \lesssim 2.4 \times 10^{-3} M_{\rm Pl}$.

Material	ρ (g/cm^3)
source mass (aluminum)	2.7
vacuum (6×10^{-10} Torr)	6.6×10^{-17}
vacuum chamber walls (steel)	7

Table 4.1: Densities of the materials in the experiment.

4.3 Numerical Method

We integrate the chameleon equation of motion (4.9) through successive under-relaxation with intermediate steps calculated by the Gauss-Siedel scheme [261]. This method is briefly reviewed in the Appendix. We demand that the first derivative of ϕ vanish at the edge of the simulation box, which is justified so long as ϕ has minimized its effective potential by that point. This assumption works because the Compton wavelength of the chameleon particle is always much smaller than the width of the vacuum chamber walls for the parameter range of interest.

The convergence time of this method is highly dependent upon the initial guess for the field configuration. There is a delicate tradeoff — within dense regions (*i.e.*, source sphere and chamber walls), the equation of motion is highly nonlinear, and small steps are required to ensure convergence; within the vacuum region, on the other hand, the equation is approximately linear but can take many steps to reach the much larger field value. Steps small enough to ensure convergence in the dense regions make the convergence time in the vacuum region intolerably large, while steps large enough to converge inside the vacuum make the numerical scheme unstable in dense regions.

To address this issue we begin with a course-grained simulation, where ϕ in the dense areas is forced to minimize its effective potential as a boundary condition. This is done only in regions where the Compton wavelength is more than an order of

magnitude smaller than the grid spacing, so the chameleon is expected to minimize $V_{\rm eff}$ everywhere in the region. The resulting course-grained output for ϕ is then interpolated into an initial guess for a higher resolution run. This method allows ϕ to quickly relax to its solution in the vacuum, while holding ϕ fixed in the numerically unstable regions.

Numerical Algorithm

In this Section we offer some details on the numerical approach used to integrate the chameleon equation of motion (4.9). This equation is a non-linear Poisson-Boltzmann equation of the form:

$$\nabla^2\phi = \rho(x,\phi) \ . \tag{4.19}$$

Let us illustrate the method with the simplest case of one spatial dimension. In that case the Laplacian operator on the left-hand side with a finite difference operator [261]

$$\frac{1}{(\Delta x)^2}\Big(\phi(x+\Delta x) - 2\phi(x) + \phi(x-\Delta x)\Big) = \rho(x,\phi) \ . \tag{4.20}$$

This approximation follows from the second-order Taylor expansion of ϕ, and becomes exact as $\Delta x \to 0$ for smooth functions. Isolating $\phi(x)$ gives a relation that may be used to iteratively solve for ϕ:

$$\phi(x) = \frac{1}{2}\Big(\phi(x+\Delta x) + \phi(x-\Delta x) - (\Delta x)^2\rho(x,\phi)\Big) \ . \tag{4.21}$$

To use this equation, we begin with an initial guess for $\phi(x)$ and apply this equation at each point successively from one edge of the integration to the other. This process is repeated iteratively until $\phi(x)$ converges on a solution. If the neighboring ϕ values on the right-hand side come from the previous iteration, this is known as the Jacobi

method. Using the most recently computed value of ϕ on the right-hand side converges more quickly and is known as the Gauss-Seidel method. We follow the latter method in our numerical integration.

This process generalizes straightforwardly to three dimensions. Here the finite difference expression becomes

$$\begin{aligned}\phi(x,y,z) = \frac{1}{6}\Big(&\phi(x+h,y,z) + \phi(x-h,y,z) \\ &\phi(x,y+h,z) + \phi(x,y-h,z) \\ &\phi(x,y,z+h) + \phi(x,y,z-h) - h^2\rho(x,y,z,\phi)\Big)\ ,\end{aligned} \tag{4.22}$$

where h is the grid spacing. Care must be taken at the edges. In this case we replace any occurrence of the type $\phi(x,-h,z)$ with $\phi(x,h,z)$. This effectively imposes the boundary condition that the normal derivative of ϕ vanish at the edge of the simulation.

Depending on the form of ρ, this algorithm may converge very slowly, or it may not converge at all. We can cure such speed/stability issues by introducing an over/under correction scheme:

$$\phi^{(n+1)}(x) = \phi^{(n)} + \alpha\left(\phi^* - \phi^{(n)}\right)\ . \tag{4.23}$$

Here, $\phi^{(i)}$ represents the i-th iteration of ϕ, and ϕ^* is predicted by Gauss-Seidel based on the previous iteration. Meanwhile, α is the relaxation parameter and can take any value in the interval $0 < \alpha < 2$. For $0 < \alpha < 1$, the algorithm converges more slowly than Gauss-Seidel, but allows for numerical instabilities to be tamed. For $\alpha = 1$ the right-hand side reduces to ϕ^*, hence the method reduces to Gauss-Seidel. If $1 < \alpha < 2$, the method will converge more quickly, but is also more likely to be

unstable. Due to the non-linear nature of the chameleon equation, we encountered significant numerical instabilities, especially in the dense regions. This was cured by taking $\alpha < 1$.

4.4 Successive Steps Towards Realistic Set-Up

In this Section we describe the results of the numerical integration, presented as successive steps towards the realistic experimental set-up. First, to make contact with our earlier analysis, we use the 3D code to check the approximate analytical expression used in [96] to place constraints on the chameleon parameter space. Remarkably, we find only a 20% difference. As our next step, we compare the realistic cylindrical vacuum chamber to a spherical vacuum chamber of the same radius. This will determine how sensitive the force calculation is to the "spherical cow" approximation. Here, we find an 18% difference in the resulting acceleration at the interferometer between these two cases. Next we examine the impact of offsetting the source mass from the center of the vacuum chamber, as is done in the actual experiment. We find the difference in acceleration at the location of the interferometer to be negligible. As our final step, we examine the effect of accounting for a circular bore through the source mass, as in the experiment. Again, we find the difference in acceleration to be negligible. For all the checks performed in this Section (except Sec. 4.4), we assume $\Lambda = \Lambda_0 = 2.4$ meV, $M = 10^{-3} M_{\rm Pl}$, and focus on the power-law $n = 1$ following [96].

Comparison to analytic approximation

As a check on the code, we integrate the chameleon equation of motion under the same conditions as those explored in [96]: a spherical vacuum chamber of radius $R_{\rm vac} = 5$ cm. (As already mentioned, the actual vacuum chamber is not a sphere, and a better estimate for its effective radius is 6 cm, but for the purpose of comparing

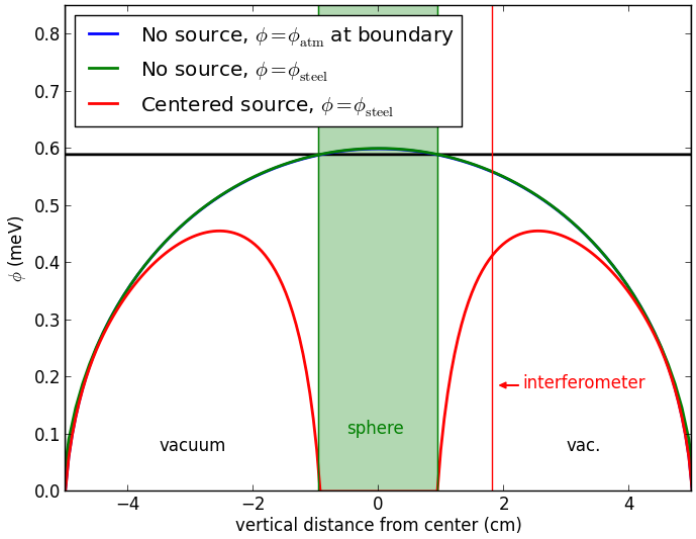

Figure 4.4: The chameleon field as a function of distance along the center of the spherical vacuum chamber. The black horizontal line marks the central value of ϕ predicted inside an empty chamber using (4.18). The red vertical line denotes the location of the interferometer. We find essentially no difference between letting ϕ minimize its potential in atmosphere *vs* in steel at the walls.

with earlier work we use the same parameters as [96]. This includes matching the parameters[24] $\Lambda = 0.1$ meV, $M = 10^{-3} M_{\rm Pl}$.) The field profile is calculated everywhere inside the chamber for 3 separate cases:

1. Without source mass (*i.e.*, empty vacuum chamber), and with boundary condition $\phi \to \phi_{\rm atm}$ at $r = R_{\rm vac}$.

2. Without source mass, and with boundary condition $\phi \to \phi_{\rm steel}$ at $r = R_{\rm vac}$.

3. Including a source mass of radius $r_{\rm s} = 1$ cm at the center of the chamber, imposing the same boundary condition as in Case 2.

The density of the different parts of the experiment are listed in Table 4.1. (For Case 1, we use $\rho = 10^{-3}$ g/cm^3 for atmospheric density.)

[24]The $\Lambda = 0.1$ meV value is chosen solely for the purpose of comparison with the 1D numerical results of [96]. For the rest of our analysis we will use the fiducial dark energy value $\Lambda = \Lambda_0 = 2.4$ meV.

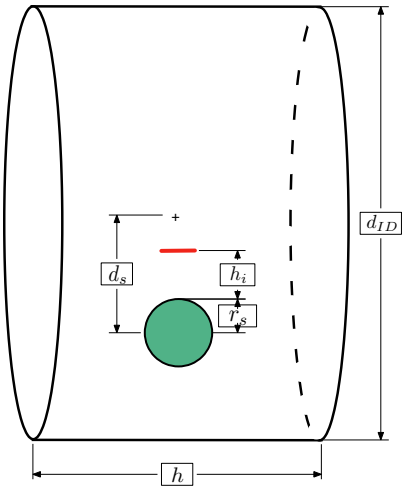

Spherical source radius	$r_{\rm s}$	0.95 cm
Diameter of bore through source	$r_{\rm bore}$	0.30 cm
Location of spherical source	$d_{\rm s}$	2.55 cm
Location of interferometer	$h_{\rm i}$	0.88 cm
Inner diameter of vacuum chamber	$d_{\rm ID}$	12.2 cm
Vacuum chamber height	h	7.1 cm

Figure 4.5: **Diagram and dimensions of experimental setup.** The cross marks the center of the vacuum chamber. The vacuum chamber walls are ~ 2 cm thick, which is much greater than the Compton wavelength of the chameleon inside steel in all cases examined.

The results are shown in Fig. 4.4. The chameleon field profiles in Cases 1 and 2 (*i.e.*, the cases without source mass), shown as the blue and green curves respectively, are virtually identical, leading us to conclude that the boundary conditions imposed at the vacuum chamber walls are unimportant to the dynamics near the center of the vacuum chamber. The black horizontal line indicates the central ϕ value predicted by (4.18) with $\xi = 0.55$, as found in [96]. We see that Cases 1 and 2 closely match this approximate constant solution near the center, in particular at the location of the interferometer (red vertical line), confirming that the code's results are consistent with [96].

Case 3, shown as the red curve, includes the source mass and allows us to calculate the acceleration on a test atom exactly and directly using (4.10). The acceleration is attractive (pointing towards the center) near the source mass, but is repulsive (pointing away from the center, and towards the chamber walls) further out. At

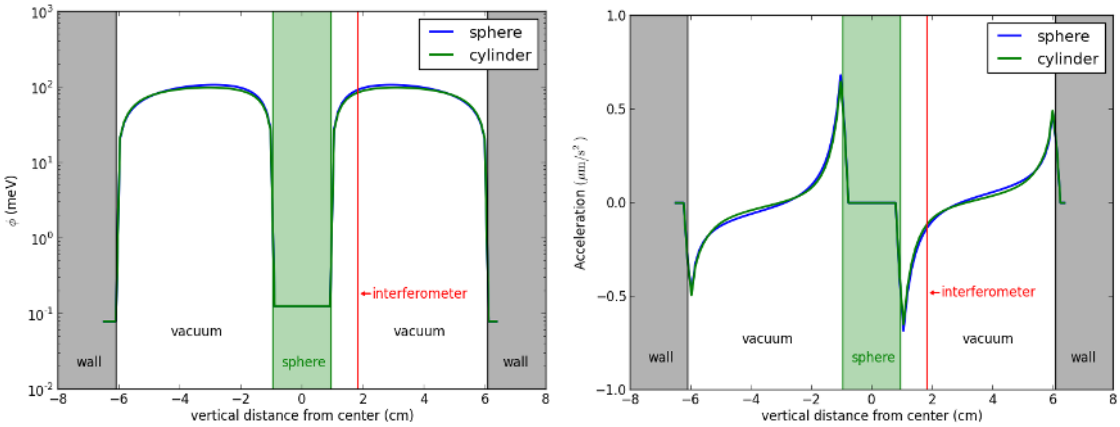

(a) Field profile (b) Acceleration

Figure 4.6: **Spherical *vs* cylindrical vacuum chamber.** Chameleon profile and acceleration as a function of distance from the center of the spherical source mass, for a spherical (blue curve) and cylindrical (green curve) vacuum chamber. The dimensions of the cylindrical vacuum chamber are chosen to match that of the experiment in [96] and are shown in Fig. 4.5. The radius of the sphere is chosen to match the inner radius of the cylinder. At the location of the interferometer (red vertical line), the acceleration in the spherical case is 18% larger than in the cylindrical chamber.

the location of the interferometer,[25] the answer is $a = 5.0 \times 10^{-10}$ m/s^2 towards the source mass. The value calculated in [96] using the approximate "thin-shell" expression (4.16) was 6.4×10^{-10} m/s^2, an overestimate of approximately 20%. (As already mentioned, however, this is compensated by a slight underestimate of the vacuum chamber radius. The actual radius is 6 cm, resulting in a larger acceleration at the location of the interferometer.)

Comparison: spherical vs cylindrical vacuum chamber

Next we examine the effect of approximating the cylindrical vacuum chamber as a sphere. For this purpose we assume a cylindrical geometry that matches the actual vacuum chamber used in the experiment [96]. As shown in Fig. 4.5 (except that the source mass in the present case is centered rather than offset), the vacuum cham-

[25]The atoms actually traverse nearly 5 mm during the acceleration measurement. Following [96], we approximate the atoms' average distance from the source mass as 8.8 mm.

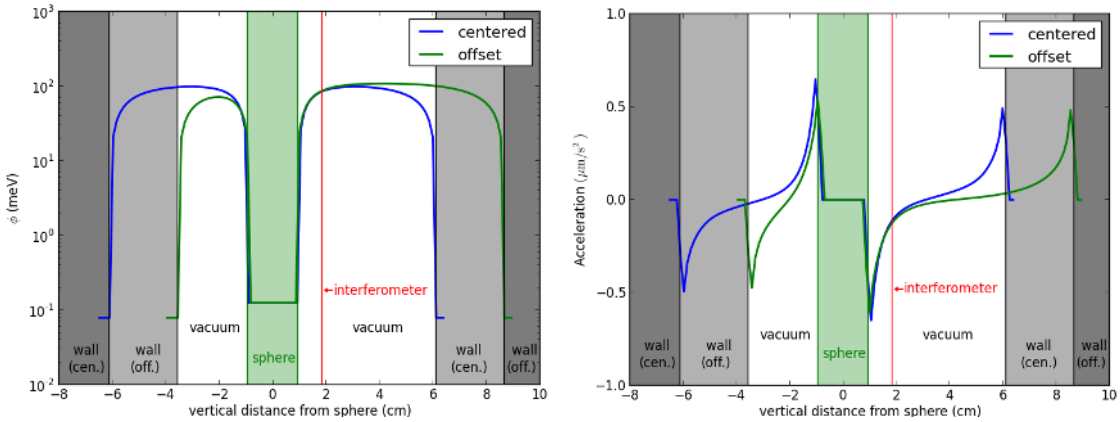

(a) Field profile (b) Acceleration

Figure 4.7: **Source mass centered** *vs* **offset.** Same plot as the previous figure, now comparing a source mass at the center (blue curve) and offset by 2.55 cm from the center (green curve), as in the actual experiment. As in the previous figure, the dimensions of the cylindrical chamber match those of the experiment. Although the field profile is altered by the offset, the acceleration at the interferometer (red vertical line) changes by less than 1%.

ber is a short cylinder, with inner radius of 6.1 cm, turned so that the axis of the cylinder is perpendicular to Earth's gravity. For comparison, we choose a sphere of the same radius, $R_{\rm vac} = 6.1$ cm, such that the distance between the source mass and the vacuum chamber wall is the same in the direction of the interferometer. This makes for a fair comparison since, keeping the distance between the source mass and interferometer fixed, the chameleon gradient at the location of the interferometer is primarily influenced by its distance from the vacuum chamber wall [225]. Recall also that we are now going back to the cosmologically-motivated value of $\Lambda = \Lambda_0 = 2.4$ meV.

The results, shown in Fig. 4.6, demonstrate a minor departure between the cylinder *vs* the sphere. In particular, the acceleration at the interferometer is 18% larger for the sphere than for the cylinder.

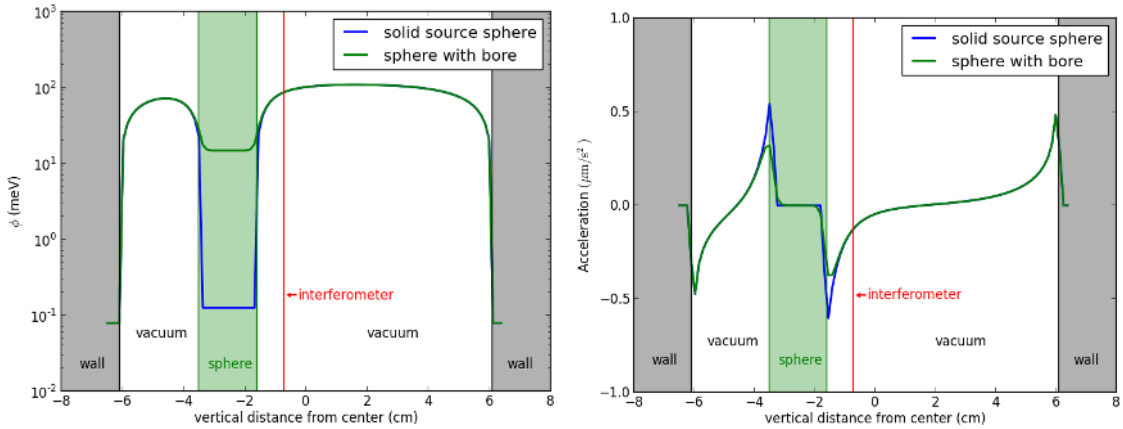

(a) Field profile (b) Acceleration

Figure 4.8: **Source mass with *vs* without bore.** Same as the previous two figures, but now comparing a solid source mass (blue curve) against one with a 3 mm diameter circular bore through the center (green curve), as in the experiment. All other dimensions are chosen to match those of the experiment. The only significant difference is inside the sphere, as the green line passes through the center of the bore, so it is still in vacuum. The acceleration at the interferometer (red vertical line) again changes by less than 1%.

Comparison: source mass offset vs centered

We now examine the effect of moving the source mass away from the center of the cylindrical vacuum chamber. For this purpose we once again assume a cylindrical geometry that matches the actual vacuum chamber used in the experiment [96], with dimensions listed in Fig. 4.5 (except with a solid source mass). We compare the chameleon profile and acceleration between a source mass at the center and a source mass located 2.55 cm below the center, as in the actual experiment. The distance to the interferometer is kept fixed. The results, shown in Fig. 4.7, demonstrate that although the acceleration profiles are different in certain regions of the vacuum chamber, the difference at the interferometer is negligible. Had the interferometer been located further away from the source, the difference in acceleration would have been more significant.

Comparison: solid source mass vs source mass with bore

As a final step towards the experimentally realistic setup, we examine the effect of a vertical circular bore through the center of the spherical source mass. We use the dimensions listed Fig. 4.5, only in one case without the bore. The results, shown in Fig. 4.8, show that the difference in acceleration at the interferometer is again negligible. The difference is, however, significant within the source mass. This is because the plot shows the chameleon profile through the center of the bore, a path which is in vacuum from wall to wall. Indeed, when inside the sphere the bore acts as a miniature vacuum chamber, and the chameleon field reaches a value such that the Compton wavelength is comparable to the radius of the bore.

4.5 Simulation of the Experiment

We are now in position to simulate the experiment [96] and derive realistic constraints on chameleon parameters. Once again the dimensions of the vacuum chamber are sketched and listed in Fig. 4.5. The material densities are listed in Table 4.1. Following [96] and as assumed in the previous Section, we focus on the power-law $n = 1$ and assume $\Lambda = \Lambda_0 = 2.4$ meV.

The chameleon profiles are plotted in Fig. 4.9, for M ranging from $10^{-5}M_{\rm Pl}$ to $M_{\rm Pl}$. The first thing to note from Fig. 4.9 is that the field profile inside the vacuum region is relatively insensitive to M. This can be understood as follows. On the one hand, in the vacuum region the density is effectively zero. Since M only appears in the equation of motion as ρ/M, the chameleon equation of motion is essentially independent of M in that region. The only dependence comes from the dense regions (source mass and chamber walls). But even so, the chameleon is screened and minimizes its effective potential at a very small field value in those dense regions, and for all intents and

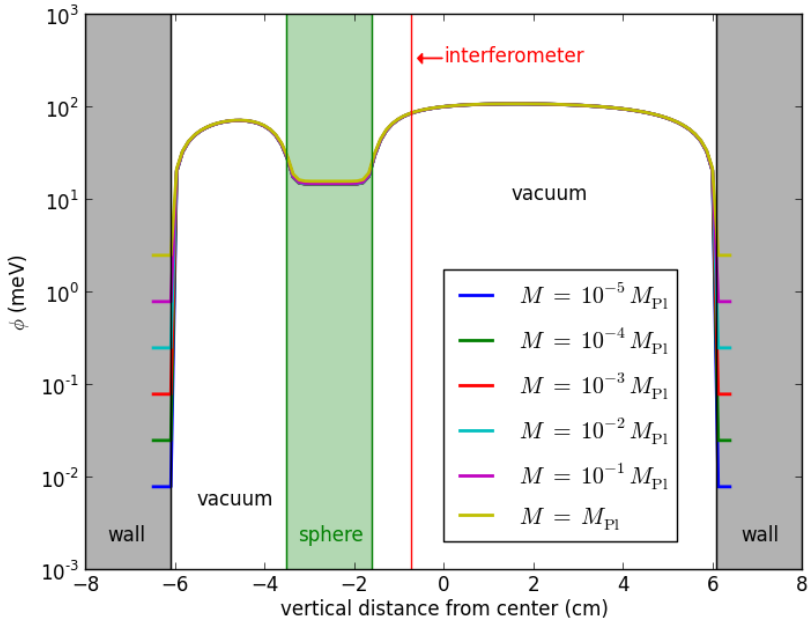

Figure 4.9: Simulation of the experimental configuration, for values of M ranging from $10^{-5}M_{\rm Pl}$ to $M_{\rm Pl}$. We find that the profiles in vacuum are nearly identical, differing only in the walls. The field values inside the metal of the source mass also scale with M, but we are showing a path that passes through the center of the bore in the source mass. The bore acts as a miniature vacuum chamber, so instead the chameleon field goes to an M-independent value such that the Compton wavelength is of order the radius of the bore.

purposes $\phi \simeq 0$ there relative to the much larger field value in the bulk of the chamber. This is why the profile is quite insensitive to M inside the chamber. (For larger values of M than considered here, the source mass and chamber walls eventually become unscreened and this argument would no longer hold.)

The acceleration at the interferometer can be calculated using the gradient of the chameleon profiles. Since $\vec{\nabla}\phi$ at that position is essentially independent of M, the only dependence on this parameter comes from the prefactor of $1/M$ in the expression (4.10) for the acceleration. We find the acceleration due to the chameleon field at the interferometer to be

$$a = \frac{\vec{\nabla}\phi}{M} = 1.2 \times 10^{-4}\ \frac{M_{\rm Pl}}{M}\ \mu{\rm m/s}^2\ . \tag{4.24}$$

As a particular example, with $M = 10^{-4}\ M_{\rm Pl}$ this yields an acceleration at the interferometer of 1.2 μm/s^2. The thin-shell approximate method used in [95, 96] yields an acceleration of 1.4 μm/s^2, a difference of $\sim 20\%$.

The atom interferometry experiment [96] placed an upper limit of $a < 5.5\ \mu$m/s^2 (95% confidence level) on the chameleon acceleration. As can now be calculated from (4.24), this corresponds to $M \leq 2.3 \times 10^{-5} M_{\rm Pl}$. Remarkably, this is the *same constraint* as quoted in [96] using the approximations describe above. The reason for this coincidence is that these authors slightly *underestimated* the radius of the vacuum chamber (5 cm instead of the actual 6 cm), which just so happens to compensate the *overestimate* inherent in the approximate thin-shell method.

The latest atom interferometry measurement, derived using the techniques developed here, measured the anomalous acceleration to be $a < 50$ nm/s^2 at the 95% confidence level [4]. This rules out $M \leq 2.4 \times 10^{-3} M_{\rm Pl}$. Since M is not expected to be much larger than $M_{\rm Pl}$, the window for chameleon theories with $n = 1$ and $\Lambda = 2.4$ meV is rapidly closing!

4.6 Forecasts for ongoing and upcoming experiments

In this Section we describe two upcoming experiments that will place even tighter constraints on the chameleon theory's parameters. The first is an improvement upon the experiment [96], performed by the same authors, and is currently underway. The second is a proposed experiment for NASA's Cold Atom Laboratory aboard the International Space Station.

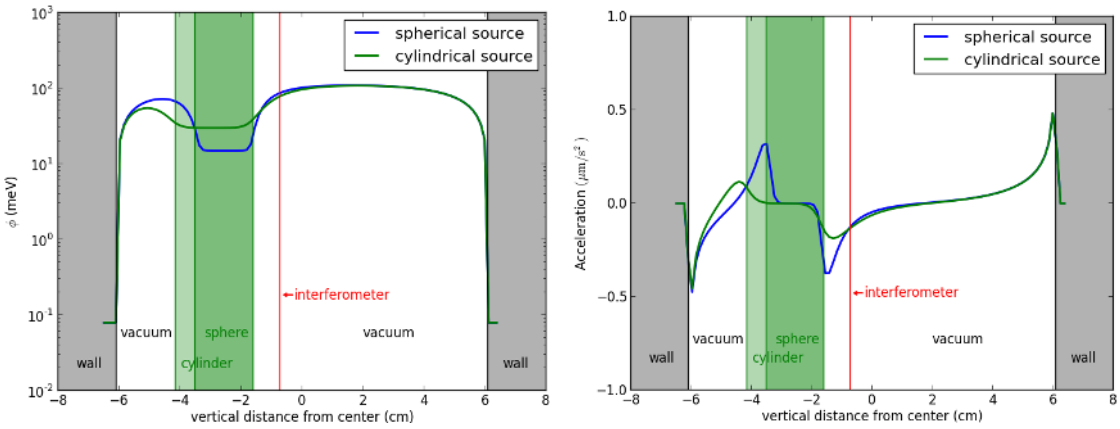

(a) Field profile (b) Acceleration

Figure 4.10: **Spherical source mass** *vs* **cylindrical source.** Comparison between two experimental setups: that of [96] (blue line) and of an improved version of the experiment that is currently underway (green line). The main difference is that the latter employs a tungsten cylinder as the source mass, while the former used an aluminum sphere. The cylinder has a wedge cut out of it, allowing for vastly improved control over systematics. These show that the cutout comes at no cost to the chameleon signal, in fact, the cylinder confers a 5% stronger chameleon force over the previous setup.

Laboratory experiment: cylindrical source with wedge

This experiment is similar to [96], except with greater sensitivity thanks to a variety of technical improvements such as colder atoms, additional vibration isolation, and the atoms are now launched upwards (rather than dropped) to allow them to spend more time near the source mass. Another key difference is that the source mass is now a tungsten hollow cylinder with a wedge cutout. This geometry was chosen so that the source mass may be moved away from the interferometer without breaking the atom/laser beam line, allowing for better control of the systematic errors.

To evaluate the sensitivity of this new setup, we perform a comparison against the geometry described in the previous Section. As before, we assume $\Lambda = 2.4$ meV, $M = 10^{-3} M_{\rm Pl}$, and $n = 1$. The source mass is a hollow cylinder with an outer diameter of 2.54 cm, inner diameter 0.99 cm, and length 2.56 cm. It is made of

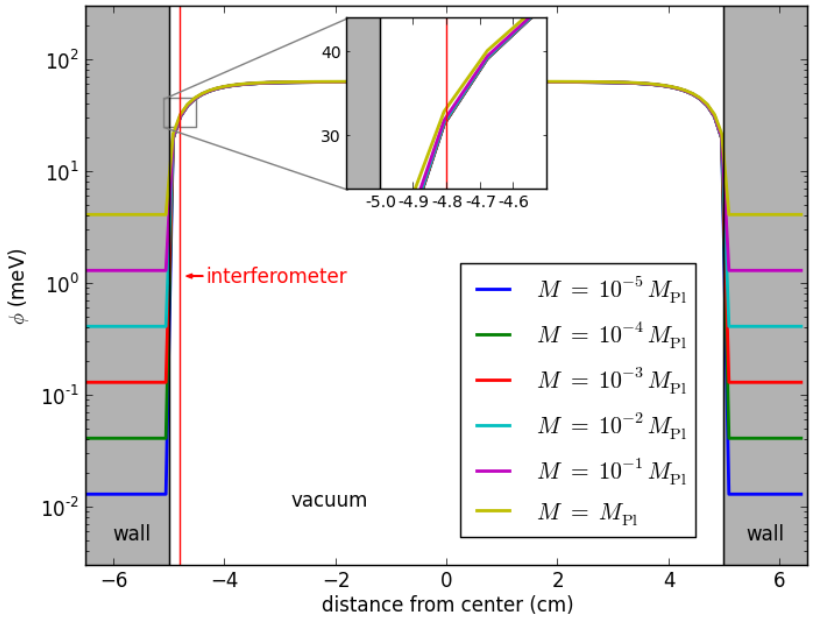

Figure 4.11: Same plot as Fig. 4.9, but for the empty rectangular vacuum chamber of the CAL experiment. The field profiles are taken along the long axis of the vacuum chamber. Again, we find that the profiles in vacuum are nearly identical.

tungsten, which has a density of 19.25 g/cm^3 . There is a wedge cut out of one side with thickness 0.50 cm.

The results, plotted in Fig. 4.10, show that the new setup produces an acceleration that is 5% larger than the previous one. This comes with a large improvement in systematic errors as well, which will allow for much greater sensitivity. The new setup, reported in [4], improved upon the limit from [96] by 2 orders of magnitude, yielding a new experimental bound of $M \leq 2.4 \times 10^{-3} M_{\rm Pl}$.

Space-based experiment: Cold Atom Laboratory

This experiment is proposed to take place inside NASA's Cold Atom Laboratory aboard the International Space Station, and is currently scheduled to be launched in 2017. Ground-based experiments are limited in that Earth's gravity causes the atoms to only spend a limited amount of time near the source mass. Performing the

experiment in space obviates this issue, allowing for greater sensitivity.[26]

The experiment consists of an empty rectangular vacuum chamber with 3×3 cm cross section and length 10 cm. Interferometry is performed with atoms located on an axis parallel, and close, to the central long axis of the vacuum chamber. The atoms' acceleration may be measured anywhere along this path (up to within ~ 0.5 mm of the walls). The walls are made of glass, with a density of roughly 2.5 g/cm^3. We assume the same chameleon parameters as in the previous Section.

The resulting chameleon field profiles along the long axis of the vacuum chamber are shown in Fig. 4.11. If the measurement is performed 2 mm from the vacuum chamber walls, we find an acceleration

$$a = 2.7 \times 10^{-3} \ \frac{M_{\rm Pl}}{M} \ \mu{\rm m/s}^2 \ , \tag{4.25}$$

towards the wall. This value is independent of M (to within 5%) as long as $M \lesssim M_{\rm Pl}$.

This demonstrates that, thanks to how close the atoms may get to the walls, the magnitude of the chameleonic acceleration is similar to that of the ground-based experiments. This result, combined with the much longer interaction times between the source and the atoms, as well as common-mode rejection of the influence of vibrations achieved by running two simultaneous atom interferometers with potassium and rubidium atoms, respectively, gives hope for much tighter restrictions on chameleon parameter space. An optimized version could in principle be designed to be sensitive to the entire parameter space $M \lesssim M_{\rm Pl}$.

[26]Long interaction times may also be achieved in ground-based experiments by dropping both the source mass and the atoms, such as in an Einstein elevator or in a zero-gravity flight [262].

4.7 Conclusions

In this Chapter we have, for the first time, solved the three-dimensional nonlinear PDE governing the chameleon scalar field inside a vacuum chamber, for static configurations. Along the way, through a series of increasingly realistic runs, we have explored the impact of various approximations made in earlier work. In particular, approximating the cylindrical vacuum chamber with a sphere while keeping the distance between the interferometer and the nearest chamber wall fixed, results in an 18% difference in acceleration at the location of the interferometer. Moving the source mass away from the center while keeping the distance to the interferometer fixed, has negligible effect on the measured acceleration. We then solved for the chameleon field in an experimentally realistic setup for $10^{-5}M_{\rm Pl} \leq M \leq M_{\rm Pl}$, finding that the chameleon profile is largely independent of M inside the vacuum chamber. We have ruled out $M < 2.4\times10^{-3}M_{\rm Pl}$ at the 95% confidence level for $n = 1$ and $\Lambda = \Lambda_0$, based on the upper bound on the acceleration reported in [4]. Finally, we have performed a preliminary analysis for upcoming experiments which can, in principle, sense the entire parameter space $M \lesssim M_{\rm Pl}$.

In the future it will be interesting to use the techniques described here to explore the effects of different source mass geometries, as it may be possible to optimize experiments for greater sensitivity. Additionally, as experimental results become more precise, so too should the theoretical predictions. This may necessitate more accurate modeling of the vacuum chamber geometry. Our method may also prove to be an invaluable tool for such a purpose.

Chapter 5

Constraints on Symmetron Field Theories

The symmetron is another theory of modified gravity whose effects could potentially be detected by atom interferometry. The symmetron mechanism [252] (see also the earlier related models [253, 254]) relies on two key ingredients: a nonzero vacuum expectation value (VEV) that depends on the local matter density, and a coupling to matter that depends on the VEV. When the local matter density is small, the VEV is non-zero and so is the matter coupling, so the scalar field mediates an attractive force. When the local density is large, the VEV becomes zero and the coupling vanishes, shutting off the scalar force. This allows the symmetron to mediate an $O(1)$ modification to gravity while going undetected in our solar system, because the local density is enough to suppress the force.

Similar to the previous Chapter with chameleons, this Chapter will detail the theoretical and numerical methods for predicting the symmetron force inside atom interferometry experiments. This is a critical step for accurately placing bounds on symmetron theories. These methods originally appeared in [4].

Symmetrons have seen application to cosmology [255], inflation [263], and as a potential explanation for dark matter [264]. A version where the symmetron mechanism arises from radiative corrections was studied in [265], and a supersymmetric symmetron was introduced in [266].

Existing tests of symmetrons fall into three categories: cosmological, astrophysical, and laboratory. One might imagine that we would need the Earth and Sun to be screened, but it is sufficient (and more conservative) to require instead that the Milky Way is screened [252]. Roughly speaking, doing so also satisfies cosmological tests at linear scales [7]. Symmetron constraints from torsion balance experiments were analyzed in [267]. Data from neutron bounce experiments can also be used to constrain symmetrons, but at the moment these limits are weaker than those derived from atom interferometry [268]. Constraints on the symmetron parameters will be presented briefly in Section 5.1.

We will be interested in what constraints atom interferometry may place on symmetron fields. This experiment used a setup very similar to that of the previous chapter — the acceleration of atoms near a small, marble sized source mass is measured to high precision, allowing one to look for anomalous fifth forces between the atoms and the source mass [4].

Once again, we wish for our constraints on symmetrons to be as precise as possible, carefully accounting for the geometry of the source mass and the vacuum chamber. To gain intuition, we begin with an analytic calculation that approximates the source mass as a sphere. We highlight some important differences from the chameleon calculation, including an effect in which the symmetron field becomes zero everywhere if the size of the vacuum chamber is smaller than the symmetron Compton wavelength. We then go on to repeat the calculation using a numerical strategy that solves for the field on a uniform three-dimensional grid, allowing us to supply the exact experimental setup. We find that the region of parameter space that is excluded by atom interferometry is complementary to the constraints from torsion balance experiments. This Chapter is based on work that first appeared in [4].

5.1 Symmetrons: A Brief Review

A simple example of a theory that exhibits the symmetron mechanism has a self-interaction potential and matter coupling

$$V(\phi) = -\frac{1}{2}\mu^2\phi^2 + \frac{1}{4}\lambda\phi^4 \ , \qquad A(\phi) = 1 + \frac{1}{M^2}\phi^2 \ . \tag{5.1}$$

This potential consists of all renormalizable operators that are invariant under the $\mathbb{Z}_2$ symmetry $\phi \to -\phi$, and the coupling consists of the leading order term that respects that symmetry. These choices yield an effective potential

$$V_{\text{eff}}(\phi) = \frac{1}{2}\left(\frac{\rho}{M^2} - \mu^2\right)\phi^2 + \frac{1}{4}\lambda\phi^4 \ , \tag{5.2}$$

with a corresponding equation of motion

$$\Box\phi = \left(\frac{\rho}{M^2} - \mu^2\right)\phi + \lambda\phi^3 \ . \tag{5.3}$$

The matter coupling is quadratic in ϕ, so the fluctuations in the scalar field see a matter coupling that is dependent on the local scalar field value. If we split the field into background and fluctuations as $\phi = \bar{\phi} + \delta\phi$, then the fluctuations $\delta\phi$ see a matter coupling $\frac{\bar{\phi}}{M^2}\rho$.

In regions of low density, $\frac{\rho}{M^2} \ll \mu^2$, the quadratic term in Eq. (5.2) is negative and the field acquires a nonzero VEV: $\phi_0 \equiv \mu/\sqrt{\lambda}$. However, in high density regions where $\frac{\rho}{M^2} \gg \mu^2$, the quadratic term becomes positive and the potential has a minimum $\phi = 0$. Since the matter coupling is dependent on the local field value, the symmetron decouples from matter in dense environments. This is the essence of the symmetron screening mechanism: the matter coupling vanishes inside large, dense

objects, causing the symmetron force sourced by such objects to be much weaker than their ordinary gravitational pull.

The symmetron parameters are typically chosen such that the force on a test particle in vacuum is an $O(1)$ modification to gravity, $\phi/M^2 \sim 1/M_{\rm Pl}$. The symmetry-breaking density is also typically chosen to be approximately the mean cosmic density today $\mu^2 M^2 \sim H_0^2 M_{\rm Pl}^2$ [252, 268]. Current tests focus on the possibility $\mu \sim$ meV, for this choice the excluded region is approximately $M \gtrsim$ 10 GeV and $\lambda < 1$ [267].

We will be interested in static, spherically symmetric solutions of Eq. (5.3). To this end, we solve for the symmetron field profile around a sphere of density $\rho \gg M^2\mu^2$ and radius R in a vacuum.

Expanding the symmetron effective potential Eq. (5.2) to quadratic order around the minima inside and outside the object, the linearized equation of motion may be solved in the two regions separately:

$$\begin{aligned} \phi(r < R) &= A\frac{R}{r}\sinh\left(r\sqrt{\frac{\rho}{M^2} - \mu^2}\right) \ , \\ \phi(r > R) &= B\frac{R}{r}e^{-\sqrt{2}\mu r} + \phi_0 \ , \end{aligned} \tag{5.4}$$

where the constants A, B are determined by matching ϕ and ϕ' at $r = R$. The exact relationship form of A, B depends on the dimensionless parameter $\alpha \equiv \frac{\rho R^2}{M^2} = 6\frac{M_{\rm Pl}^2}{M^2}\Phi$. There are two limiting cases to consider:

$$B = \begin{cases} -\phi_0 \frac{\alpha}{3} & \alpha \ll 1 \quad \text{(unscreened)} \ , \\ \phi_0\left(-1 + \frac{1}{\sqrt{\alpha}}\right) & \alpha \gg 1 \quad \text{(screened)} \ . \end{cases} \tag{5.5}$$

The acceleration of a test particle due to the symmetron force follows from Eq. (A.19)

as

$$\vec{a}_\phi = \frac{\phi_0}{M^2}\vec{\nabla}\phi \ . \tag{5.6}$$

Dividing the screened force by the unscreened one leads to the screening factor

$$\lambda_i = \min\left(\frac{1}{\alpha_i}, 1\right) \tag{5.7}$$

for an object with a surface Newtonian potential Φ_i.

Note that Eq. (5.4) implies an exponential dropoff in the scalar acceleration beyond μ^{-1}. Beyond this point, the force is much harder to detect. For a given μ there is therefore a maximum distance from the surface of the source mass to the atoms Δ which will still result in a measurable force. So the experiment will only measure a significant force if $\Delta \lesssim \mu^{-1}$.

We must also consider the finite size of the vacuum chamber. For a given μ, there is a minimum size vacuum chamber which can result in a nonzero symmetron field [267]. To see this, consider a 1-dimensional gap of length d, where $\rho = 0$ inside the gap, and the walls are infinitely dense so $\phi_{\text{walls}} = 0$. The symmetron field will reach its VEV at roughly a distance $m_{\text{vac}}^{-1} = \mu^{-1}$ from the walls. Approximating the field as linear[27], so $\vec{\nabla}\phi \approx \mu^2/\sqrt{\lambda}$, the Hamiltonian simplifies as

$$\begin{aligned} H &= \int dx \left(\frac{1}{2}(\vec{\nabla}\phi)^2 + V_{\text{eff}}(\phi)\right) \ , \\ &\approx \frac{\mu^4}{\lambda} m_{\text{vac}}^{-1} - \frac{1}{4}\frac{\mu^4}{\lambda} d \ . \end{aligned} \tag{5.8}$$

The Hamiltonian is negative for $d \gtrsim m_{\text{vac}}^{-1}$, that is, $d \gtrsim \mu^{-1}$. Therefore it is only for gaps larger than this that a nontrivial field profile is energetically favorable to

[27] A more detailed calculation in [267], which integrated the solutions to the equation of motion, differs in its final answer by a factor of π.

remaining at $\phi = 0$ everywhere, where $H = 0$.

This translates to a fairly narrow window of sensitivity in μ for atom interferometry experiments. For a given experimental setup, a non-negligible symmetron force will only exist for $d^{-1} \lesssim \mu \lesssim \Delta^{-1}$. Since $\Delta/d \approx 10$ to 100, there is at most only 1-2 orders of magnitude in μ which are testable. In the latest atom interferometry experiment [4] the window is roughly $10^{-2} \lesssim \mu \lesssim 10^{-1}$ meV.

5.2 Numerical analysis

Our goal is to solve the static symmetron equation of motion for an arbitrary matter distribution $\rho = \rho(\vec{x})$:

$$\vec{\nabla}^2\phi = \left(\frac{\rho}{M^2} - \mu^2\right)\phi + \lambda\phi^3 \ . \tag{5.9}$$

This equation appears to have three free parameters: μ, M, and λ. However, the solutions' dependence on λ turns out to be trivial, and is easily inferred by considering the field redefinition $\hat{\phi} \equiv \sqrt{\lambda}\phi$. Under such a change the parameter λ drops out completely, telling us that the combination $\sqrt{\lambda}\phi$ is independent of λ.

Similarly, in vacuum $\rho/M^2 \ll \mu^2$, and for all practical purposes $\rho \approx 0$, while in the source mass or vacuum chamber walls the opposite is true, and $\rho \approx \infty$. We therefore expect the field profiles will be largely independent of M, since it only appears in the combination ρ/M in Eq. 5.9. Of course, the symmetron force still depends sensitively on M via Eq. (5.6).

These findings simplify matters considerably. Rather than scan a parameter space of three independent parameters, we merely perform a single computation for each value of μ we are interested in. Furthermore, the range of testable μ in atom interferometry is only 1-2 orders of magnitude, allowing us to fully predict the symmetron force for

a large range of M and *all* λ with a relatively small computational requirement.

We adopt the same technique used for chameleons, solving for the field on a uniform grid with the Gauss-Seidel relaxation scheme detailed in Chapter 4. Once again, the solution is highly unstable inside dense regions, so we provide boundary conditions that set the field to minimize its effective potential there. This is justified so long as the grid size is much less than the thin-shell width ΔR. Computing the thin-shell width from the screening factor (Eq. (5.7), see also Appendix A) as $\lambda_{\rm source} \sim \Delta R/R$, we find

$$\Delta R = \frac{M^2}{M_{\rm Pl}^2}\frac{R}{6\Phi} \ . \tag{5.10}$$

Another bit of relevant physics that cannot be captured by the simulation is the screening of the atom. The radius of an atom is many orders of magnitude smaller than the grid spacing (which is roughly 0.1 mm). This is not a problem if the atoms are unscreened — in this limit, the atoms behave as ideal test particles, obeying Eq. (1.5). The non-linear effects due to the source mass and the vacuum chamber walls are fully captured in our solution of ϕ. We can account for atomic screening by simply adding the screening factor to Eq. (1.5):

$$\vec{a} = \lambda_{\rm atom}\frac{\phi}{M^2}\vec{\nabla}\phi \ . \tag{5.11}$$

The resulting field profile is shown in Fig. 5.1. We have plotted the combination $\lambda\phi\vec{\nabla}\phi$ along the vertical axis of the experiment. This term is proportional to the scalar acceleration and is independent of M and λ. We have plotted for two values of μ, which are both within the allowed window which still yields measurable forces. The larger value of μ results in a force that is stronger, yet shorter-ranged force since the effective symmetron mass is $\sim \mu$. The smaller value of μ results in a force with

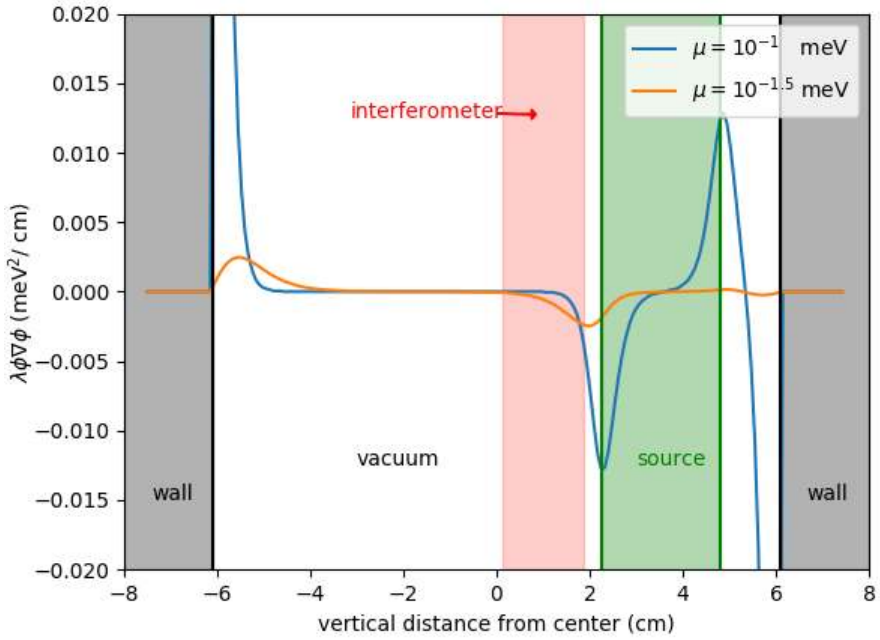

Figure 5.1: Symmetron field profiles for $M = 10^3$ GeV, $\lambda = 10^{-5}$, and $\mu = 10^{-1}, 10^{-1.5}$ meV, plotted along the vertical axis of the vacuum chamber. The atoms follow a vertical path that takes them near the source mass; the interferometry measurement occurs in the red region near the apex of their trajectory. The combination $\lambda\phi\vec{\nabla}\phi$ is displayed because it is independent of M and λ and is easily relatable to the scalar acceleration Eq. (5.11). (Note that this is the λ that appears in the Lagrangian, not the thin-shell factor $\lambda_{\rm atom}$.) The two curves illustrate the window of measurable μ nicely: for larger μ, the overall force is stronger, yet shorter-ranged, and much larger μ would result in a force that cannot reach to the interferometer. For smaller μ, the force is weaker yet longer-ranged, suppressed because the vacuum chamber is not large enough for the field to reach its VEV.

longer range, but it is is suppressed by the finite size of the vacuum chamber. Smaller values of μ would result in a field that remains at $\phi = 0$ everywhere inside the vacuum chamber, causing the scalar force to vanish.

Finally, in light of the fact that the experiment measures the average acceleration felt by the atoms during a measurement of finite time, we integrate the above acceleration assuming that the atoms follow the classical path $z(t)$ determined by their initial

position and velocity:

$$a_{\rm avg} = \frac{1}{t_{\rm f} - t_{\rm i}} \int_{t_{\rm i}}^{t_{\rm f}} a(z(t)) {\rm d}t \ , \tag{5.12}$$

where $t_{\rm i}$ and $t_{\rm f}$ are the beginning and end of the measurement (the first and third laser pulses, respectively).

The constraints on the parameters are plotted in Fig. 5.2. The symmetron force gets stronger with decreasing M, hence the power-law seen in the figure. When $M \lesssim 1$ GeV the atoms no longer behave as test particles and begin to be screened, so the exclusion plot flattens. Finally, below $M \sim 10^{-4}$ GeV, the vacuum density is large enough that the symmetry remains unbroken, so $\rho/M^2 > \mu^2$ everywhere in the experiment and the symmetron force vanishes.

We see that constraints from atom interferometry have rapidly sharpened since the first study was published in 2015. Furthermore, they are somewhat complementary to torsion balance experiments [113], providing two ways to test different regimes of the theory.

5.3 Conclusion

We have examined symmetron fields within the context of atom interferometry experiments. We began with an analytic derivation of the symmetron force, gaining intuition for the problem by deriving the screening factors and thin-shell widths for the atom and sphere, and carefully analyzing the behavior of the symmetron field in a vacuum chamber of finite size. These findings were further supported by a numerical calculation that more accurately accounts for the experimental setup. Finally, these results were used to exclude regions of allowed parameter space for symmetron fields.

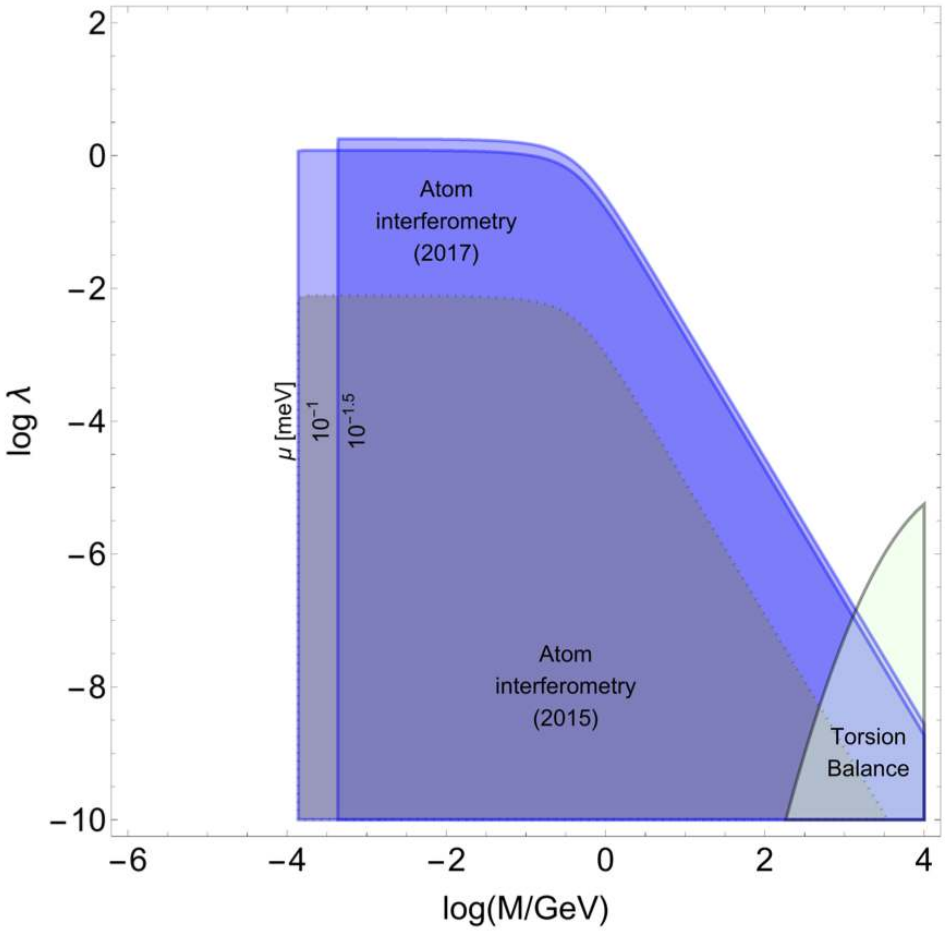

Figure 5.2: Shaded areas are excluded regions of parameter space. The areas in blue are constrained by the latest atom interferometry data [4]. For comparison we have included older atom interferometry [96], as well as data from torsion balance experiments [225].

Chapter 6

Conclusions

This Thesis has explored several related questions concerning the viability of scalar field theories. In Chapter 2 we constructed a healthy theory that violates the null energy condition, providing a powerful counterexample to the notion that violating the NEC always goes with an instability. This model, which was published several years ago, has already helped inspire a new generation of NEC-violating theories, which make several major improvements to our own. One major drawback of our model was that at late times the scalar field becomes strongly coupled and the EFT breaks down. Several of these new theories have fixed this issue [185, 187], providing a graceful exit to the NEC-violating phase.

In Chapter 3 we presented a positive energy theorem for $P(X)$ theories. Perhaps one of the most surprising findings was that the Ghost Condensate model (Eq. 1.11) with $\alpha = -1$, which is known to be locally pathological, was discovered to have global positive energy. This result highlights the distinction between local and global criteria for a healthy field theory, with the latter likely being more difficult to violate. Looking forward, it will be interesting to see if a positive energy theorem can be proven for galileons.

Chapters 4 and 5 considered questions of phenomenological viability, focusing in particular on what may be learned from atom interferometry experiments. Atom interferometry is a relative newcomer to the ongoing search for evidence of scalar fields, yet it is already competitive with, and complimentary to, many of the long-

established experimental techniques. Time will only improve their sensitivity, and it is entirely possible that some models (such as the simple $n = 1$ chameleon) are close to being ruled out completely. The calculational tools we presented have already been invaluable for understanding and interpreting experimental results and optimizing sensitivity. In the future, these methods could be extended to a wider range of theories (*i.e.* $P(X)$ and galileons) as well as to other experimental setups, ranging from torsion balance experiments to galaxy-wide measurements, possibly even to tests and theories that have yet to be imagined.

Appendix A

Screening Factors

In this Appendix we make precise the statements about screening in or near "sufficiently" large or dense objects. As a model problem, we will calculate the force between a large sphere of radius R_A and a much smaller sphere of radius R_B, both of uniform density $\rho_{A,B}$. Both are surrounded by a background density ρ_0.

A.1 The field from a single object

We begin by finding the scalar field due to A by itself. Inside and outside the object, we expand the Lagrangian to quadratic order around the value that minimizes its effective potential in that region: $\phi = \phi_i + \varphi_i$, where $V_{\rm eff},_{\phi_i} = 0$. The quadratic Lagrangian for perturbations φ is

$$\begin{aligned}\mathcal{L}_\varphi &= -\frac{1}{2}(\partial\varphi)^2 - \frac{1}{2}V_{\rm eff},_{\phi\phi}(\phi_i)\varphi^2 \ , \\ &= -\frac{1}{2}(\partial\varphi)^2 - \frac{1}{2}m_{\rm eff}^2\varphi^2 \ ,\end{aligned} \tag{A.1}$$

where we have defined the effective mass of the perturbations $m_{\rm eff}^2 = V_{\rm eff},_{\phi\phi}$. The resulting equation of motion is

$$\varphi'' + \frac{2}{r}\varphi' = m_{\rm eff}^2\varphi \ , \tag{A.2}$$

where we have specialized to static and spherically symmetric solutions. Assuming the mass is constant, the solution is

$$\varphi = \frac{C_1 e^{-mr}}{r} + \frac{C_2 e^{mr}}{r} \ . \tag{A.3}$$

In general m can vary with the local environmental density. We therefore solve for the field piecewise inside and outside the sphere, and then matching ϕ and its first derivative at the boundary.

Inside the sphere, we require ϕ' to vanish at the origin, giving

$$\phi(r < R_A) = \phi_{\rm in} - \frac{A \sinh(m_{\rm in} r)}{r} \ . \tag{A.4}$$

For the solution outside the sphere we demand that the field tend to a constant at infinity, so

$$\phi(r > R_A) = \phi_{\rm out} + \frac{B e^{-m_{\rm out}(r-R)}}{4\pi r} \ . \tag{A.5}$$

The coefficients A, B are determined by matching ϕ, ϕ' at the boundary R_A. Only B is of present interest:

$$B = 4\pi(\phi_{\rm out} - \phi_{\rm in}) R \left(\frac{m_{\rm in} R - \tanh(m_{\rm in} R)}{m_{\rm in} R + m_{\rm out} R \tanh(m_{\rm in} R)} \right) \ . \tag{A.6}$$

This term is the "scalar charge" of the object.

We can gain some intuition by considering an alternate derivation of the scalar force [219]. Consider the scalar equation of motion,

$$\vec{\nabla}^2 \phi = \frac{\partial V}{\partial \phi} + \alpha \rho \ , \tag{A.7}$$

where α is an expansion of the coupling function $A(\phi)$. Our goal is to write the exterior solution as

$$\phi = \phi_{\rm out} - \frac{\lambda \alpha M}{4\pi r} \ . \tag{A.8}$$

This is very similar to Eq. (A.5), except we have included only the monopole contribution, and have expressed the total scalar charge as $B = \lambda \alpha M$, where M is the mass of the object, α is the coupling strength, and λ is a screening factor which varies between 0 and 1 based on how screened the object is.

Assuming that the field is able to minimize its effective potential inside the object, it sits at a constant value $\phi_{\rm in}$ everywhere inside, except for a thin shell near the surface. The field only varies within the thin shell, where rises from the minimum to meet the surface boundary condition.

To get a rough idea for the thickness ΔR of the thin shell, we approximate Eq. (A.7) as

$$\frac{1}{R} \frac{\phi_{\rm out} - \phi_{\rm in}}{\Delta R} \approx \alpha \rho \ . \tag{A.9}$$

Defining the mass of the object $M = \rho 4\pi R^3/3$, the thin shell thickness is

$$\frac{\Delta R}{R} \approx \frac{\phi_{\rm out}}{6 \alpha M_{\rm Pl}^2 \Phi} \ , \tag{A.10}$$

where we have assumed $\phi_{\rm out} \gg \phi_{\rm in}$ and have used the surface Newtonian potential of the object $\Phi = GM/R.$. Since only the matter inside the thin shell is relevant to the external field, the screening factor λ must be the fraction of the volume inside the

thin shell:

$$\begin{aligned}\lambda &= 3\frac{\Delta R}{R} \ , \\ &= \frac{\phi_{\rm out}}{2\alpha M_{\rm Pl}^2 \Phi} \ ,\end{aligned} \tag{A.11}$$

This quantity expresses the fraction of the "bare charge" αM of the object that is felt by external test particles. An unscreened object has $\lambda \sim 1$, and a strongly screened object has $\lambda \sim 0$.

A.2 Motion of an extended object

In the previous Section we calculated the scalar field due to a spherical object. We would now like to understand how an object moves in the presence of the scalar field.

A point particle feels an acceleration given by Eq. (1.5). An extended object, on the other hand, may be screened, as seen in the previous Section. We follow an approach originally introduced for GR by Einstein, Infeld, and Hoffman [258], and later applied to scalar field theories in [219] .

The momentum of the object is

$$P_i = \int d^3x T_i{}^0 \ , \tag{A.12}$$

where the energy-momentum tensor is a combination from the matter and the scalar field: $T_{\mu\nu} = T^{\rm m}_{\mu\nu} + T^{\phi}_{\mu\nu}$. The volume is performed over a spherical volume that is large enough encompass the entire object, so that $T^{\rm m}_{\mu\nu}$ vanishes at the surface. The sphere should also be small enough that the matter dominates $T_{\mu\nu}$ inside the sphere, so that Eq. (A.12) is a good approximation for the motion of the object itself.

The change in the momentum with time is

$$\begin{aligned}\dot{P}_i &= \int d^3x \partial_0 T_i{}^0 \ , \\ &= -\int dS_j T^{\phi}_i{}^j \ . \end{aligned} \tag{A.13}$$

where we have used conservation of the energy-momentum tensor $\partial_\nu T^{\mu\nu} = 0$ and Gauss' Law to turn it into a surface integral. Finally, since the matter energy-momentum tensor vanishes at the surface of the spherical volume, only the contribution from the scalar field survives.

The scalar field is a sum of the background contribution, presumably sourced by some object far away, and a piece sourced by the object itself:

$$\phi = \phi_0(\vec{x}) + \phi_1(r) \ . \tag{A.14}$$

The background field is assumed to be linear on the length scale of the object:

$$\phi_0 \approx \phi_0(0) + \partial_i \phi_0(0) x^i \ , \tag{A.15}$$

where the origin of the coordinates x^i is the center of the object. At the moment, all we require of $\phi_1(r)$ is that it is spherically symmetric.

We substitute our expression for the field into the scalar energy-momentum tensor:

$$T^{\phi}_{\mu\nu} = \partial_\mu \phi \partial_\nu \phi - \eta_{\mu\nu} \left(\frac{1}{2} (\partial\phi)^2 + V_{\text{eff}}(\phi) \right) \ , \tag{A.16}$$

and plug in to Eq. (A.13). Remarkably, we find

$$\dot{P}_i = -4\pi r^2 \partial_i \phi_0 \partial_r \phi_1(r) \ . \tag{A.17}$$

The simplicity of this final expression is due to a number of cancellations in the surface integral. The term like $\partial_i\phi_0\partial_j\phi_0$ is neglected because gradients of the background field are small, the term like $\partial_i\phi_1\partial_j\phi_0$ integrates to zero because it is a surface integral of a uniform vector field, and the term like $\partial_i\phi_1\partial_j\phi_1$ integrates to zero because both terms are spherically symmetric. The second part of $T^{\phi}_{\mu\nu}$ is sub-leading, because we have in mind that the field is mainly sourced by the object itself rather than its potential.

If we assume ϕ_1 is of the form in Eq. (A.5), then the scalar force on the object is

$$F_i = -\partial_i\phi_0(1 + m_{\rm out}R)\lambda\alpha M \ , \tag{A.18}$$

where we have performed the integral at the surface of the object (so that $r = R$), and have equated the change in momentum with a force acting on the center of mass of the object.

Assuming that the field from A is also given by Eq. (A.5), we are now able to find the scalar force between two objects A and B, separated by a distance r, where $M_B \ll M_A$. It is:

$$F_\phi = -(\lambda_A\alpha M_A)(\lambda_B\alpha M_B)(1 + m_{\rm out}r)(1 + m_{\rm out}R_B)\frac{e^{-m_{\rm out}(r-R_A)}}{4\pi r^2} \ . \tag{A.19}$$

This expression gives the force between two extended objects (where A is much larger than B) in any theory with potential screening. Of particular interest is the appearance of *two* screening factors, one for each object, as well as a Yukawa-type force law.

Taken together, we see that screening very efficiently suppresses the force between two large, massive objects or over long distances. The force laws derived for chameleons and symmetrons, in Chapters 4 and 5 respectively, are special cases of this expression.

References

[1] B. Elder, A. Joyce, and J. Khoury, "From Satisfying to Violating the Null Energy Condition," *Phys. Rev.*, vol. D89, no. 4, p. 044027, 2014.

[2] B. Elder, A. Joyce, J. Khoury, and A. J. Tolley, "Positive energy theorem for $P(X, \phi)$ theories," *Phys. Rev.*, vol. D91, no. 6, p. 064002, 2015.

[3] B. Elder, J. Khoury, P. Haslinger, M. Jaffe, H. Müller, and P. Hamilton, "Chameleon Dark Energy and Atom Interferometry," *Phys. Rev.*, vol. D94, no. 4, p. 044051, 2016.

[4] M. Jaffe, P. Haslinger, V. Xu, P. Hamilton, A. Upadhye, B. Elder, J. Khoury, and H. Müller, "Testing sub-gravitational forces on atoms from a miniature, in-vacuum source mass," *Nat. Phys.*, 2016.

[5] S. Deser, "Selfinteraction and gauge invariance," *Gen. Rel. Grav.*, vol. 1, pp. 9–18, 1970.

[6] T. Clifton, P. G. Ferreira, A. Padilla, and C. Skordis, "Modified Gravity and Cosmology," *Phys. Rept.*, vol. 513, pp. 1–189, 2012.

[7] A. Joyce, B. Jain, J. Khoury, and M. Trodden, "Beyond the Cosmological Standard Model," *Phys. Rept.*, vol. 568, pp. 1–98, 2015.

[8] C. Brans and R. H. Dicke, "Mach's principle and a relativistic theory of gravitation," *Phys. Rev.*, vol. 124, pp. 925–935, 1961.

[9] M. Born and L. Infeld, "Foundations of the new field theory," *Proc. Roy. Soc. Lond.*, vol. A144, pp. 425–451, 1934.

[10] R. G. Leigh, "Dirac-Born-Infeld Action from Dirichlet Sigma Model," *Mod. Phys. Lett.*, vol. A4, p. 2767, 1989.

[11] T. Padmanabhan, "Accelerated expansion of the universe driven by tachyonic matter," *Phys. Rev.*, vol. D66, p. 021301, 2002.

[12] N. Arkani-Hamed, H.-C. Cheng, M. A. Luty, and S. Mukohyama, "Ghost condensation and a consistent infrared modification of gravity," *JHEP*, vol. 05, p. 074, 2004.

[13] C. Armendariz-Picon, T. Damour, and V. F. Mukhanov, "k - inflation," *Phys. Lett.*, vol. B458, pp. 209–218, 1999.

[14] C. Armendariz-Picon, V. F. Mukhanov, and P. J. Steinhardt, "A Dynamical solution to the problem of a small cosmological constant and late time cosmic acceleration," *Phys. Rev. Lett.*, vol. 85, pp. 4438–4441, 2000.

[15] P. Brax, C. Burrage, and A.-C. Davis, "Screening fifth forces in k-essence and DBI models," *JCAP*, vol. 1301, p. 020, 2013.

[16] C. Burrage and J. Khoury, "Screening of scalar fields in Dirac-Born-Infeld theory," *Phys. Rev.*, vol. D90, no. 2, p. 024001, 2014.

[17] M. Greiter, F. Wilczek, and E. Witten, "Hydrodynamic Relations in Superconductivity," *Mod. Phys. Lett.*, vol. B3, p. 903, 1989.

[18] L. Berezhiani and J. Khoury, "Dark Matter Superfluidity and Galactic Dynamics," *Phys. Lett.*, vol. B753, pp. 639–643, 2016.

[19] L. Berezhiani and J. Khoury, "Theory of dark matter superfluidity," *Phys. Rev.*, vol. D92, p. 103510, 2015.

[20] J. Khoury, "Another Path for the Emergence of Modified Galactic Dynamics from Dark Matter Superfluidity," *Phys. Rev.*, vol. D93, no. 10, p. 103533, 2016.

[21] A. Hodson, H. Zhao, J. Khoury, and B. Famaey, "Galaxy Clusters in the Context of Superfluid Dark Matter," 2016.

[22] G. R. Dvali, G. Gabadadze, and M. Porrati, "4-D gravity on a brane in 5-D Minkowski space," *Phys. Lett.*, vol. B485, pp. 208–214, 2000.

[23] A. Nicolis and R. Rattazzi, "Classical and quantum consistency of the DGP model," *JHEP*, vol. 06, p. 059, 2004.

[24] A. Nicolis, R. Rattazzi, and E. Trincherini, "The Galileon as a local modification of gravity," *Phys. Rev.*, vol. D79, p. 064036, 2009.

[25] M. Ostrogradsky, "Mmoires sur les quations diffrentielles, relatives au problme des isoprimtres," *Mem. Acad. St. Petersbourg*, vol. 6, no. 4, pp. 385–517, 1850.

[26] K. Hinterbichler, M. Trodden, and D. Wesley, "Multi-field galileons and higher co-dimension branes," *Phys. Rev.*, vol. D82, p. 124018, 2010.

[27] D. B. Fairlie, J. Govaerts, and A. Morozov, "Universal field equations with covariant solutions," *Nucl. Phys.*, vol. B373, pp. 214–232, 1992.

[28] D. B. Fairlie and J. Govaerts, "Euler hierarchies and universal equations," *J. Math. Phys.*, vol. 33, pp. 3543–3566, 1992.

[29] D. B. Fairlie and J. Govaerts, "Universal field equations with reparametrization invariance," *Phys. Lett.*, vol. B281, pp. 49–53, 1992.

[30] T. L. Curtright and D. B. Fairlie, "A Galileon Primer," 2012.

[31] G. Goon, K. Hinterbichler, A. Joyce, and M. Trodden, "Galileons as Wess-Zumino Terms," *JHEP*, vol. 06, p. 004, 2012.

[32] A. Anisimov, E. Babichev, and A. Vikman, "B-inflation," *JCAP*, vol. 0506, p. 006, 2005.

[33] T. Kobayashi, M. Yamaguchi, and J. Yokoyama, "G-inflation: Inflation driven by the Galileon field," *Phys. Rev. Lett.*, vol. 105, p. 231302, 2010.

[34] C. Burrage, C. de Rham, D. Seery, and A. J. Tolley, "Galileon inflation," *JCAP*, vol. 1101, p. 014, 2011.

[35] P. Creminelli, G. D'Amico, M. Musso, J. Norena, and E. Trincherini, "Galilean symmetry in the effective theory of inflation: new shapes of non-Gaussianity," *JCAP*, vol. 1102, p. 006, 2011.

[36] K. Kamada, T. Kobayashi, M. Yamaguchi, and J. Yokoyama, "Higgs G-inflation," *Phys. Rev.*, vol. D83, p. 083515, 2011.

[37] A. De Felice and S. Tsujikawa, "Generalized Galileon cosmology," *Phys. Rev.*, vol. D84, p. 124029, 2011.

[38] T. Kobayashi, "Cosmic expansion and growth histories in Galileon scalar-tensor models of dark energy," *Phys. Rev.*, vol. D81, p. 103533, 2010.

[39] A. De Felice and S. Tsujikawa, "Primordial non-Gaussianities in general modified gravitational models of inflation," *JCAP*, vol. 1104, p. 029, 2011.

[40] T. Kobayashi, M. Yamaguchi, and J. Yokoyama, "Primordial non-Gaussianity from G-inflation," *Phys. Rev.*, vol. D83, p. 103524, 2011.

[41] S. Renaux-Petel, S. Mizuno, and K. Koyama, "Primordial fluctuations and non-Gaussianities from multifield DBI Galileon inflation," *JCAP*, vol. 1111, p. 042, 2011.

[42] M. Fasiello, "Trispectrum from Co-dimension 2(n) Galileons," *JCAP*, vol. 1312, p. 033, 2013.

[43] K. S. Kumar, J. C. Bueno Snchez, C. Escamilla-Rivera, J. Marto, and P. Vargas Moniz, "DBI Galileon inflation in the light of Planck 2015," *JCAP*, vol. 1602, no. 02, p. 063, 2016.

[44] R. Herrera, "G-Warm inflation," *JCAP*, vol. 1705, no. 05, p. 029, 2017.

[45] P. Creminelli, A. Nicolis, and E. Trincherini, "Galilean Genesis: An Alternative to inflation," *JCAP*, vol. 1011, p. 021, 2010.

[46] K. Hinterbichler and J. Khoury, "The Pseudo-Conformal Universe: Scale Invariance from Spontaneous Breaking of Conformal Symmetry," *JCAP*, vol. 1204, p. 023, 2012.

[47] L. Perreault Levasseur, R. Brandenberger, and A.-C. Davis, "Defrosting in an Emergent Galileon Cosmology," *Phys. Rev.*, vol. D84, p. 103512, 2011.

[48] Y. Wang and R. Brandenberger, "Scale-Invariant Fluctuations from Galilean Genesis," *JCAP*, vol. 1210, p. 021, 2012.

[49] Z.-G. Liu, J. Zhang, and Y.-S. Piao, "A Galileon Design of Slow Expansion," *Phys. Rev.*, vol. D84, p. 063508, 2011.

[50] K. Hinterbichler, A. Joyce, and J. Khoury, "Non-linear Realizations of Conformal Symmetry and Effective Field Theory for the Pseudo-Conformal Universe," *JCAP*, vol. 1206, p. 043, 2012.

[51] K. Hinterbichler, A. Joyce, J. Khoury, and G. E. J. Miller, "DBI Realizations of the Pseudo-Conformal Universe and Galilean Genesis Scenarios," *JCAP*, vol. 1212, p. 030, 2012.

[52] K. Hinterbichler, A. Joyce, J. Khoury, and G. E. J. Miller, "Dirac-Born-Infeld Genesis: An Improved Violation of the Null Energy Condition," *Phys. Rev. Lett.*, vol. 110, no. 24, p. 241303, 2013.

[53] P. Creminelli, K. Hinterbichler, J. Khoury, A. Nicolis, and E. Trincherini, "Subluminal Galilean Genesis," *JHEP*, vol. 02, p. 006, 2013.

[54] S. Nishi and T. Kobayashi, "Generalized Galilean Genesis," *JCAP*, vol. 1503, no. 03, p. 057, 2015.

[55] N. Chow and J. Khoury, "Galileon Cosmology," *Phys. Rev.*, vol. D80, p. 024037, 2009.

[56] F. P. Silva and K. Koyama, "Self-Accelerating Universe in Galileon Cosmology," *Phys. Rev.*, vol. D80, p. 121301, 2009.

[57] T. Kobayashi, H. Tashiro, and D. Suzuki, "Evolution of linear cosmological perturbations and its observational implications in Galileon-type modified gravity," *Phys. Rev.*, vol. D81, p. 063513, 2010.

[58] A. De Felice, R. Kase, and S. Tsujikawa, "Matter perturbations in Galileon cosmology," *Phys. Rev.*, vol. D83, p. 043515, 2011.

[59] A. De Felice, S. Mukohyama, and S. Tsujikawa, "Density perturbations in general modified gravitational theories," *Phys. Rev.*, vol. D82, p. 023524, 2010.

[60] A. De Felice and S. Tsujikawa, "Cosmology of a covariant Galileon field," *Phys. Rev. Lett.*, vol. 105, p. 111301, 2010.

[61] R. Gannouji and M. Sami, "Galileon gravity and its relevance to late time cosmic acceleration," *Phys. Rev.*, vol. D82, p. 024011, 2010.

[62] A. Ali, R. Gannouji, and M. Sami, "Modified gravity a la Galileon: Late time cosmic acceleration and observational constraints," *Phys. Rev.*, vol. D82, p. 103015, 2010.

[63] D. F. Mota, M. Sandstad, and T. Zlosnik, "Cosmology of the selfaccelerating third order Galileon," *JHEP*, vol. 12, p. 051, 2010.

[64] A. Barreira, B. Li, C. M. Baugh, and S. Pascoli, "Linear perturbations in Galileon gravity models," *Phys. Rev.*, vol. D86, p. 124016, 2012.

[65] C. Burrage, D. Parkinson, and D. Seery, "Beyond the growth rate of cosmic structure: Testing modified gravity models with an extra degree of freedom," 2015.

[66] M. Zumalacrregui, E. Bellini, I. Sawicki, and J. Lesgourgues, "hi_class: Horndeski in the Cosmic Linear Anisotropy Solving System," 2016.

[67] G. Gabadadze and S. Yu, "Nonlocal Galileons and Self-Acceleration," *Phys. Lett.*, vol. B768, pp. 397–403, 2017.

[68] M. W. Hossain, "First and second order cosmological perturbations in light mass Galileon models," *Phys. Rev.*, vol. D96, no. 2, p. 023506, 2017.

[69] G. Koutsoumbas, K. Ntrekis, E. Papantonopoulos, and E. N. Saridakis, "Unification of Dark Matter - Dark Energy in Generalized Galileon Theories," 2017.

[70] J. Renk, M. Zumalacrregui, F. Montanari, and A. Barreira, "Galileon Gravity in Light of ISW, CMB, BAO and H_0 data," 2017.

[71] R. Banerjee, S. Chakraborty, A. Mitra, and P. Mukherjee, "Cosmological implications of shift symmetric Galileon field," 2017.

[72] C. de Rham and G. Gabadadze, "Generalization of the Fierz-Pauli Action," *Phys. Rev.*, vol. D82, p. 044020, 2010.

[73] J. Khoury, J.-L. Lehners, and B. A. Ovrut, "Supersymmetric Galileons," *Phys. Rev.*, vol. D84, p. 043521, 2011.

[74] M. Koehn, J.-L. Lehners, and B. Ovrut, "Supersymmetric cubic Galileons have ghosts," *Phys. Rev.*, vol. D88, no. 2, p. 023528, 2013.

[75] M. Koehn, J.-L. Lehners, and B. A. Ovrut, "Cosmological super-bounce," *Phys. Rev.*, vol. D90, no. 2, p. 025005, 2014.

[76] F. Farakos, C. Germani, and A. Kehagias, "On ghost-free supersymmetric galileons," *JHEP*, vol. 11, p. 045, 2013.

[77] R. Deen and B. Ovrut, "Supergravitational Conformal Galileons," 2017.

[78] G. W. Horndeski, "Second-order scalar-tensor field equations in a four-dimensional space," *Int. J. Theor. Phys.*, vol. 10, pp. 363–384, 1974.

[79] C. Deffayet, G. Esposito-Farese, and A. Vikman, "Covariant Galileon," *Phys. Rev.*, vol. D79, p. 084003, 2009.

[80] R. L. Arnowitt, S. Deser, and C. W. Misner, "Dynamical Structure and Definition of Energy in General Relativity," *Phys. Rev.*, vol. 116, pp. 1322–1330, 1959.

[81] R. Schon and S.-T. Yau, "On the Proof of the positive mass conjecture in general relativity," *Commun. Math. Phys.*, vol. 65, pp. 45–76, 1979.

[82] E. Witten, "A Simple Proof of the Positive Energy Theorem," *Commun. Math. Phys.*, vol. 80, p. 381, 1981.

[83] T. Parker and C. H. Taubes, "On Witten's Proof of the Positive Energy Theorem," *Commun. Math. Phys.*, vol. 84, p. 223, 1982.

[84] J. A. Nester, "A New gravitational energy expression with a simple positivity proof," *Phys. Lett.*, vol. A83, p. 241, 1981.

[85] P. K. Townsend, "Positive Energy and the Scalar Potential in Higher Dimensional (Super)gravity Theories," *Phys. Lett.*, vol. 148B, pp. 55–59, 1984.

[86] W. Boucher, "POSITIVE ENERGY WITHOUT SUPERSYMMETRY," *Nucl. Phys.*, vol. B242, pp. 282–296, 1984.

[87] P. J. E. Peebles and B. Ratra, "The Cosmological constant and dark energy," *Rev. Mod. Phys.*, vol. 75, pp. 559–606, 2003.

[88] S. Tsujikawa, "Quintessence: A Review," *Class. Quant. Grav.*, vol. 30, p. 214003, 2013.

[89] S. Weinberg, "The Cosmological Constant Problem," *Rev. Mod. Phys.*, vol. 61, pp. 1–23, 1989.

[90] C. M. Will, "The Confrontation between General Relativity and Experiment," *Living Rev. Rel.*, vol. 17, p. 4, 2014.

[91] T. Jenke, P. Geltenbort, H. Lemmel, and H. Abele, "Realization of a gravity-resonance-spectroscopy technique," *Nature Phys.*, vol. 7, pp. 468–472, 2011.

[92] T. Jenke *et al.*, "Gravity Resonance Spectroscopy Constrains Dark Energy and Dark Matter Scenarios," *Phys. Rev. Lett.*, vol. 112, p. 151105, 2014.

[93] G. Cronenberg, H. Filter, M. Thalhammer, T. Jenke, H. Abele, and P. Geltenbort, "A Gravity of Earth Measurement with a qBOUNCE Experiment," *PoS*, vol. EPS-HEP2015, p. 408, 2015.

[94] C. Burrage, E. J. Copeland, and E. A. Hinds, "Probing Dark Energy with Atom Interferometry," *JCAP*, vol. 1503, no. 03, p. 042, 2015.

[95] C. Burrage and E. J. Copeland, "Using Atom Interferometry to Detect Dark Energy," *Contemp. Phys.*, vol. 57, no. 2, pp. 164–176, 2016.

[96] P. Hamilton, M. Jaffe, P. Haslinger, Q. Simmons, H. Müller, and J. Khoury, "Atom-interferometry constraints on dark energy," *Science*, vol. 349, pp. 849–851, 2015.

[97] K. S. Stelle, "Renormalization of Higher Derivative Quantum Gravity," *Phys. Rev.*, vol. D16, pp. 953–969, 1977.

[98] K. S. Stelle, "Classical Gravity with Higher Derivatives," *Gen. Rel. Grav.*, vol. 9, pp. 353–371, 1978.

[99] A. A. Starobinsky, "A New Type of Isotropic Cosmological Models Without Singularity," *Phys. Lett.*, vol. 91B, pp. 99–102, 1980.

[100] S. Capozziello, "Curvature quintessence," *Int. J. Mod. Phys.*, vol. D11, pp. 483–492, 2002.

[101] S. Capozziello, S. Carloni, and A. Troisi, "Quintessence without scalar fields," *Recent Res. Dev. Astron. Astrophys.*, vol. 1, p. 625, 2003.

[102] S. M. Carroll, V. Duvvuri, M. Trodden, and M. S. Turner, "Is cosmic speed - up due to new gravitational physics?," *Phys. Rev.*, vol. D70, p. 043528, 2004.

[103] T. Chiba, "1/R gravity and scalar - tensor gravity," *Phys. Lett.*, vol. B575, pp. 1–3, 2003.

[104] A. Nunez and S. Solganik, "The Content of f(R) gravity," 2004.

[105] G. Dvali, G. F. Giudice, C. Gomez, and A. Kehagias, "UV-Completion by Classicalization," *JHEP*, vol. 08, p. 108, 2011.

[106] S. M. Carroll, M. Hoffman, and M. Trodden, "Can the dark energy equation - of - state parameter w be less than -1?," *Phys. Rev.*, vol. D68, p. 023509, 2003.

[107] J. M. Cline, S. Jeon, and G. D. Moore, "The Phantom menaced: Constraints on low-energy effective ghosts," *Phys. Rev.*, vol. D70, p. 043543, 2004.

[108] M. E. Peskin and D. V. Schroeder, *An Introduction to quantum field theory*. Reading, USA: Addison-Wesley, 1995.

[109] C. De Rham, L. Keltner, and A. J. Tolley, "Generalized galileon duality," *Phys. Rev.*, vol. D90, no. 2, p. 024050, 2014.

[110] A. Adams, N. Arkani-Hamed, S. Dubovsky, A. Nicolis, and R. Rattazzi, "Causality, analyticity and an IR obstruction to UV completion," *JHEP*, vol. 10, p. 014, 2006.

[111] S. R. Coleman and E. J. Weinberg, "Radiative Corrections as the Origin of Spontaneous Symmetry Breaking," *Phys. Rev.*, vol. D7, pp. 1888–1910, 1973.

[112] A. Upadhye, W. Hu, and J. Khoury, "Quantum Stability of Chameleon Field Theories," *Phys. Rev. Lett.*, vol. 109, p. 041301, 2012.

[113] E. G. Adelberger, B. R. Heckel, S. A. Hoedl, C. D. Hoyle, D. J. Kapner, and A. Upadhye, "Particle Physics Implications of a Recent Test of the Gravitational Inverse Sqaure Law," *Phys. Rev. Lett.*, vol. 98, p. 131104, 2007.

[114] C. de Rham and R. H. Ribeiro, "Riding on irrelevant operators," *JCAP*, vol. 1411, no. 11, p. 016, 2014.

[115] M. A. Luty, M. Porrati, and R. Rattazzi, "Strong interactions and stability in the DGP model," *JHEP*, vol. 09, p. 029, 2003.

[116] A. Nicolis, R. Rattazzi, and E. Trincherini, "Energy's and amplitudes' positivity," *JHEP*, vol. 05, p. 095, 2010. [Erratum: JHEP11,128(2011)].

[117] B. P. Abbott *et al.*, "Observation of Gravitational Waves from a Binary Black Hole Merger," *Phys. Rev. Lett.*, vol. 116, no. 6, p. 061102, 2016.

[118] M. Kasevich and S. Chu, "Atomic interferometry using stimulated Raman transitions," *Phys. Rev. Lett.*, vol. 67, pp. 181–184, 1991.

[119] A. D. Cronin, J. Schmiedmayer, and D. E. Pritchard, "Optics and interferometry with atoms and molecules," *Rev. Mod. Phys.*, vol. 81, pp. 1051–1129, 2009.

[120] F. Terranova and G. M. Tino, "Testing the a_μ anomaly in the electron sector through a precise measurement of h/M," *Phys. Rev.*, vol. A89, no. 5, p. 052118, 2014.

[121] S. Dimopoulos and A. A. Geraci, "Probing submicron forces by interferometry of Bose-Einstein condensed atoms," *Phys. Rev.*, vol. D68, p. 124021, 2003.

[122] R. Penrose, "Gravitational collapse and space-time singularities," *Phys. Rev. Lett.*, vol. 14, pp. 57–59, 1965.

[123] E. Curiel, "A Primer on Energy Conditions," *Einstein Stud.*, vol. 13, pp. 43–104, 2017.

[124] M. Visser and C. Barcelo, "Energy conditions and their cosmological implications," in *Proceedings, 3rd International Conference on Particle Physics and the Early Universe (COSMO 1999): Trieste, Italy, September 27-October 3, 1999*, pp. 98–112, 2000.

[125] S. Dubovsky, T. Gregoire, A. Nicolis, and R. Rattazzi, "Null energy condition and superluminal propagation," *JHEP*, vol. 03, p. 025, 2006.

[126] I. Sawicki and A. Vikman, "Hidden Negative Energies in Strongly Accelerated Universes," *Phys. Rev.*, vol. D87, no. 6, p. 067301, 2013.

[127] P. Creminelli, M. A. Luty, A. Nicolis, and L. Senatore, "Starting the Universe: Stable Violation of the Null Energy Condition and Non-standard Cosmologies," *JHEP*, vol. 12, p. 080, 2006.

[128] V. A. Rubakov, "Consistent NEC-violation: towards creating a universe in the laboratory," *Phys. Rev.*, vol. D88, p. 044015, 2013.

[129] M. Gasperini and G. Veneziano, "Pre - big bang in string cosmology," *Astropart. Phys.*, vol. 1, pp. 317–339, 1993.

[130] M. Gasperini and G. Veneziano, "The Pre - big bang scenario in string cosmology," *Phys. Rept.*, vol. 373, pp. 1–212, 2003.

[131] M. Gasperini and G. Veneziano, "String Theory and Pre-big bang Cosmology," *Nuovo Cim.*, vol. C38, no. 5, p. 160, 2016.

[132] J. Khoury, B. A. Ovrut, P. J. Steinhardt, and N. Turok, "The Ekpyrotic universe: Colliding branes and the origin of the hot big bang," *Phys. Rev.*, vol. D64, p. 123522, 2001.

[133] R. Y. Donagi, J. Khoury, B. A. Ovrut, P. J. Steinhardt, and N. Turok, "Visible branes with negative tension in heterotic M theory," *JHEP*, vol. 11, p. 041, 2001.

[134] J. Khoury, B. A. Ovrut, N. Seiberg, P. J. Steinhardt, and N. Turok, "From big crunch to big bang," *Phys. Rev.*, vol. D65, p. 086007, 2002.

[135] J. Khoury, B. A. Ovrut, P. J. Steinhardt, and N. Turok, "Density perturbations in the ekpyrotic scenario," *Phys. Rev.*, vol. D66, p. 046005, 2002.

[136] D. H. Lyth, "The Primordial curvature perturbation in the ekpyrotic universe," *Phys. Lett.*, vol. B524, pp. 1–4, 2002.

[137] R. Brandenberger and F. Finelli, "On the spectrum of fluctuations in an effective field theory of the Ekpyrotic universe," *JHEP*, vol. 11, p. 056, 2001.

[138] P. J. Steinhardt and N. Turok, "Cosmic evolution in a cyclic universe," *Phys. Rev.*, vol. D65, p. 126003, 2002.

[139] A. Notari and A. Riotto, "Isocurvature perturbations in the ekpyrotic universe," *Nucl. Phys.*, vol. B644, pp. 371–382, 2002.

[140] F. Finelli, "Assisted contraction," *Phys. Lett.*, vol. B545, pp. 1–7, 2002.

[141] S. Tsujikawa, R. Brandenberger, and F. Finelli, "On the construction of nonsingular pre - big bang and ekpyrotic cosmologies and the resulting density perturbations," *Phys. Rev.*, vol. D66, p. 083513, 2002.

[142] S. Gratton, J. Khoury, P. J. Steinhardt, and N. Turok, "Conditions for generating scale-invariant density perturbations," *Phys. Rev.*, vol. D69, p. 103505, 2004.

[143] A. J. Tolley, N. Turok, and P. J. Steinhardt, "Cosmological perturbations in a big crunch / big bang space-time," *Phys. Rev.*, vol. D69, p. 106005, 2004.

[144] B. Craps and B. A. Ovrut, "Global fluctuation spectra in big crunch / big bang string vacua," *Phys. Rev.*, vol. D69, p. 066001, 2004.

[145] J. Khoury, P. J. Steinhardt, and N. Turok, "Inflation versus cyclic predictions for spectral tilt," *Phys. Rev. Lett.*, vol. 91, p. 161301, 2003.

[146] J. Khoury, P. J. Steinhardt, and N. Turok, "Designing cyclic universe models," *Phys. Rev. Lett.*, vol. 92, p. 031302, 2004.

[147] J. Khoury, "A Briefing on the ekpyrotic / cyclic universe," in *Proceedings, 6th RESCEU International Symposium on Frontiers in Astroparticle Physics and Cosmology: Tokyo, Japan, 4-7 Nov 2003*, 2004.

[148] P. Creminelli, A. Nicolis, and M. Zaldarriaga, "Perturbations in bouncing cosmologies: Dynamical attractor versus scale invariance," *Phys. Rev.*, vol. D71, p. 063505, 2005.

[149] J.-L. Lehners, P. McFadden, N. Turok, and P. J. Steinhardt, "Generating ekpyrotic curvature perturbations before the big bang," *Phys. Rev.*, vol. D76, p. 103501, 2007.

[150] E. I. Buchbinder, J. Khoury, and B. A. Ovrut, "New Ekpyrotic cosmology," *Phys. Rev.*, vol. D76, p. 123503, 2007.

[151] E. I. Buchbinder, J. Khoury, and B. A. Ovrut, "On the initial conditions in new ekpyrotic cosmology," *JHEP*, vol. 11, p. 076, 2007.

[152] E. I. Buchbinder, J. Khoury, and B. A. Ovrut, "Non-Gaussianities in new ekpyrotic cosmology," *Phys. Rev. Lett.*, vol. 100, p. 171302, 2008.

[153] P. Creminelli and L. Senatore, "A Smooth bouncing cosmology with scale invariant spectrum," *JCAP*, vol. 0711, p. 010, 2007.

[154] K. Koyama and D. Wands, "Ekpyrotic collapse with multiple fields," *JCAP*, vol. 0704, p. 008, 2007.

[155] K. Koyama, S. Mizuno, and D. Wands, "Curvature perturbations from ekpyrotic collapse with multiple fields," *Class. Quant. Grav.*, vol. 24, pp. 3919–3932, 2007.

[156] K. Koyama, S. Mizuno, F. Vernizzi, and D. Wands, "Non-Gaussianities from ekpyrotic collapse with multiple fields," *JCAP*, vol. 0711, p. 024, 2007.

[157] J.-L. Lehners and P. J. Steinhardt, "Non-Gaussian density fluctuations from entropically generated curvature perturbations in Ekpyrotic models," *Phys. Rev.*, vol. D77, p. 063533, 2008. [Erratum: Phys. Rev.D79,129903(2009)].

[158] J.-L. Lehners and P. J. Steinhardt, "Intuitive understanding of non-gaussianity in ekpyrotic and cyclic models," *Phys. Rev.*, vol. D78, p. 023506, 2008. [Erratum: Phys. Rev.D79,129902(2009)].

[159] J.-L. Lehners and P. J. Steinhardt, "Non-Gaussianity Generated by the Entropic Mechanism in Bouncing Cosmologies Made Simple," *Phys. Rev.*, vol. D80, p. 103520, 2009.

[160] Y.-F. Cai, D. A. Easson, and R. Brandenberger, "Towards a Nonsingular Bouncing Cosmology," *JCAP*, vol. 1208, p. 020, 2012.

[161] T. Qiu, J. Evslin, Y.-F. Cai, M. Li, and X. Zhang, "Bouncing Galileon Cosmologies," *JCAP*, vol. 1110, p. 036, 2011.

[162] J. Khoury and P. J. Steinhardt, "Adiabatic Ekpyrosis: Scale-Invariant Curvature Perturbations from a Single Scalar Field in a Contracting Universe," *Phys. Rev. Lett.*, vol. 104, p. 091301, 2010.

[163] J. Khoury and P. J. Steinhardt, "Generating Scale-Invariant Perturbations from Rapidly-Evolving Equation of State," *Phys. Rev.*, vol. D83, p. 123502, 2011.

[164] A. Joyce and J. Khoury, "Scale Invariance via a Phase of Slow Expansion," *Phys. Rev.*, vol. D84, p. 023508, 2011.

[165] J. Fonseca and D. Wands, "Tilted Ekpyrosis," *Phys. Rev.*, vol. D84, p. 101303, 2011.

[166] C. Lin, R. H. Brandenberger, and L. Perreault Levasseur, "A Matter Bounce By Means of Ghost Condensation," *JCAP*, vol. 1104, p. 019, 2011.

[167] B. Craps, T. Hertog, and N. Turok, "On the Quantum Resolution of Cosmological Singularities using AdS/CFT," *Phys. Rev.*, vol. D86, p. 043513, 2012.

[168] V. A. Rubakov, "Harrison-Zeldovich spectrum from conformal invariance," *JCAP*, vol. 0909, p. 030, 2009.

[169] M. Osipov and V. Rubakov, "Scalar tilt from broken conformal invariance," *JETP Lett.*, vol. 93, pp. 52–55, 2011.

[170] M. Libanov and V. Rubakov, "Cosmological density perturbations from conformal scalar field: infrared properties and statistical anisotropy," *JCAP*, vol. 1011, p. 045, 2010.

[171] M. Libanov, S. Mironov, and V. Rubakov, "Properties of scalar perturbations generated by conformal scalar field," *Prog. Theor. Phys. Suppl.*, vol. 190, pp. 120–134, 2011.

[172] M. Libanov, S. Ramazanov, and V. Rubakov, "Scalar perturbations in conformal rolling scenario with intermediate stage," *JCAP*, vol. 1106, p. 010, 2011.

[173] M. Libanov, S. Mironov, and V. Rubakov, "Non-Gaussianity of scalar perturbations generated by conformal mechanisms," *Phys. Rev.*, vol. D84, p. 083502, 2011.

[174] M. Osipov and V. Rubakov, "Galileon bounce after ekpyrotic contraction," *JCAP*, vol. 1311, p. 031, 2013.

[175] J. De-Santiago, J. L. Cervantes-Cota, and D. Wands, "Cosmological phase space analysis of the F(X) - V(ϕ) scalar field and bouncing solutions," *Phys. Rev.*, vol. D87, no. 2, p. 023502, 2013.

[176] A. Nayeri, R. H. Brandenberger, and C. Vafa, "Producing a scale-invariant spectrum of perturbations in a Hagedorn phase of string cosmology," *Phys. Rev. Lett.*, vol. 97, p. 021302, 2006.

[177] Z.-G. Liu and Y.-S. Piao, "A Galileon Design of Slow Expansion: Emergent universe," *Phys. Lett.*, vol. B718, pp. 734–739, 2013.

[178] C. Deffayet, O. Pujolas, I. Sawicki, and A. Vikman, "Imperfect Dark Energy from Kinetic Gravity Braiding," *JCAP*, vol. 1010, p. 026, 2010.

[179] C. de Rham and A. J. Tolley, "DBI and the Galileon reunited," *JCAP*, vol. 1005, p. 015, 2010.

[180] S. L. Dubovsky and S. M. Sibiryakov, "Spontaneous breaking of Lorentz invariance, black holes and perpetuum mobile of the 2nd kind," *Phys. Lett.*, vol. B638, pp. 509–514, 2006.

[181] R. M. Wald, "Black hole entropy is the Noether charge," *Phys. Rev.*, vol. D48, no. 8, pp. R3427–R3431, 1993.

[182] V. Iyer and R. M. Wald, "A Comparison of Noether charge and Euclidean methods for computing the entropy of stationary black holes," *Phys. Rev.*, vol. D52, pp. 4430–4439, 1995.

[183] P. Creminelli, M. Serone, and E. Trincherini, "Non-linear Representations of the Conformal Group and Mapping of Galileons," *JHEP*, vol. 10, p. 040, 2013.

[184] C. de Rham, M. Fasiello, and A. J. Tolley, "Galileon Duality," *Phys. Lett.*, vol. B733, pp. 46–51, 2014.

[185] A. Ijjas and P. J. Steinhardt, "Classically stable nonsingular cosmological bounces," *Phys. Rev. Lett.*, vol. 117, no. 12, p. 121304, 2016.

[186] A. Ijjas and P. J. Steinhardt, "Fully stable cosmological solutions with a non-singular classical bounce," *Phys. Lett.*, vol. B764, pp. 289–294, 2017.

[187] M. Libanov, S. Mironov, and V. Rubakov, "Generalized Galileons: instabilities of bouncing and Genesis cosmologies and modified Genesis," *JCAP*, vol. 1608, no. 08, p. 037, 2016.

[188] P. Creminelli, D. Pirtskhalava, L. Santoni, and E. Trincherini, "Stability of Geodesically Complete Cosmologies," *JCAP*, vol. 1611, no. 11, p. 047, 2016.

[189] D. A. Easson, I. Sawicki, and A. Vikman, "When Matter Matters," *JCAP*, vol. 1307, p. 014, 2013.

[190] V. A. Rubakov, "The Null Energy Condition and its violation," *Phys. Usp.*, vol. 57, pp. 128–142, 2014. [Usp. Fiz. Nauk184,no.2,137(2014)].

[191] R. V. Buniy, S. D. H. Hsu, and B. M. Murray, "The Null energy condition and instability," *Phys. Rev.*, vol. D74, p. 063518, 2006.

[192] D. A. Easson, I. Sawicki, and A. Vikman, "G-Bounce," *JCAP*, vol. 1111, p. 021, 2011.

[193] P. Creminelli, A. Joyce, J. Khoury, and M. Simonovic, "Consistency Relations for the Conformal Mechanism," *JCAP*, vol. 1304, p. 020, 2013.

[194] D. Lovelock, "The Einstein tensor and its generalizations," *J. Math. Phys.*, vol. 12, pp. 498–501, 1971.

[195] G. Goon, K. Hinterbichler, and M. Trodden, "Symmetries for Galileons and DBI scalars on curved space," *JCAP*, vol. 1107, p. 017, 2011.

[196] M. Alishahiha, E. Silverstein, and D. Tong, "DBI in the sky," *Phys. Rev.*, vol. D70, p. 123505, 2004.

[197] S. Mukohyama, "Ghost condensate and generalized second law," *JHEP*, vol. 09, p. 070, 2009.

[198] R. P. Woodard, "Avoiding dark energy with 1/r modifications of gravity," *Lect. Notes Phys.*, vol. 720, pp. 403–433, 2007.

[199] S. M. Carroll, *Spacetime and geometry: An introduction to general relativity.* 2004.

[200] A. Komar, "Positive-Definite Energy Density and Global Consequences for General Relativity," *Phys. Rev.*, vol. 129, no. 4, p. 1873, 1963.

[201] P. Breitenlohner and D. Z. Freedman, "Positive Energy in anti-De Sitter Backgrounds and Gauged Extended Supergravity," *Phys. Lett.*, vol. 115B, pp. 197–201, 1982.

[202] L. F. Abbott and S. Deser, "Stability of Gravity with a Cosmological Constant," *Nucl. Phys.*, vol. B195, pp. 76–96, 1982.

[203] G. W. Gibbons, S. W. Hawking, G. T. Horowitz, and M. J. Perry, "Positive Mass Theorems for Black Holes," *Commun. Math. Phys.*, vol. 88, p. 295, 1983.

[204] L. Mezincescu and P. K. Townsend, "Stability at a Local Maximum in Higher Dimensional Anti-de Sitter Space and Applications to Supergravity," *Annals Phys.*, vol. 160, p. 406, 1985.

[205] T. Shiromizu, D. Ida, and T. Torii, "Gravitational energy, dS / CFT correspondence and cosmic no hair," *JHEP*, vol. 11, p. 010, 2001.

[206] D. Kastor and J. H. Traschen, "A Positive energy theorem for asymptotically de Sitter space-times," *Class. Quant. Grav.*, vol. 19, pp. 5901–5920, 2002.

[207] S. Deser and B. Tekin, "Conformal Properties of Charges in Scalar-Tensor Gravities," *Class. Quant. Grav.*, vol. 23, pp. 7479–7482, 2006.

[208] E. Silverstein and D. Tong, "Scalar speed limits and cosmology: Acceleration from D-cceleration," *Phys. Rev.*, vol. D70, p. 103505, 2004.

[209] V. F. Mukhanov and A. Vikman, "Enhancing the tensor-to-scalar ratio in simple inflation," *JCAP*, vol. 0602, p. 004, 2006.

[210] C. Armendariz-Picon, V. F. Mukhanov, and P. J. Steinhardt, "Essentials of k essence," *Phys. Rev.*, vol. D63, p. 103510, 2001.

[211] E. Babichev, C. Deffayet, and R. Ziour, "k-Mouflage gravity," *Int. J. Mod. Phys.*, vol. D18, pp. 2147–2154, 2009.

[212] A. J. Tolley and M. Wyman, "The Gelaton Scenario: Equilateral non-Gaussianity from multi-field dynamics," *Phys. Rev.*, vol. D81, p. 043502, 2010.

[213] M. Nozawa and T. Shiromizu, "Modeling scalar fields consistent with positive mass," *Phys. Rev.*, vol. D89, no. 2, p. 023011, 2014.

[214] S. Dubovsky, L. Hui, A. Nicolis, and D. T. Son, "Effective field theory for hydrodynamics: thermodynamics, and the derivative expansion," *Phys. Rev.*, vol. D85, p. 085029, 2012.

[215] C. Burrage and J. Sakstein, "A Compendium of Chameleon Constraints," *JCAP*, vol. 1611, no. 11, p. 045, 2016.

[216] J. Wang, L. Hui, and J. Khoury, "No-Go Theorems for Generalized Chameleon Field Theories," *Phys. Rev. Lett.*, vol. 109, p. 241301, 2012.

[217] P. Brax, A.-C. Davis, and B. Li, "Modified Gravity Tomography," *Phys. Lett.*, vol. B715, pp. 38–43, 2012.

[218] P. Brax, C. Burrage, and A.-C. Davis, "Laboratory Tests of the Galileon," *JCAP*, vol. 1109, p. 020, 2011.

[219] L. Hui, A. Nicolis, and C. Stubbs, "Equivalence Principle Implications of Modified Gravity Models," *Phys. Rev.*, vol. D80, p. 104002, 2009.

[220] B. Jain and J. VanderPlas, "Tests of Modified Gravity with Dwarf Galaxies," *JCAP*, vol. 1110, p. 032, 2011.

[221] P. Chang and L. Hui, "Stellar Structure and Tests of Modified Gravity," *Astrophys. J.*, vol. 732, p. 25, 2011.

[222] A.-C. Davis, E. A. Lim, J. Sakstein, and D. Shaw, "Modified Gravity Makes Galaxies Brighter," *Phys. Rev.*, vol. D85, p. 123006, 2012.

[223] B. Jain, V. Vikram, and J. Sakstein, "Astrophysical Tests of Modified Gravity: Constraints from Distance Indicators in the Nearby Universe," *Astrophys. J.*, vol. 779, p. 39, 2013.

[224] D. J. Kapner, T. S. Cook, E. G. Adelberger, J. H. Gundlach, B. R. Heckel, C. D. Hoyle, and H. E. Swanson, "Tests of the gravitational inverse-square law below the dark-energy length scale," *Phys. Rev. Lett.*, vol. 98, p. 021101, 2007.

[225] A. Upadhye, "Dark energy fifth forces in torsion pendulum experiments," *Phys. Rev.*, vol. D86, p. 102003, 2012.

[226] D. M. Harber, J. M. Obrecht, J. M. McGuirk, and E. A. Cornell, "Measurement of the Casimir-Polder force through center-of-mass oscillations of a Bose-Einstein condensate," *Phys. Rev.*, vol. A72, p. 033610, 2005.

[227] A. N. Ivanov, R. Hollwieser, T. Jenke, M. Wellenzohen, and H. Abele, "Influence of the chameleon field potential on transition frequencies of gravitationally bound quantum states of ultracold neutrons," *Phys. Rev.*, vol. D87, no. 10, p. 105013, 2013.

[228] P. Brax and G. Pignol, "Strongly Coupled Chameleons and the Neutronic Quantum Bouncer," *Phys. Rev. Lett.*, vol. 107, p. 111301, 2011.

[229] P. Brax, G. Pignol, and D. Roulier, "Probing Strongly Coupled Chameleons with Slow Neutrons," *Phys. Rev.*, vol. D88, p. 083004, 2013.

[230] H. Lemmel, P. Brax, A. N. Ivanov, T. Jenke, G. Pignol, M. Pitschmann, T. Potocar, M. Wellenzohn, M. Zawisky, and H. Abele, "Neutron Interferometry constrains dark energy chameleon fields," *Phys. Lett.*, vol. B743, pp. 310–314, 2015.

[231] K. Li *et al.*, "Neutron Limit on the Strongly-Coupled Chameleon Field," *Phys. Rev.*, vol. D93, no. 6, p. 062001, 2016.

[232] A. S. Chou *et al.*, "A Search for chameleon particles using a photon regeneration technique," *Phys. Rev. Lett.*, vol. 102, p. 030402, 2009.

[233] J. H. Steffen, A. Upadhye, A. Baumbaugh, A. S. Chou, P. O. Mazur, R. Tomlin, A. Weltman, and W. Wester, "Laboratory constraints on chameleon dark energy and power-law fields," *Phys. Rev. Lett.*, vol. 105, p. 261803, 2010.

[234] G. Rybka *et al.*, "A Search for Scalar Chameleons with ADMX," *Phys. Rev. Lett.*, vol. 105, p. 051801, 2010.

[235] P. Brax and K. Zioutas, "Solar Chameleons," *Phys. Rev.*, vol. D82, p. 043007, 2010.

[236] C. Burrage, A.-C. Davis, and D. J. Shaw, "Detecting Chameleons: The Astronomical Polarization Produced by Chameleon-like Scalar Fields," *Phys. Rev.*, vol. D79, p. 044028, 2009.

[237] B. Ratra and P. J. E. Peebles, "Cosmological Consequences of a Rolling Homogeneous Scalar Field," *Phys. Rev.*, vol. D37, p. 3406, 1988.

[238] C. Wetterich, "Cosmology and the Fate of Dilatation Symmetry," *Nucl. Phys.*, vol. B302, pp. 668–696, 1988.

[239] J. Khoury and A. Weltman, "Chameleon fields: Awaiting surprises for tests of gravity in space," *Phys. Rev. Lett.*, vol. 93, p. 171104, 2004.

[240] J. Khoury and A. Weltman, "Chameleon cosmology," *Phys. Rev.*, vol. D69, p. 044026, 2004.

[241] I. Zlatev, L.-M. Wang, and P. J. Steinhardt, "Quintessence, cosmic coincidence, and the cosmological constant," *Phys. Rev. Lett.*, vol. 82, pp. 896–899, 1999.

[242] P. J. Steinhardt, L.-M. Wang, and I. Zlatev, "Cosmological tracking solutions," *Phys. Rev.*, vol. D59, p. 123504, 1999.

[243] P. Binetruy, M. K. Gaillard, and Y.-Y. Wu, "Modular invariant formulation of multi - gaugino and matter condensation," *Nucl. Phys.*, vol. B493, pp. 27–55, 1997.

[244] T. Barreiro, B. de Carlos, and E. J. Copeland, "On nonperturbative corrections to the Kahler potential," *Phys. Rev.*, vol. D57, pp. 7354–7360, 1998.

[245] P. Binetruy, M. K. Gaillard, and Y.-Y. Wu, "Supersymmetry breaking and weakly versus strongly coupled string theory," *Phys. Lett.*, vol. B412, pp. 288–295, 1997.

[246] S. S. Gubser and J. Khoury, "Scalar self-interactions loosen constraints from fifth force searches," *Phys. Rev.*, vol. D70, p. 104001, 2004.

[247] S. Schlgel, S. Clesse, and A. Fzfa, "Probing Modified Gravity with Atom-Interferometry: a Numerical Approach," *Phys. Rev.*, vol. D93, no. 10, p. 104036, 2016.

[248] L. Kraiselburd, S. J. Landau, M. Salgado, D. Sudarsky, and H. Vucetich, "Equivalence Principle in Chameleon Models," 2015.

[249] P. Brax, C. van de Bruck, A.-C. Davis, J. Khoury, and A. Weltman, "Detecting dark energy in orbit - The Cosmological chameleon," *Phys. Rev.*, vol. D70, p. 123518, 2004.

[250] D. F. Mota and D. J. Shaw, "Strongly coupled chameleon fields: New horizons in scalar field theory," *Phys. Rev. Lett.*, vol. 97, p. 151102, 2006.

[251] D. F. Mota and D. J. Shaw, "Evading Equivalence Principle Violations, Cosmological and other Experimental Constraints in Scalar Field Theories with a Strong Coupling to Matter," *Phys. Rev.*, vol. D75, p. 063501, 2007.

[252] K. Hinterbichler and J. Khoury, "Symmetron Fields: Screening Long-Range Forces Through Local Symmetry Restoration," *Phys. Rev. Lett.*, vol. 104, p. 231301, 2010.

[253] K. A. Olive and M. Pospelov, "Environmental dependence of masses and coupling constants," *Phys. Rev.*, vol. D77, p. 043524, 2008.

[254] M. Pietroni, "Dark energy condensation," *Phys. Rev.*, vol. D72, p. 043535, 2005.

[255] K. Hinterbichler, J. Khoury, A. Levy, and A. Matas, "Symmetron Cosmology," *Phys. Rev.*, vol. D84, p. 103521, 2011.

[256] P. Brax, C. van de Bruck, A.-C. Davis, B. Li, B. Schmauch, and D. J. Shaw, "Linear Growth of Structure in the Symmetron Model," *Phys. Rev.*, vol. D84, p. 123524, 2011.

[257] P. Brax, C. van de Bruck, A.-C. Davis, B. Li, and D. J. Shaw, "Nonlinear Structure Formation with the Environmentally Dependent Dilaton," *Phys. Rev.*, vol. D83, p. 104026, 2011.

[258] A. Einstein, L. Infeld, and B. Hoffmann, "The Gravitational equations and the problem of motion," *Annals Math.*, vol. 39, pp. 65–100, 1938.

[259] K. Jones-Smith and F. Ferrer, "Detecting Chameleon Dark Energy via Electrostatic Analogy," *Phys. Rev. Lett.*, vol. 108, p. 221101, 2012.

[260] R. Pourhasan, N. Afshordi, R. B. Mann, and A. C. Davis, "Chameleon Gravity, Electrostatics, and Kinematics in the Outer Galaxy," *JCAP*, vol. 1112, p. 005, 2011.

[261] W. H. Press, S. A. Teukolsky, W. T. Vetterling, and B. P. Flannery, *Numerical Recipes in C (2Nd Ed.): The Art of Scientific Computing*. New York, NY, USA: Cambridge University Press, 1992.

[262] R. Geiger, V. Ménoret, G. Stern, N. Zahzam, P. Cheinet, B. Battelier, A. Villing, F. Moron, M. Lours, Y. Bidel, A. Bresson, A. Landragin, and P. Bouyer, "Detecting inertial effects with airborne matter-wave interferometry," *Nature Communications*, vol. 2, p. 474, Sept. 2011.

[263] R. Dong, W. H. Kinney, and D. Stojkovic, "Symmetron Inflation," *JCAP*, vol. 1401, p. 021, 2014.

[264] C. Burrage, E. J. Copeland, and P. Millington, "Radial acceleration relation from symmetron fifth forces," *Phys. Rev.*, vol. D95, no. 6, p. 064050, 2017. [Erratum: Phys. Rev.D95,no.12,129902(2017)].

[265] C. Burrage, E. J. Copeland, and P. Millington, "Radiative Screening of Fifth Forces," *Phys. Rev. Lett.*, vol. 117, no. 21, p. 211102, 2016.

[266] P. Brax, A.-C. Davis, and J. Sakstein, "SUPER-Screening," *Phys. Lett.*, vol. B719, pp. 210–217, 2013.

[267] A. Upadhye, "Symmetron dark energy in laboratory experiments," *Phys. Rev. Lett.*, vol. 110, no. 3, p. 031301, 2013.

[268] C. Burrage, A. Kuribayashi-Coleman, J. Stevenson, and B. Thrussell, "Constraining symmetron fields with atom interferometry," *JCAP*, vol. 1612, p. 041, 2016.